

High-spin molecules of phosphorus and nitrogen-centered radicals

Citation for published version (APA):

Wienk, M. M. (1997). *High-spin molecules of phosphorus and nitrogen-centered radicals*. [Phd Thesis 1 (Research TU/e / Graduation TU/e), Chemical Engineering and Chemistry]. Technische Universiteit Eindhoven. <https://doi.org/10.6100/IR477523>

DOI:

[10.6100/IR477523](https://doi.org/10.6100/IR477523)

Document status and date:

Published: 01/01/1997

Document Version:

Publisher's PDF, also known as Version of Record (includes final page, issue and volume numbers)

Please check the document version of this publication:

- A submitted manuscript is the version of the article upon submission and before peer-review. There can be important differences between the submitted version and the official published version of record. People interested in the research are advised to contact the author for the final version of the publication, or visit the DOI to the publisher's website.
- The final author version and the galley proof are versions of the publication after peer review.
- The final published version features the final layout of the paper including the volume, issue and page numbers.

[Link to publication](#)

General rights

Copyright and moral rights for the publications made accessible in the public portal are retained by the authors and/or other copyright owners and it is a condition of accessing publications that users recognise and abide by the legal requirements associated with these rights.

- Users may download and print one copy of any publication from the public portal for the purpose of private study or research.
- You may not further distribute the material or use it for any profit-making activity or commercial gain
- You may freely distribute the URL identifying the publication in the public portal.

If the publication is distributed under the terms of Article 25fa of the Dutch Copyright Act, indicated by the "Taverne" license above, please follow below link for the End User Agreement:

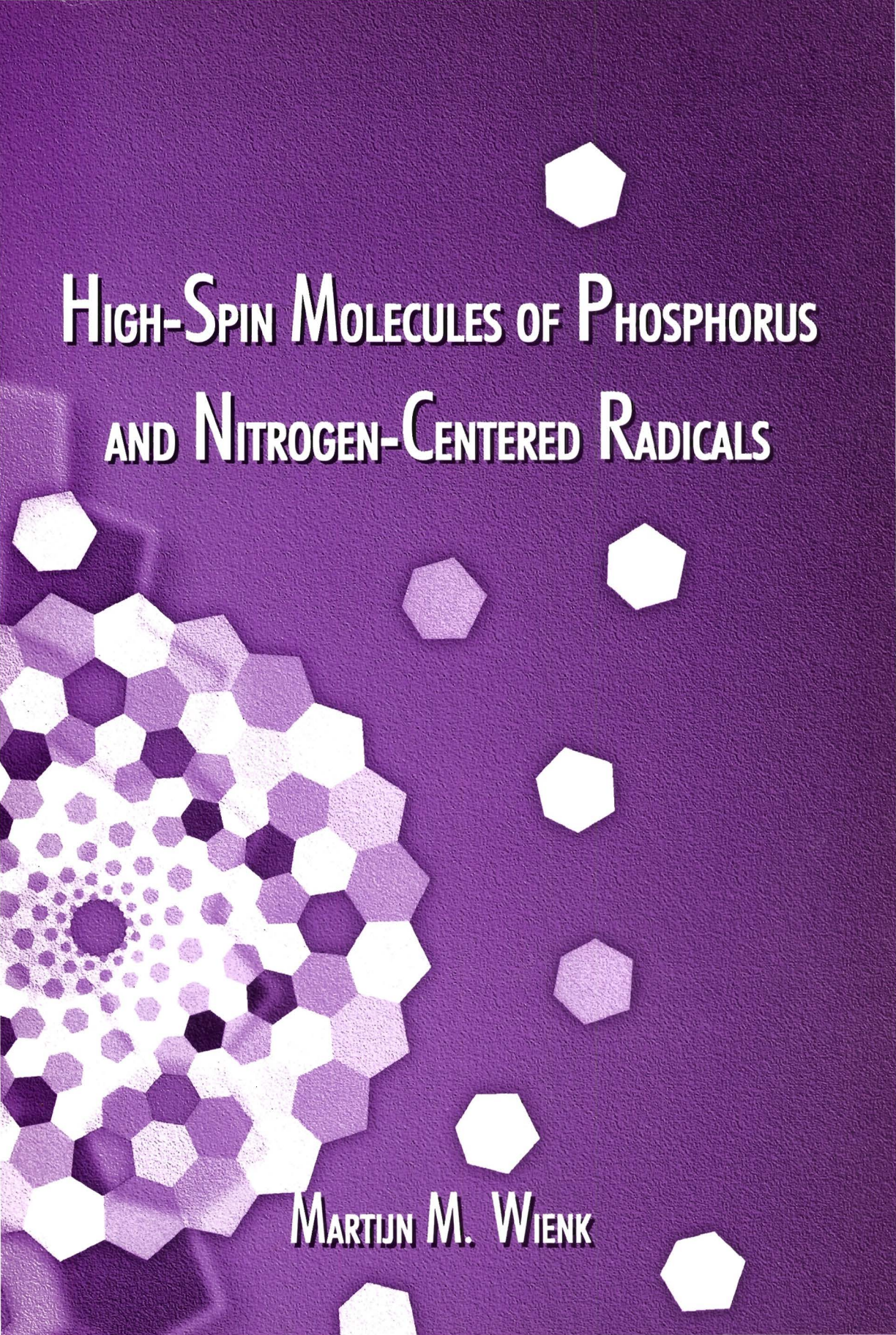
www.tue.nl/taverne

Take down policy

If you believe that this document breaches copyright please contact us at:

openaccess@tue.nl

providing details and we will investigate your claim.



**HIGH-SPIN MOLECULES OF PHOSPHORUS
AND NITROGEN-CENTERED RADICALS**

MARTIJN M. WIENK

High-Spin Molecules of Phosphorus and Nitrogen-Centered Radicals

High-Spin Molecules of Phosphorus and Nitrogen-Centered Radicals

PROEFSCHRIFT

ter verkrijging van de graad van doctor aan de Technische Universiteit Eindhoven, op gezag van de Rector Magnificus, prof. dr. M. Rem, voor een commissie aangewezen door het College van Dekanen in het openbaar te verdedigen op maandag 21 april 1997 om 16.00 uur.

Door

Martinus Maria Wienk

geboren te Oldenzaal

Dit proefschrift is goedgekeurd door de promotoren:

prof. dr. E. W. Meijer

en

prof. dr. E. J. R. Sudhölter

Copromotor:

dr. ir. R. A. J. Janssen

CIP-DATA LIBRARY TECHNISCHE UNIVERSITEIT EINDHOVEN

Wienk, Martinus M.

High-spin molecules of phosphorus and nitrogen-centered radicals / by
Martinus M. Wienk. - Eindhoven : Technische Universiteit Eindhoven, 1997.

Proefschrift. -

ISBN 90-386-0998-1

NUGI 813

Trefw.: vrije radicalen / elektronenspinresonantie / ferromagnetisme

Subject headings: radicals / electron spin resonance / ferromagnetism / high-spin molecules

"Hij doet de duizend kleine dingen die nodig zijn voor de geringste vooruitgang. Hij voert de vervelendste manipulaties uit met een eindeloos geduld, omdat er een doel achter zit. Hij ziet in gespannen verwachting en met grimmige vastberadenheid, hoe de natuur zich houdt onder het kruisverhoor, dat op wetenschappelijke wijze wordt afgenomen. Hij past de dwangmiddelen op de stof toe, met eerbied in het hart.

Hij heeft maling aan mensen met schoone handen en nette pakken, en is volkomen gelukkig."

*Dr. R. S. Tjaden Modderman
in "de Geest der Chemie"*

Order out of Chaos....

Contents

Chapter 1	Introduction	
1.1	High-Spin Molecules	1
1.2	Aims of Research	3
1.3	Scope of the Thesis	3
1.4	References	4
Chapter 2	High-Spin Molecules	
2.1	Introduction	5
2.2	Cooperative Magnetic Behavior	5
2.3	Organic Ferromagnets	6
2.4	Intramolecular Spin Alignment	7
2.4.1	Exchange Interaction	7
2.4.2	Molecular Orbital Degeneracy	9
2.4.3	Valence Bond Models and Spin Polarization	11
2.5	Intermolecular Spin Alignment	13
2.5.1	Spin Exchange	13
2.5.2	Charge-Transfer Complexes	14
2.6	Literature Survey	14
2.6.1	Carbenes	14
2.6.2	Triarylmethyl Radicals	16
2.6.3	Other Carbon-Centered Radicals	18
2.6.4	Nitroxyl Radicals	19
2.6.5	Nitrenes	20
2.6.6	Charged High-Spin Molecules	21
2.6.7	High-Spin Polymers	22
2.6.8	Ferromagnetic Molecular Assemblies	24
2.7	Analytical Methods	25
2.7.1	ESR Spectroscopy	25
2.7.2	Magnetization and Magnetic Susceptibility	27
2.8	Concluding Remarks	29
2.9	References	29
Chapter 3	Triplet-State Phosphinyl Diradicals	
3.1	Introduction	35
3.2	Synthesis	36
3.3	ESR Spectroscopy	37

3.4	Determination of the Ground State	39
3.5	Conclusion	40
3.6	Experimental Section	40
	3.6.1 General Methods	40
	3.6.2 Synthesis	41
3.7	References	42
Chapter 4	Triplet-State Phosphoryl Diradicals	
4.1	Introduction	45
4.2	Synthesis	47
4.3	X-Ray Analysis	47
4.4	NMR Analysis	48
4.5	ESR Spectroscopy	49
4.6	Determination of Ground States	55
4.7	Structure Assignment of Radicals	56
4.8	Discussion	56
4.9	Acylphosphine Oxides as Precursor	57
	4.9.1 Introduction	57
	4.9.2 Synthesis	58
	4.9.3 ESR Spectroscopy	59
4.10	Conclusion	62
4.11	Experimental Section	63
	4.11.1 General Methods	63
	4.11.2 Synthesis	63
4.12	References	66
Chapter 5	High-Spin Cation Radicals of Methylene Phosphoranes	
5.1	Introduction	69
5.2	Synthesis of Methylene Phosphoranes	71
5.3	Cyclic Voltammetry	72
5.4	ESR Spectroscopy	73
5.5	Determination of Ground States	78
5.6	Synthesis of Bis and Trisphosphines	79
5.7	Cyclic Voltammetry	80
5.8	Conclusion	81
5.9	Experimental Section	82
	5.9.1 General Methods	82
	5.9.2 Synthesis	82
5.10	References	85

Chapter 6	Stable High-Spin Cation Radicals of <i>m-p-N</i>-Phenylaniline Oligomers	
6.1	Introduction	87
6.2	Synthesis	89
6.3	Cyclic Voltammetry	90
6.4	UV/visible/nearIR Spectroscopy	93
6.5	Electrospray Mass Spectrometry	96
6.6	ESR Spectroscopy	97
6.7	Determination of Ground States	101
	6.7.1 Variable Temperature ESR Spectroscopy	101
	6.7.2 Magnetization Measurements	102
6.8	Discussion	103
6.9	Conclusion	105
6.10	Experimental Section	105
	6.10.1 General Methods	105
	6.10.2 Synthesis	105
6.11	References	107
Chapter 7	Stable High-Spin Cation Radicals of <i>m-p</i>-Aniline Oligomers by “Acid Doping”	
7.1	Introduction	111
7.2	Synthesis	112
7.3	Cyclic Voltammetry	114
7.4	UV/visible/nearIR Spectroscopy	115
7.5	“Acid Doping”	116
7.6	ESR Spectroscopy	117
7.7	Determination of Ground States	119
7.8	Conclusion	120
7.9	Experimental Section	120
	7.9.1 General Methods	120
	7.9.2 Synthesis	121
7.10	References	124
Epilogue		125
Summary		126
Samenvatting		128
Curriculum Vitae		130

Chapter 1

Introduction

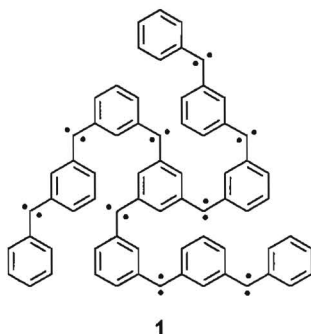
1.1 High-Spin Molecules

In recent years, high-spin molecules have attracted increasing attention as model compounds for organic ferromagnets.¹⁻³ High-spin molecules consist of organic radicals as spin-carrying moieties, covalently linked via ferromagnetic coupling units, in such a way that the individual electron spins are aligned in a parallel fashion. Without such spin coupling, electron spins will act as independent entities. Coupling units generally consist of π -conjugated segments, and the sign and strength of the spin-spin interaction are determined by the topology of these units. In case of ferromagnetic coupling, the magnetic moments, associated with the individual electron spins are parallel and the magnetic moment of the molecule is proportional to the number of aligned spins. Ultimately, this may lead to high-spin polymers or even ferromagnetic materials, since ferromagnetism emanates from the cooperative behavior of a large number unpaired electrons with parallel spins. In the meantime, high-spin molecules are excellent tools to study the behavior of and interaction between unpaired electrons in organic molecules.

The application of organic compounds to achieve ferromagnetic properties, has been considered only recently. Traditionally, ferromagnets have been associated with metals such as iron, chrome and cobalt, because unpaired electrons are intrinsic to these materials. Due to the fact that electron pairing is one of the basic principles of chemical bonds in organic chemistry, unpaired electrons are less common in organic molecules and materials. Therefore, the preparation of purely organic materials exhibiting ferromagnetic interactions in three dimensions poses a scientific challenge. The study of high-spin molecules, which focuses on intramolecular spin alignment is only one of the strategies pursued at the moment.⁴⁻⁶ Other approaches aim at the intermolecular spin ordering via spatial arrangement of stable organic radicals in the crystalline phase. The major advantage of high-spin molecules is the strong intramolecular spin coupling. Furthermore, the mechanisms governing this intramolecular interaction are well understood and generally have a good predicting value, allowing rational design of new architectures.^{1,2}

Combination of different radical sites with the available ferromagnetic coupling units has led to various high-spin molecules. For example, nonacarbene **1** has been prepared, which has 18 unpaired electrons, all of which are ferromagnetically coupled, resulting in a nonadecet

($S = 9$) ground state; the highest reported spin number for a high-spin molecule to date.⁷ Other frequently used spin-carrying units are nitrenes and triarylmethyl radicals. Because of their stability, nitroxyl radicals have also extensively been employed, but these open-shell moieties exhibit relatively limited spin delocalization and consequently weak spin-spin interactions. At the moment research is aimed at the development of new spin carrying units, which should be reasonably stable and have a significant overlap with the ferromagnetic coupling unit, allowing interaction between the individual spins.



A particularly interesting strategy towards high-spin polymers is that of a polaronic ferromagnetic chain, in which unpaired electrons can be introduced by reduction or oxidation of dopable segments.⁸⁻¹⁰ This process is well established for π -conjugated polymers, leading to conducting materials. Spin alignment between the polaronic (ionic) units can be achieved by linkage via ferromagnetic coupling units (Figure 1.1). Various polymers have been prepared that demonstrate the feasibility of this concept. If the doping level of such a polymer can be tuned accurately and the polaronic units are stable enough, this concept may afford a very convenient route towards high-spin polymers.

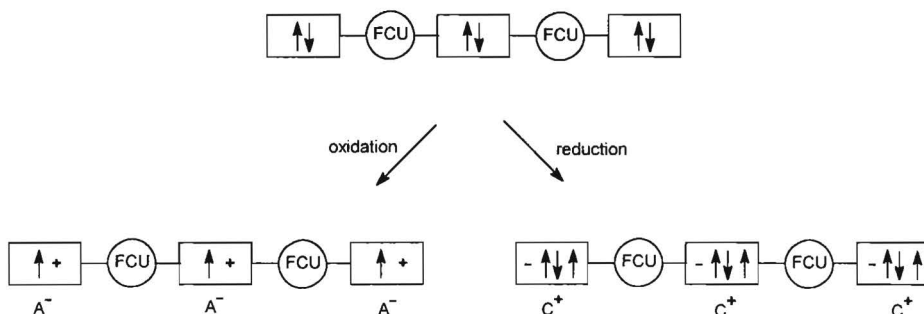


Figure 1.1 Schematic representation of a polaronic ferromagnetic chain.

1.2 Aims of Research

The primary goal of this research was the evaluation of new organic radicals as spin-carrying moiety in high-spin molecules. In all cases, *m*-phenylene, which is the most commonly used ferromagnetic linker, was chosen as coupling unit. For effective spin-coupling between radical sites, the spin density at the coupling unit must be high. In contrast, the stability of a radical usually increases with extension of the delocalization of the unpaired electron. This intrinsic dichotomy between localization and delocalization of spin necessitates an extensive search for novel organic radicals that can be incorporated in high-spin systems.

When this research started, all known high-spin molecules exclusively comprised radical sites localized on first-row elements like carbon and nitrogen. To broaden the scope, we set out to investigate the possibility to use heavy-atom radicals instead. Phosphorus was chosen as second-row element, because of the existing expertise in the field of phosphorus-centered radicals.¹¹⁻¹³ While various new phosphorus-related high-spin molecules could be prepared, they lacked the desired stability under ambient conditions.¹⁴⁻¹⁶ Therefore, the focus of research was eventually shifted to polaronic radicals, investigating whether it is possible to apply the concepts used in the area of (semi)conducting polymers to prepare high-spin molecules with intramolecular ferromagnetic coupling. Conducting polyaniline served as a model, because of the open-shell character of the charge carriers in this polymer. This has led to various high-spin aniline oligomers, which are stable under ambient conditions.¹⁷⁻¹⁹

1.3 Scope of the Thesis

In Chapter 2 of this thesis an introduction is given into the mechanisms governing spin-spin interactions in organic systems. Furthermore, a literature survey as well as an overview of the most commonly used analytical techniques are presented. In the following chapters different organic radicals are evaluated as spin-carrying units in high-spin molecules. Initially research was focused on phosphorus-centered radicals as spin-carrying units for high-spin molecules. Chapters 3 and 4 are devoted to triplet phosphinyl and phosphoryl diradicals, respectively. These diradicals, which are the first high-spin molecules based on heavy-atom radicals, confirm the effectiveness of *m*-phenylene as a ferromagnetic coupling unit. The major challenge turned out to be the efficient generation of the radicals. Attempts to improve the efficiency of the generation of phosphoryl radicals using acylphosphine oxides as precursors failed, due to instability of the phosphoryl radicals and very facile side reactions (Chapter 5). Cation radicals, generated by oxidation of neutral methylene phosphoranes are the subject of Chapter 6. In addition to a triplet di(cation radical), a tri(cation radical) with a quartet ground state has been prepared. These cation radicals are much more stable than the

phosphinyl and phosphoryl radicals, and can be kept in solution at temperatures below 200 K.

In the last two Chapters, 7 and 8, aniline oligomers are introduced as model compounds for polaronic ferromagnetic polymers. It is shown that these oligomers can efficiently be oxidized to the corresponding high-spin oligo(cation radical)s, which are stable at ambient conditions. An alternating *meta* and *para* connectivity of the aniline units ensures ferromagnetic spin alignment and chemical stability of these polaronic oligomers. Extension to higher spin multiplicities in one and two dimensions has been achieved, demonstrating that these systems are promising building blocks for future polaronic ferromagnets.

1.4 References

- 1 Rajca, A. *Chem. Rev.* **1994**, *94*, 871.
- 2 Iwamura, H. *Adv. Phys. Org. Chem.* **1990**, *26*, 179.
- 3 Iwamura, H.; Koga, N. *Acc. Chem. Res.* **1993**, *26*, 346.
- 4 Magnetic Molecular Materials; Gatteschi, D., Kahn, O., Miller, J. S., Palacio, F., Eds; Kluwer Academic Publishers: Dordrecht, The Netherlands, 1991.
- 5 *Chemistry and Physics of Molecular Based Magnetic Materials. Molecular Crystals and Liquid Crystals*; Iwamura, H., Miller, J. S., Eds.; Gordon and Breach Publishers: New York, 1993; Vol. 232, pp 1-360.
- 6 Miller, J. S.; Epstein, A. J. *Angew. Chem., Int. Ed. Engl.* **1994**, *33*, 385.
- 7 Nakamura N.; Inoue, K.; Iwamura, H. *Angew. Chem., Int. Ed. Engl.* **1993**, *32*, 872.
- 8 Fukutome, H.; Takahashi, I.; Ozaki, M. *Chem. Phys. Lett.* **1987**, *133*, 34.
- 9 Kaisaki, D. A.; Chang, W.; Dougherty, D. A. *J. Am. Chem. Soc.* **1991**, *113*, 2764.
- 10 Tanaka, K.; Ago, H.; Yamabe, T. *Synth. Met.* **1995**, *72*, 225.
- 11 Aagaard, O. M.; Janssen, R. A. J.; de Waal, B. F. M.; Kanters, J. A.; Schouten, A.; Buck, H. M. *J. Am. Chem. Soc.* **1990**, *112*, 5432.
- 12 de Waal, B. F. M.; Aagaard, O. M.; Janssen, R. A. J. *J. Am. Chem. Soc.* **1991**, *113*, 9471.
- 13 Janssen, R. A. J.; Aagaard, O. M.; Cabbolet, M. T. J. F.; de Waal, B. F. M. *J. Phys. Chem.* **1991**, *95*, 9256.
- 14 Wienk, M. M.; Janssen, R. A. J.; Meijer, E. W. *J. Phys. Chem.* **1995**, *99*, 9331.
- 15 Wienk, M. M.; Janssen, R. A. J.; Meijer, E. W. *Synth. Met.* **1995**, *71*, 1833.
- 16 Wienk, M. M.; Janssen, R. A. J. *Chem. Commun.* **1996**, 1919.
- 17 Wienk, M. M.; Janssen, R. A. J. *Chem. Commun.* **1996**, 267.
- 18 Wienk, M. M.; Janssen, R. A. J. *J. Am. Chem. Soc.* **1996**, *118*, 10626.
- 19 Wienk, M. M.; Janssen, R. A. J. *J. Am. Chem. Soc.* **1997**, accepted for publication.

Chapter 2

High-Spin Molecules

2.1 Introduction

High-spin molecules attract considerable interest as model compounds for organic ferromagnetic materials.^{1,2} In this chapter, a short introduction into magnetism is given and the prerequisites for organic ferromagnets will be addressed. Furthermore, the most important developments and analytical techniques commonly used in this discipline will be discussed.

2.2 Cooperative Magnetic Behavior

Ferromagnetism is a materials property, which results from the cooperative behavior of a large number of minute magnetic moments that are associated with the electron spin. The spin of an electron is either up (\uparrow) or down (\downarrow) and the corresponding magnetic moments have opposite signs. Generally, organic molecules have a closed-shell configuration in which each electron is accompanied by an electron with opposite spin. Consequently, the magnetic moments cancel out and the corresponding material is *diamagnetic* (Figure 2.1). Radicals are open-shell molecules, but to arrive at macroscopic magnetic properties, the interaction between the individual unpaired electrons is of eminent importance. If no interaction is present, the material is called *paramagnetic*; the spins and corresponding magnetic moments will be randomly oriented, which also causes cancellation of the spins. When interactions give rise to a parallel alignment of the spins, they are called *ferromagnetic*. This orientation leads to a material in which the individual magnetic moments add up to a macroscopic phenomenon. *Antiferromagnetic* interactions, on the other hand, favor an alternate orientation of the spins and *ferrimagnetic* interactions arise when spins of unequal size are aligned alternately. In this case the spins can only partly cancel out, and consequently this effect also leads to magnetic materials.

A magnetic material generally consists of several magnetic domains. Within such a domain the spins all are aligned over a long range and in three dimensions. In α -iron, the microcrystalline particles that form single domain structures contain ca. 5000 coupled spins. This spin alignment only occurs if the spin-spin interaction energies are larger than the thermal energy (kT) of the system. This implies that spin alignment will only occur below a certain critical temperature, called the Curie temperature (T_C).

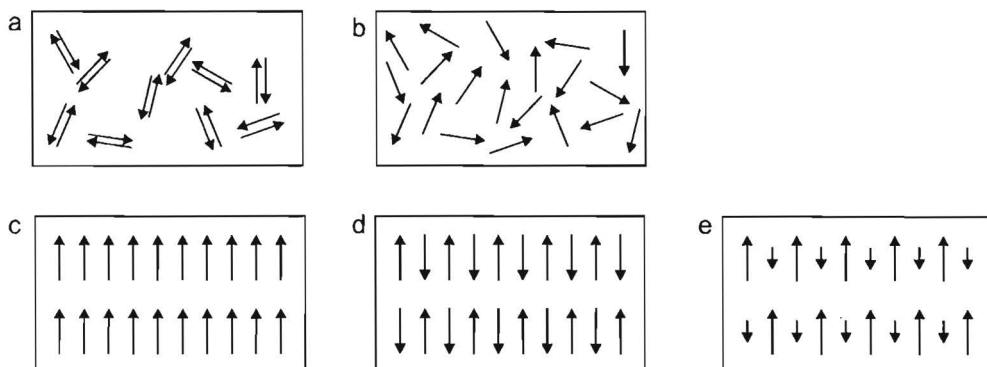


Figure 2.1. Schematic representation of materials exhibiting a) diamagnetism b) paramagnetism c) ferromagnetism d) antiferromagnetism e) ferrimagnetism

2.3 Organic Ferromagnets

In classical magnets the electron spins are more or less localized at single atoms in d or f orbital spin sites. They are prepared by high-temperature metallurgical methods. Recently, organic molecule-based magnetic materials have been developed, which can be prepared through low-temperature synthetic procedures.³ Two categories of molecule-based magnets can be distinguished. The first category comprises organometallic materials in which the interplay between organic molecules and metals gives rise to long-range spin coupling. Materials of this category with Curie temperatures well above room temperature have been prepared.³ The second category is comprised solely of organic molecules or polymers.⁴⁻⁶ In these materials, the s and p orbitals not only have to accommodate the spins, but also have to provide a mechanism of spin coupling.

Organic radicals contain unpaired electrons and can, therefore, be used as spin carrying moiety. To arrive at a ferromagnetic material, the interaction between individual unpaired electrons has to be controlled in such a way that parallel spin alignment is favored. In general, two different approaches to organic ferromagnets are pursued: one focusing on *intermolecular*, the other on *intramolecular* interactions. The first approach aims at the spatial organization of radicals in a crystal structure. Even though the intermolecular spin-spin interactions are relatively weak, a number of purely organic ferromagnetic materials have been prepared this way (see 2.6.8). The weakness of the spin-spin interaction, however, is reflected in the Curie temperatures of these materials, most of which are well below 10 K.

The second approach uses interactions between unpaired electrons within the same molecule, creating so-called high-spin molecules. These open-shell molecules contain several unpaired electrons which align ferromagnetically. An advantage of this approach is the

generally much stronger spin coupling. In addition, intramolecular spin-spin interactions are well understood, making a rational molecular design of high-spin systems possible. However, in order to obtain ferromagnetic materials, intermolecular spin coupling between such high-spin molecules has to be achieved as well.

In this chapter, several models describing both intramolecular and intermolecular spin-spin interactions will be evaluated.

2.4 Intramolecular Spin Alignment

For the creation of high-spin molecules, intramolecular ferromagnetic spin alignment is essential. Over the years, a number of models has been developed describing the interaction between unpaired electrons in organic multi-spin molecules. Generally, these models have a good predicting value, allowing a rational design of new high-spin systems.

2.4.1 Exchange Interaction

In a diradical, the simplest of multi-spin systems, two unpaired electrons are located in two (near) degenerate singly occupied molecular orbitals (SOMOs) φ_a and φ_b . The ground state can be either a low-spin singlet (S: antiferromagnetic coupling of spins) or a high-spin triplet (T: ferromagnetic coupling of spins). The spin-spin interaction can be described by the Heisenberg-Hamiltonian:

$$\hat{H} = -2 \sum_{i < j} \sum J_{ij} \hat{s}_i \hat{s}_j \quad (1)$$

in which \hat{s}_i and \hat{s}_j are spin operators and J_{ij} is the exchange coupling constant between the electrons i and j , which can be either positive or negative, leading to ferromagnetic or antiferromagnetic spin alignment, respectively. The energy gap between the singlet and triplet state ($E_S - E_T = \Delta E_{ST}$) is given by $2J$ and should be positive for ferromagnetic interaction to occur. According to the Heitler-London model, J basically has the following form:⁷

$$J = 2\beta S + K \quad (2)$$

with
$$S = \langle \varphi_a | \varphi_b \rangle \quad (3)$$

$$\beta = \langle \varphi_a | \hat{H} | \varphi_b \rangle \quad (4)$$

and
$$K = \langle \varphi_a(1)\varphi_b(2) | e^2/r_{12} | \varphi_a(2)\varphi_b(1) \rangle \quad (5)$$

The value of J is determined by two terms of opposite sign. The product of the resonance integral β with the overlap integral S is always negative since β and S are of opposite sign. This factor can be seen as the antiferromagnetic contribution to J . On the other hand, the ferromagnetic contribution is accounted for by the two-electron exchange integral, K , which is necessarily positive. The exchange interaction arises from the antisymmetrization of the wave function as required by the Pauli exclusion principle. This principle forbids electrons with the same spin to occupy the same region of space. As a result, the motions of electrons with alike spins are more correlated than when the signs of the spins would have been opposite. This correlated motion of electrons keeps them further apart and therefore they experience a smaller Coulomb repulsion, resulting in a lower overall energy.

In general, $2\beta S$ dominates, resulting in a negative value for J and a singlet ground state. Ferromagnetic interaction occurs, when S approaches zero, i.e. when φ_a and φ_b are (quasi) orthogonal. A zero overlap integral does not necessarily lead to a strong stabilization of the triplet state; in addition the exchange integral K must be substantial. Because K qualitatively corresponds to the overlap integral, disregarding the sign, this is achieved when the two SOMOs φ_a and φ_b occupy the same region of space, somewhere in the molecule.

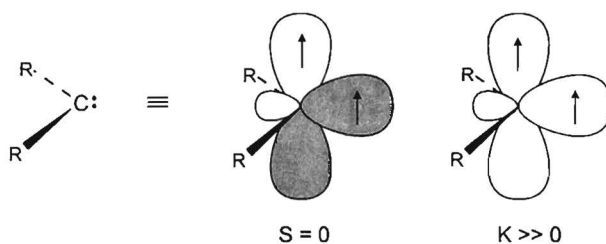


Figure 2.2. Perpendicular orbitals at a carbene center, illustrating the exact cancellation of the overlap integral S and a substantial value for the exchange integral K .

The implications of the above can be illustrated by looking at a carbene which is a prototype structure of a triplet diradical (Figure 2.2). The two unpaired electrons are located in two near degenerate MOs located on the same carbon atom. One electron occupies a sp^2 -hybridized orbital, the other a p orbital, perpendicular to the sp^2 orbital. Consequently, the positive overlap exactly cancels out the negative overlap, i.e. the SOMOs are orthogonal and S is zero. For K cancellation does not occur and since both MOs are located on the same carbon atom, electron-electron interactions are substantial. Therefore, the ground state will be a triplet state, in which the destabilizing Coulomb interactions are greatly diminished by the correlated motion of the parallel spins, as compared to the singlet state. In fact, because in the case of

carbenes the SOMOs are located on one atom, this is an implication of Hund's rule which applies to atomic orbitals.

Summarizing, in order to create high-spin molecules, molecules need to be designed with several (near) degenerate orbitals, which are localized within the same region of space and yet have an overlap integral that is zero or at least very small.

2.4.2 Molecular Orbital Degeneracy

A category of compounds, which is known to have degenerate orbitals is the class of non-Kekulé molecules. These alternant hydrocarbons are fully conjugated, but contain at least two atoms that are not π -bonded.^{8,9} In 1950 Longuet-Higgins proved that an alternant hydrocarbon contains at least $(N - 2T)$ singly occupied non-bonding molecular orbitals (NBMOs), where N is the number of carbon atoms and T the maximum number of double bonds that occurs in any resonance structure.¹⁰ Looking at isomeric benzoquinodimethanes, one can see that the *para* isomer **1** can be represented as a classical Kekulé structure with a total of four double bonds (Figure 2.3). Longuet-Higgins predicts $(N - 2T) = 8 - 8 = 0$ NBMOs and a closed-shell configuration. On the other hand, the *meta* isomer **2** can only be drawn in a non-Kekulé fashion, with three double bonds at the most, resulting in two NBMOs each occupied by one unpaired electron.

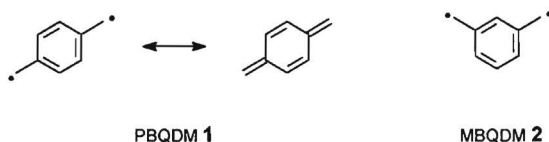


Figure 2.3. Isomeric structures of benzoquinodimethane

On the basis of Hund's rule, Longuet-Higgins predicted ferromagnetic spin alignment between the unpaired electrons in the NBMOs of a non-Kekulé molecule, and a ground-state with a spin quantum number $S = n/2$, where n is the number of unpaired electrons.

This model, however, does not account for the exchange interaction, necessary to establish effective coupling between the electron spins. As a consequence, the ground-states of only a limited number of non-Kekulé molecules are predicted accurately. Therefore, an extended model was proposed by Borden and Davidson, introducing the concept of non-disjoint NBMOs.¹¹ To illustrate this model, we consider trimethylenemethane (TMM, **3**). This is a non-Kekulé molecule with two singly occupied NBMOs. A simple Hückel

representation of the NBMOs is depicted in Figure 2.4. In this representation, or in any other, the two NBMOs span common atoms; they are so called non-disjoint. Because the electrons occupy the same region of space, the exchange interaction is substantial and the diradical has a high-spin triplet ground state

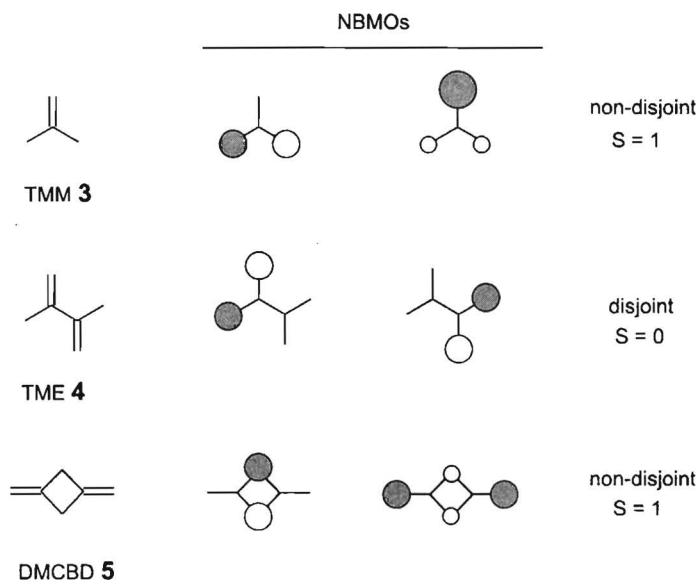


Figure 2.4. Hückel representations of the NBMO structure of non-Kekulé molecules

Tetramethyleneethane (TME, 4) is also a non-Kekulé molecule and according to the Longuet-Higgins model this structure has $(6-4) = 2$ NBMOs, and a triplet ground state. However, these two singly-occupied NBMOs can be selected in such a way that the overlap is very small; they are disjoint. Consequently, the exchange is small and the singlet and triplet state are expected to be near-degenerate. TME was found to have a triplet ground state^{12,13} and CI calculations support this observation.¹⁴ In an optimized geometry - with a twist of ca. 45° around the central bond- the triplet state lies below the singlet state. In a planar conformation the singlet is found to be lowest in energy.

In TME, two allyl radicals can be recognized, which are connected via the central carbon atoms that do not contribute to the NBMOs. Another non-Kekulé molecule can be constructed from two allyl radicals: 2,4-dimethylene-1,3-cyclobutanediyl (DMCBD, 5).¹⁵ It is a C₆H₆ and has 6 π -electrons and is considered a non-Kekulé isomer of benzene.¹⁶ In this case the connection between the two allylic halves does involve spin carrying carbon atoms. Consequently, the NBMOs are non-disjoint and the ground state is a triplet.

2.4.3 Valence Bond Models and Spin Polarization

More recently, valence bond theories have been developed, to predict ground state multiplicities of non-Kekulé molecules. The carbon atoms in an alternant hydrocarbon can be starred in such a way that no two starred atoms are adjacent. When $n^* \geq n$, the spin quantum number S is given by:^{17,18}

$$S = (n^* - n) / 2 \quad (6)$$

This theory offers a very convenient way to predict ground-state multiplicities in a large array of conjugated open-shell systems. In Figure 2.5, the model is worked out for the prototype structures that have been discussed so far. The predicted values for the spin multiplicity are in accordance with experimental results.

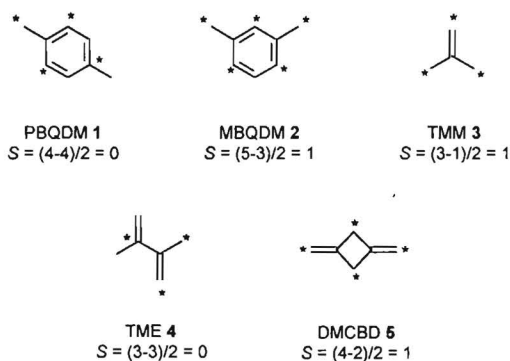


Figure 2.5. Valence bond representations and predicted spin multiplicities of some prototype alternant hydrocarbons.

In a simple Hückel-MO picture the spin density on the starred and unstarred atoms would be positive and zero, respectively. A full MO-calculation requires the admixture of excited states with partially occupied anti-bonding MOs into the ground state. This configuration interaction results in spin polarization; the additional spin density inverts on each successive atom in a π -conjugated system. Consequently, (large) positive and (small) negative spin densities are obtained on the starred and unstarred atoms, respectively (Figure 2.6). This illustrates the ferrimagnetic nature of the spin-spin coupling. Another method to predict the ground-state multiplicity, is simply counting the number of π -electrons between the open-shell units. The interaction is ferromagnetic if the spin-carrying moieties are separated by an odd number of π -electrons, whereas, the coupling is antiferromagnetic if this number is even.

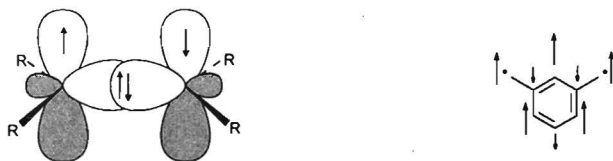


Figure 2.6. (left): Spin polarization results from Hund's rule, favoring parallel spin orientation for spins in the σ - and π -orbital on each atom. Inversion of polarization occurs because the spins of the electron pair in the σ -orbital always are opposite as dictated by the Pauli principle. (right): Ferrimagnetic nature of the spin-spin interaction in MBQDM.

The valence bond model is a very convenient model which successfully predicts the ground state of a large number of non-Kekulé molecules. Nevertheless, in some cases this description is not sufficient because it only accounts for the sign of the interaction and not for its strength. For the m,m' -isomer of a 1,1-diphenylethylene linked diradical, the VB model predicts a high-spin ground state whereas experimentally a low-spin ground state is found (Figure 2.7).^{19,20} This observation can be rationalized by considering the Borden–Davidson model which makes a distinction between joint and disjoint MOs. If the connection of the spin units involves carbon atoms that have no substantial spin density, the spin-spin interaction is very weak, which leads to a singlet-triplet degeneracy.

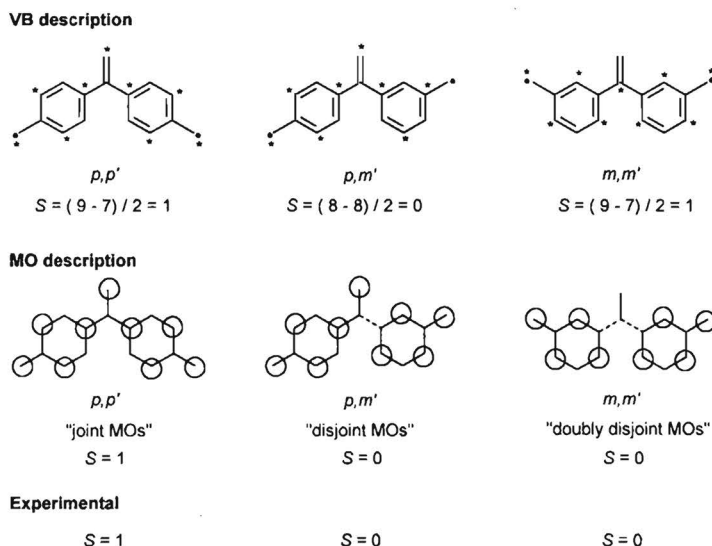


Figure 2.7. Topological isomers of a 1,1-diphenylethylene linked diradical. Valence bond description predicts a triplet ground state for the m,m' -isomer, but the MO picture illustrates that the NBMOs are (doubly) disjoint, formally leading to a singlet-triplet degeneracy (open circles mark the atoms with a large positive spin density).

2.5 Intermolecular Spin Alignment

Unless it will be possible to synthesize super-high-spin molecules with enough coupled spins to act as a single domain particle, intermolecular spin coupling between individual magnetic molecules is essential to create ferromagnetic materials. Even though this subject is beyond the scope of this thesis, some models describing such interactions will shortly be addressed.

2.5.1 Spin Exchange

The valence bond theory of topological symmetry as discussed in the previous paragraph can be considered as a through-bond interaction. For the description of the spin-spin interaction between unpaired electrons on separate molecules, a theory for through-space interactions has been put forward, which is quite similar. It was McConnell who first proposed such a mechanism (McConnell model I).²¹ For the magnetic interaction between two aromatic radicals A and B the Heisenberg-Hamiltonian can be expanded to:

$$\hat{H}^{AB} = -2 \sum_{i,j} J_{ij}^{AB} \hat{s}_i^A \hat{s}_j^B = -2 \hat{s}^A \hat{s}^B \sum_{i,j} J_{ij}^{AB} \rho_i^A \rho_j^B \quad (7)$$

Calculation of the exchange coupling constant J_{ij}^{AB} leads to an expression similar to equation 2 but with the signs inverted.^{7,22} Hence, since J_{ij}^{AB} is negative, the product of the spin densities ρ_i^A and ρ_j^B has to be negative as well, for ferromagnetic interactions between A and B to occur. In other words, exchange interaction, and thus ferromagnetic spin-coupling takes place if the interaction occurs between atoms of opposite spin density.

This prediction has been confirmed by ab initio calculations on the combination of a methyl and an allyl radical.²³ Similar calculations have been performed on stacks of benzyl radicals.²⁴⁻²⁶ In this case, only the *ortho* and *para* orientations result in ferromagnetic spin alignment (Figure 2.8), which is in good agreement with the McConnell model I.

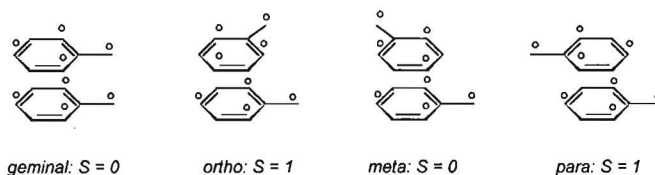


Figure 2.8. Interaction between two benzyl radicals in different orientation. Marked and unmarked atoms carry a positive and negative spin density, respectively.

2.5.2 Charge-Transfer Complexes

Generally, the unpaired electrons generated within one-dimensional alternating stacks of donor-acceptor salts ($--D^+A\cdot D^+A\cdot D^+A\cdot D^+A--$), are aligned in an antiferromagnetic fashion. This is a result of the admixing of the wave functions of the original (closed-shell) donor and acceptor components into the wave function of the CT complex. A second model proposed by McConnell (model II) predicts that, when either the donor or acceptor has a triplet ground state, the unpaired electrons in the CT complexes will align ferromagnetically.²⁷ In this case, the admixing of the wave function with the initial wave functions of donor and acceptor (one of which is a triplet), will lead to a parallel alignment of the spins in the complex.²⁸ Later, various adaptations of this model have been proposed,²⁹⁻³² but no experimental results have been reported that confirm these models.

2.6 Literature Survey

Based on the concepts discussed in the previous paragraphs, several high-spin molecules have been prepared. Ever since it has been recognized that these compounds are a first step toward organic ferromagnets, the number of papers reporting on high-spin compounds has increased enormously. In this literature survey, the most widely used organic open-shell moieties and spin-coupling units will be discussed.

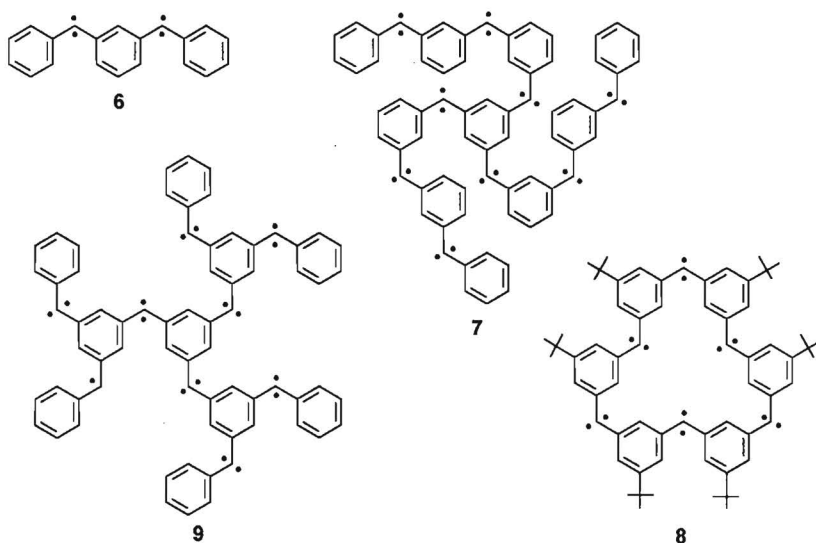
In addition some organic molecular assemblies which display bulk ferromagnetic behavior will shortly be addressed.

2.6.1 Carbenes

In 1967 Itoh³³ and Wasserman et al.³⁴ independently reported dicarbene **6** in which two phenylcarbene units are attached to the *meta* positions of a phenylene ring. This tetraradical has a quintet ($S = 2$) ground state, which results from the ferromagnetic coupling between the two triplet carbene moieties. The *meta*-substituted phenyl ring acts as a ferromagnetic coupling unit. This finding turned out to be the onset of both experimental^{35,36} and theoretical interest^{37,38} into carbenes as potential organoferromagnets.

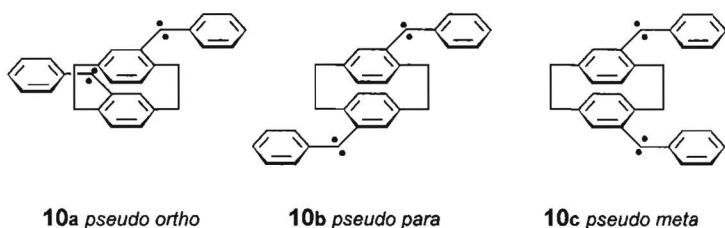
Oligocarbenes are generated photochemically at cryogenic temperatures from the corresponding diazo precursors. This is a very efficient single photon process, leaving no carbenes with unreacted diazo groups. Variable temperature experiments indicate a large ($\gg 1$ kcal per mole) energy gap between the high-spin ground state and lower spin states.

Over the years, linear oligocarbenes with ever increasing spin multiplicities have been prepared by the group of Iwamura.³⁹⁻⁴⁵ The concept was further extended into a two-dimensional framework making star-shaped compounds, with a 1,3,5-trisubstituted benzene ring as the core.^{46,47} Nonacarbene **7** has a nonadecet ($S = 9$) ground state; the highest spin state ever reported for a purely organic molecule. It is also shown that this approach can successfully be extended to a cyclic structure **8**, that eventually may lead to two-dimensional networks.



Recently, highly branched dendritic structures like **9** have been prepared, but the observed spin states were lower than expected.^{48,49} This observation is explained in terms of a facile recombination of carbene centers, due to the close proximity enforced by the molecular structure.

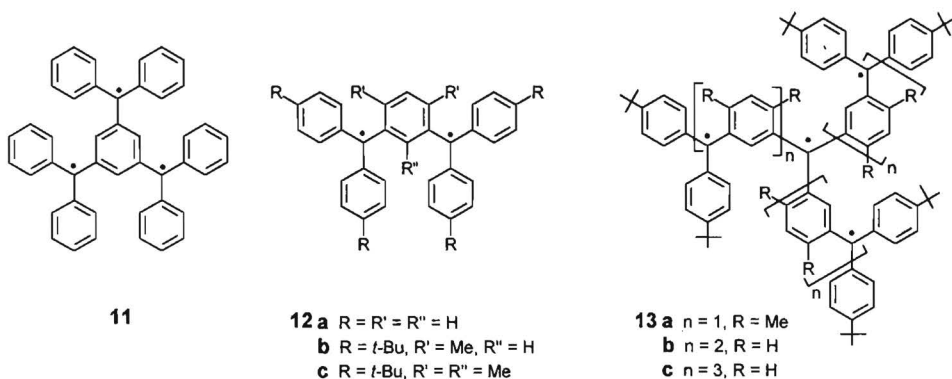
In a very elegant manner Iwamura demonstrated that spin alignment in the third direction (perpendicular to the molecular plane) is also possible, using [2,2]-paracyclophane derivatives **10**.^{50,51} The mode of interaction can be described by the McConnell model I, even though this model was originally put forward to describe intermolecular interactions. Of the three isomers, with different orientations of the two phenylmethylene substituents, only the *pseudo ortho* (**10a**) and *pseudo para* (**10b**) isomers satisfy the McConnell condition of exchange interaction between sites of opposite spin density. Accordingly, they are expected to have a quartet ($S = 2$) ground state, which was confirmed by experimental results. Exactly as predicted by the McConnell model, **10c** was found to have a singlet ($S = 0$) ground state.



Altogether, oligocarbenes have extensively been used to study the spin-spin interaction in organic multi-spin molecules. In the long run, however, carbenes suffer greatly from their intrinsic thermal instability. Unsubstituted phenylcarbenes degrade at temperatures well below 100 K, which makes it impossible to use these radicals at ambient conditions.

2.6.2 Triarylmethyl Radicals

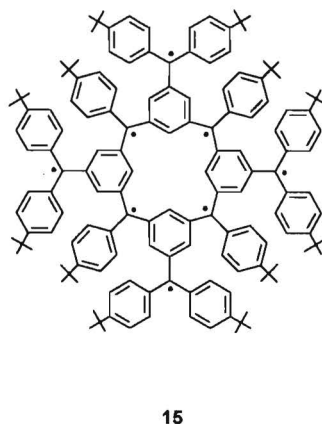
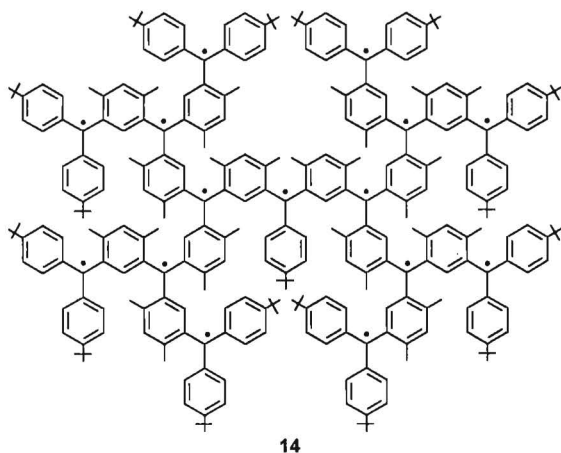
Another class of hydrocarbon-based high-spin molecules are the triarylmethyl radicals. Classical examples of this category are the Leo triradical (**11**)⁵² and Schlenk's hydrocarbon (**12a**).^{53,54} In these structures the *meta*-phenylene is also used as a ferromagnetic coupling unit between the radical sites. An advantage of this type of radicals over carbenes is their greater stability. Highly substituted triarylmethyl radicals are stable up to ambient temperatures.



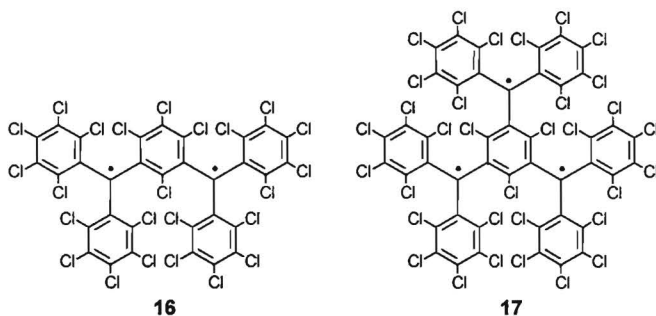
Rajca et al. have synthesized a range of alkyl substituted oligo(triarylmethyl) radicals, starting with a diradical (**12b**) and ending with a heptaradical (**13c**).⁵⁵⁻⁵⁷ These open-shell systems are prepared by oxidation of the corresponding oligo anions. To avoid reaction at the *para* positions of the alkyl rings, alkyl substituents have been introduced. This greatly stabilizes this type of radicals.

Based on the same concept, also a 1,3-connected triarylmethyl polyradical has been prepared. This polymer has an average of around 30 monomeric units linearly connected in each chain.⁵⁸ However, magnetization studies revealed a behavior that fits closely to that of a system with a spin multiplicity $S = 2$ only. This is probably due to an interrupted spin coupling within the chains. Defects which result from incomplete reactions or side reactions may be responsible for the disconnected spin-spin interactions. As a result, a chain of an average of 30 units contains a number of isolated spin-coupled segments, with an average of around four spin-carrying units per segment.

Dendritic polyradicals have also been prepared, but these also suffer from the interrupted spin coupling.^{59,60} Especially defects on the inner triarylmethyl sites are detrimental to the spin multiplicity. For example, one defect in pentadecaradical **14** may result in three isolated spin systems of $S = 3/2$, $3/2$ and $8/2$, instead of one $S = 15/2$ spin system. The dendritic polyradical **14** reveals a magnetization behavior comparable to a spin states of $7/2$ to $5/2$. The 'supposed' untriacontaradical, which is one generation higher should contain 31 unpaired electrons, but a much lower spin state ($5/2$ to $4/2$) is observed. From these results, a conversion of only 80% is estimated.



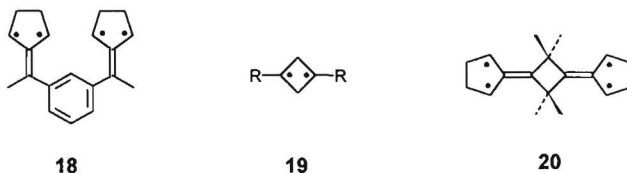
To get around the problem of interrupted spin-spin interaction in linear and branched chains, Rajca introduced the application of multiple spin-coupling pathways.^{61,62} The calix[4]arene derivative **15** represents a closed loop. In this system, two pathways for spin-coupling exist and hence such a topology is oblivious to one defect. Other structures that should even be more resilient to defects have also been proposed.



Veciana et al. have synthesized the perchlorinated derivative of the Schlenk hydrocarbon (**16**)⁶³ and a higher homologue of this compound (**17**).^{64,65} These compounds are stable in air up to 250 °C. Despite a non-planar conformation due to sterical crowding, both compounds have high-spin ground states, and the nearby lower-spin states are thermally inaccessible, indicating an energy gap $\gg 1$ kcal per mole.

2.6.3 Other Carbon-Centered Radicals

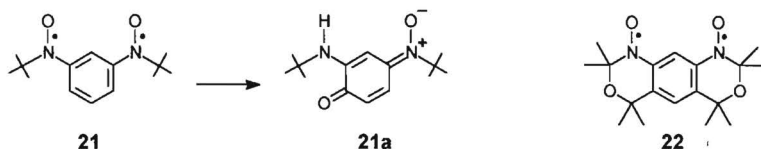
The spin-carrying unit in **18** is a derivative of TMM (see 2.4.2). Due to its topology, the two unpaired electrons in this unit interact ferromagnetically.⁶⁶ Connection of two of these triplet moieties via *m*-phenylene leads to ferromagnetic interaction and a quintet ($S = 2$) ground state.^{67,68}



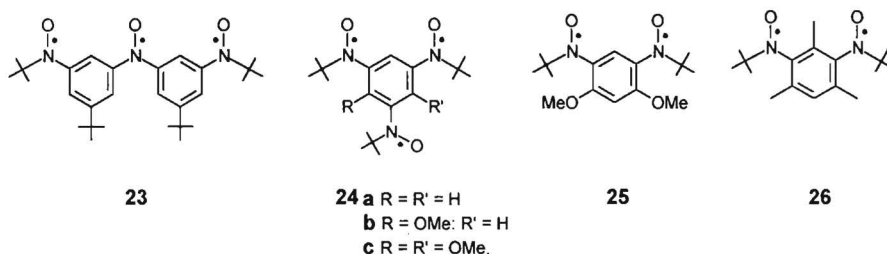
In cyclobutanediyl diradicals **19**, spin coupling occurs via a through-bond interaction, mediated by the CH_2 -groups. This results in a HOMO-LUMO degeneracy and a triplet ground state.⁶⁹ Based on this observation, Dougherty reasoned that the cyclobutane ring acts as a non-conjugated ferromagnetic coupling unit. This was demonstrated by compound **20**, which combines the triplet spin carrying unit with the cyclobutane coupling unit, and was found to have a high-spin quintet ($S = 2$) ground state, separated from the triplet state by at least a few hundreds of calories per mole.⁷⁰

2.6.4 Nitroxyl Radicals

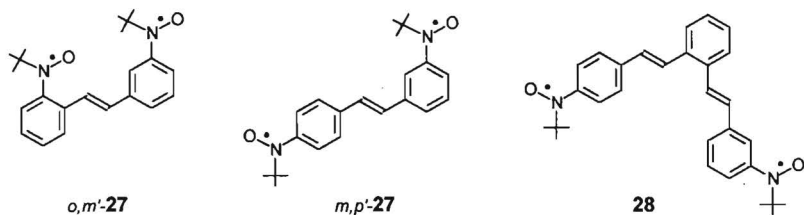
The stability of nitroxyl radicals makes these open-shell units very suitable for the generation of high-spin molecules. An early example of a nitroxyl diradical which has a high-spin ground state is compound (21).⁷¹ The energy gap between triplet ground state and the singlet state is $\gg 1$ kcal per mole. This diradical, however, is not stable. In solution, as well as in the crystalline phase it undergoes a topochemical change to the aminoquinone imine *N*-oxide 21a. In the tricyclic diradical 22 this problem was overcome, because the vulnerable positions *para* to the nitroxyl moieties are protected.⁷² ESR spectroscopy reveals a triplet state, but no studies have been undertaken to determine whether this is the ground state or a thermally populated state.



Triradical 23 has a quartet ground state and the energy gap (J/k) to the thermally excited doublet state was estimated to be 240 K (= 480 cal per mole).⁷³ This is considerably less than for any *m*-phenylene-coupled carbon based high-spin system. This is ascribed to the more localized spins of the nitroxyl radicals. The smaller spin density in the central ring makes the spin coupling weaker.



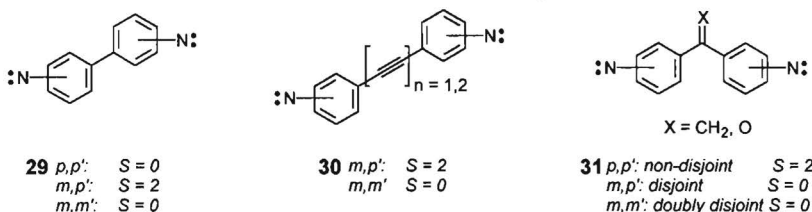
Substitution on the *m*-phenylene ring further diminishes the spin coupling, probably due to an out-of-plane twist of the nitroxyl moieties. Compound 24a has a quartet ground state, but introduction of one methoxy group (24b) leads to a reduction of the energy difference between quartet and doublet states, and a second methoxy group (24c) results in a low-spin doublet ground state.^{74,75} Similar effects are observed for compounds 25 and 26, both of which have a singlet ground state.^{76,77}



Stilbenes are of interest as ferromagnetic coupling units, because they can be used as the repeat unit of a polymer with pendant radical sites. Several connectivities of the open-shell moieties are possible, and the spin state of the different nitroxyl diradicals is always in agreement with the topology rules. So, both o,m' -27 and m,p' -27 have a triplet ground state.⁷⁸ However, the spin-spin interaction is rather weak due to a combination of the localization of the spin and the length of the π -system between the spins. If the distance between the radical sites is further increased, ΔE_{ST} decreases rapidly. For compound 28 the energy difference is only one tenth of the value for m,p' -27.⁷⁹

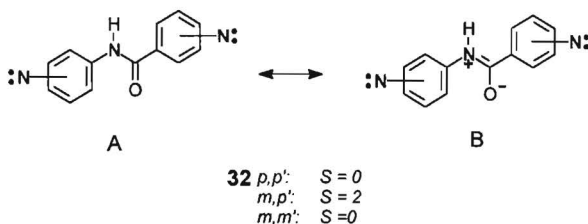
2.6.5 Nitrenes

Nitrenes are the nitrogen analogues of carbenes with two unpaired electrons localized in orthogonal orbitals on the nitrogen atom. Consequently, each nitrene unit has a triplet spin state. Like carbenes, nitrenes are thermally unstable and do not survive temperatures higher than ca. 100 K. Unlike other radical species discussed in this chapter, nitrenes have only one connection to other atoms. Consequently they can not be included in the main chain of a oligoradical, but can only be used as spin carrying pendants in side groups. This may have a certain advantage, though, since in this case incomplete conversion of the precursor groups does not necessarily lead to a disrupted connectivity.



Various π -conjugated coupling units have been tested in combination with differently oriented phenylnitrene groups (29-31).^{19,20,80} For these compounds the relation between the topology of the connecting units and the nature of the magnetic interactions is generally

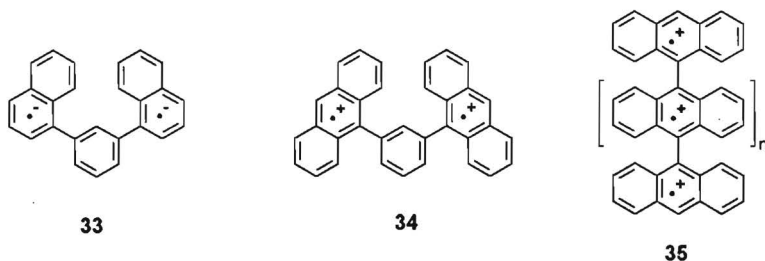
accurately predicted by the valence bond theory. Only for the *m,m'* isomer of **31** the disjoint nature of the connection has to be considered to account for the observed low-spin state (see 2.4.3).



The amide linkage also turns out to be an effective spin-coupling unit, connecting two phenylnitrene units in **32**. Both theoretical studies and experimental results indicate that the amide bond acts like the C=C double bond of a stilbene coupling unit. This is explained in terms of a stilbene-like resonance structure B.⁸¹

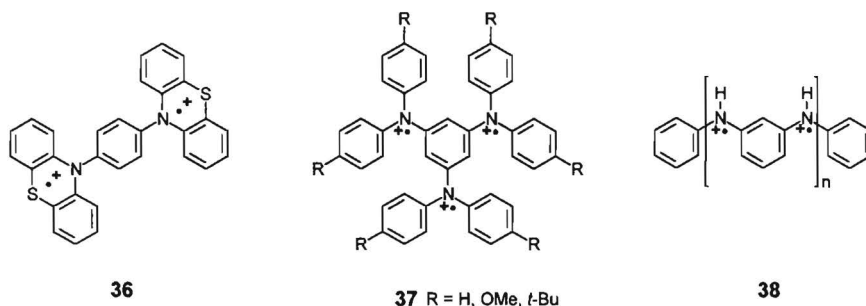
2.6.6 Charged High-Spin Molecules

In addition to the neutral radicals discussed in the previous paragraphs, also ionic spin-carrying units have been applied for the construction of high-spin molecules. Illustrative examples are compounds **33** and **34**.⁸² Reductive doping of the neutral 1,3-dinaphthylbenzene affords the corresponding di(anion radical) **33**, which has a high-spin triplet ground state. In a similar fashion oxidative doping of the dianthryl compound leads to the triplet state di(cation radical) **34**.



In an original approach, Baumgarten has also used the oxidized anthryl moiety as spin-carrying subunit for the construction of high-spin molecules.^{83,84} Instead of using a ferromagnetic coupling unit, the desired spin-spin interaction is achieved by the perpendicular alignment of the spin-carrying moiety **35**. Due to this arrangement, the singly occupied MOs are also orthogonal, which should lead to ferromagnetic spin alignment. In a number of

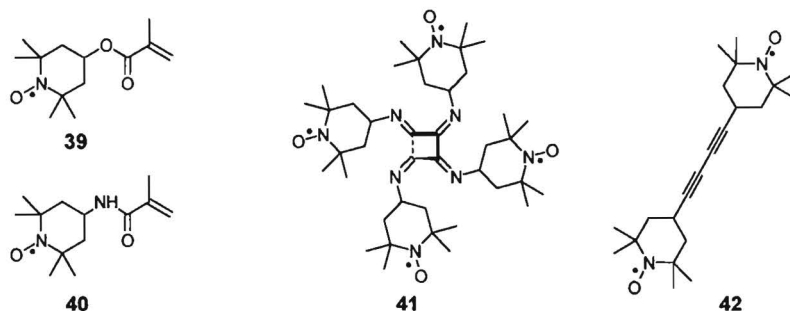
oligo(9,10-anthrylene)s, high-spin states were generated, but variable temperature ESR studies revealed that these are thermally populated.



Di(cation radical) **36**, has a triplet ground state, even though the polaronic units are connected via a *p*-phenylene ring which normally acts as an antiferromagnetic coupling unit.⁸⁵ This is rationalized by the orthogonal arrangement of the phenothiazine units, giving rise to spin alignment, similar to the oligoanthrylenes. A number of other high-spin molecules based on nitrogen cation radicals such as triarylamines **37**⁸⁶⁻⁸⁹ and oligo *m*-anilines **38**⁹⁰ have been prepared, but a major problem encountered with these compounds is the poor stability of the molecules after doping.

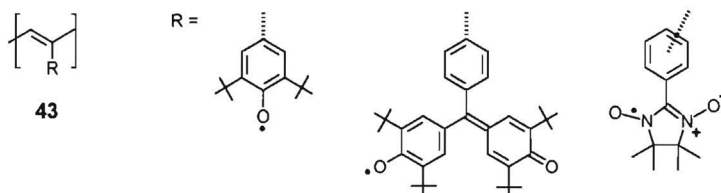
2.6.7 High-Spin Polymers

Straightforward polymerization of methylmetacrylate coupled TEMPO radicals like **39** and **40** leads to a material with weak antiferromagnetic interactions.⁹¹ Similar results are obtained with TEMPO groups attached to a polyiminoethylene backbone **41**.⁹² Despite the close packing of the spin-carrying units in this helical polymer, no magnetic ordering was observed. Replacing the TEMPO radicals by diphenylphenoxy radicals rendered no improvement.⁹³

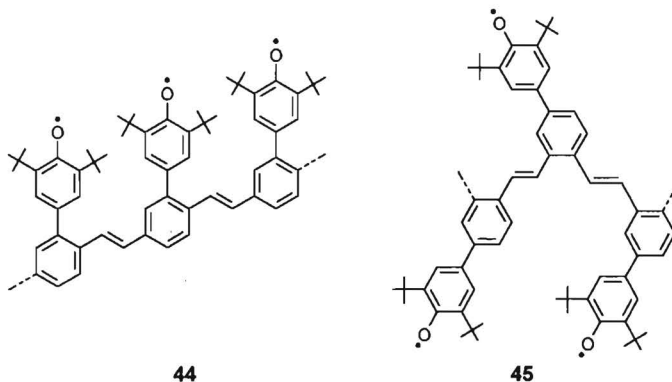


In 1986, Ovchinnikov and coworkers reported on the magnetic properties of polymeric samples obtained from the polymerization of a diacetylene monomer containing two TEMPO units **42**.⁹⁴⁻⁹⁶ However, these observations have been subject to controversy ever since. Attempts by other research groups to reproduce these results all failed.^{97,98} Other attempts to prepare high-spin polydiacetylenes failed because most of the radical sites are destroyed during polymerization.⁹⁹

Polyacetylenes with pendant stable radicals (**43**) have also been investigated as potential high-spin systems. Several spin carrying moieties have been applied, but in spite of the very high spin concentrations that were obtained, no cooperative ferromagnetic behavior was observed.¹⁰⁰⁻¹⁰⁵ The interactions were either predominantly paramagnetic or antiferromagnetic.



Regioregular poly(phenylenevinylene)s (PPVs) have recently been used as a backbone in combination with phenoxy radicals as pendant spin-carrying units. Valence bond theory and model studies on stilbene compounds provide insight into the topology required for ferromagnetic spin coupling.⁷⁸ Both the polymer with the *para* substitution pattern **44** and the polymer with the *ortho* pattern **45** display ferromagnetic spin alignment, even though the spin concentration did not exceed 0.7 spin/monomer unit.¹⁰⁶⁻¹⁰⁸ Similar results have been reported for PPVs with *tert*-butyl nitroxyl radicals as spin-carrying units.¹⁰⁹

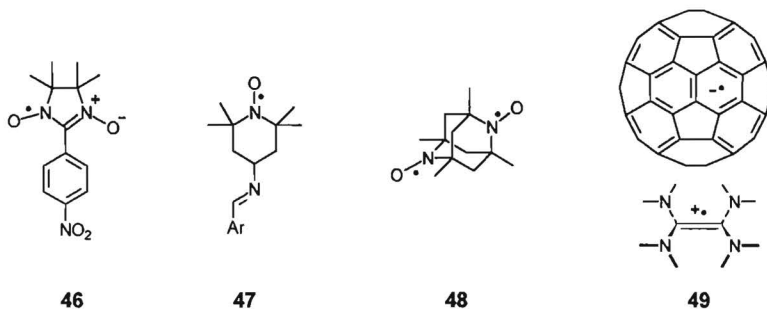


The concept of polaronic ferromagnetic polymers has been introduced by Fukutome. In this approach the spins are introduced by doping of π -conjugated segments. Connection of

these polaronic open-shell moieties via ferromagnetic coupling units should lead to parallel spin alignment.¹¹⁰⁻¹¹² Preliminary results suggest that this concept may work if problems like poor characterization and insufficiently low doping levels can be solved.¹¹³⁻¹¹⁶

2.6.8 Ferromagnetic Molecular Assemblies

The first purely organic ferromagnetic material reported was a single crystal of the stable nitronyl nitroxyl radical **46**. Three different crystal phases have been recognized, all showing ferromagnetic intermolecular interactions.¹¹⁷⁻¹¹⁹ In two crystal packings, the β -phase and the γ -phase, ferromagnetic transitions to long-range spin ordered states were observed at 0.60 K and 0.65 K, respectively.¹²⁰⁻¹²² The spin-coupling is, therefore, attributed to interaction between the SOMO, and the HOMO and/or LUMO. Several slightly different nitronyl nitroxyl radicals, which display ferromagnetic behavior to some extent in the crystalline state, have been reported.¹²³⁻¹²⁷ It appears that molecular stacks are formed in the crystal structure with relatively strong ferromagnetic interaction between the molecules within the stacks. Interaction between the stacks, however, is extremely weak and in some cases even antiferromagnetic. For crystalline samples of TEMPO radicals **47**, ferromagnetic transitions have been observed as well, but the Curie temperatures of 0.18 and 0.4 K are extremely low.



Compound **48** is a stable diradical which possesses a triplet ground state.^{128,129} This intramolecular ferromagnetic spin alignment is due to the perpendicular arrangement of the two nitroxyl moieties, which results in two orthogonal NBMOs. In the crystalline state, cooperative magnetic interactions occur. Studies reveal a positive Weiss constant $\theta = +10$ K and magnetization behavior of a $S = 6$ spin system. A ferromagnetic transition is observed at 1.48 K. Below this temperature spontaneous magnetization occurs.

The highest Curie temperature for a purely organic material has been reported for a charge-transfer complex between C₆₀ and tetrakis(dimethylamino)ethylene (TDAE) **49**.^{130,131} At 16 K a ferromagnetic transition occurs as evidenced by a sudden increase of the magnetization. The exact nature of the ferromagnetic interactions is still unclear.

2.7 Analytical Methods

Various methods can be applied to characterize the magnetic behavior of multi-spin systems.^{4,5} ESR spectroscopy is the most versatile technique to gain insight into the molecular magnetic properties, and can be used to determine spin states of paramagnetic species. Additional information, especially about intermolecular interactions can be obtained by magnetization and magnetic susceptibility measurements.¹³² In this paragraph, a short introduction into these techniques is given.

2.7.1 ESR Spectroscopy

To examine intramolecular spin-spin interactions, ESR spectroscopy is the most versatile spectroscopic technique available. In (frozen) solution, molecularly dissolved species can be studied, in absence of intermolecular interactions between the spins. Information about the localization of and distance between the unpaired electrons can be obtained.

In absence of hyperfine splitting, the spin Hamiltonian for a $S = 1/2$ molecule only contains the electron Zeeman term. If a molecule contains more than one unpaired electron, this Hamiltonian has to be extended with a term taking into account the spin-spin interactions:¹³³

$$\hat{H} = g\mu_B H \hat{S} + \hat{S} \mathbf{D} \hat{S} \quad (8)$$

In this expression g is the g factor, μ_B is the Bohr magneton, and H is the magnetic field. The spin-spin term, $\hat{S} \mathbf{D} \hat{S}$, leads to further splitting of the energy levels and therefore to additional spectral transitions. Spin-spin interactions occur regardless of the application of a magnetic field, so the effects on the energy levels are called zero-field splitting. \mathbf{D} is a tensor which can be diagonalized, leading to a new expression for the spin-spin term (equation 9). X , Y and Z are the eigenvalues of \mathbf{D} in the direction of the three principal axes. Because \mathbf{D} is a traceless tensor, these three principal values can be reduced to two, which have been denoted as D and E . Introduction of $D (= -3/2 Z)$ and $E (= -1/2 (X - Y))$ leads to equation 10 for the Hamiltonian.

$$\hat{S} \mathbf{D} \hat{S} = -X \hat{S}_x^2 - Y \hat{S}_y^2 - Z \hat{S}_z^2 \quad (9)$$

$$\begin{aligned} \hat{H} &= \mu_B H g \hat{S} + D(\hat{S}_z^2 - 1/3 \hat{S}^2) + E(\hat{S}_x^2 - \hat{S}_y^2) \\ &= \mu_B H g \hat{S} + D(\hat{S}_z^2 - 1/3 S(S+1)) + E(\hat{S}_x^2 - \hat{S}_y^2) \end{aligned} \quad (10)$$

The signs of D and E depend on which axis is chosen as Z . Both can either be positive or

negative. Usually, the absolute signs are unknown since the spectral transitions only depend on their relative signs. Therefore, D and E are often given as absolute magnitudes. Two different interactions contribute to the spin Hamiltonian: spin-spin and spin-orbit coupling. In organic molecules, the latter is negligible so that D and E are determined by the magnetic dipole-dipole interaction (equation 11). Using this expression an estimate of the distance between the interacting electrons can be made.¹³⁴

$$D = -\left(\frac{3\mu_0}{8\pi h}\right) 10^{24} g^2 \mu_B^2 \langle d^{-3} \rangle \quad (D \text{ in MHz, } d \text{ in \AA}) \quad (11)$$

(μ_0 = vacuum permeability;
 h = Planck's constant)

The energy gap between spin sub levels, and consequently the ESR transition energies are small (an X-band ESR spectrometer operates at ca. 9.3 GHz, which corresponds to an energy of ca. $6.2 \cdot 10^{-24}$ J). The population of the upper spin levels can therefore not be neglected at temperatures above 0 K, which leads to a temperature dependent ESR signal intensity. This behavior is described by the Curie law, a Boltzmann-like relation in which $\exp(\Delta W/kT)$ is reduced to $\Delta W/kT$. The Curie law states that the difference in population between lower and higher spin levels, and consequently the ESR signal intensity I , is linearly proportional to the inverse of the absolute temperature:

$$I = \frac{C}{T} \quad (12)$$

Variable temperature ESR measurements are often used to assess the ground state of high-spin molecules. If the intensity of an ESR signal of a certain spin state increases linearly with $1/T$, this indicates that no thermal population or depopulation of this state occurs. This can be interpreted in two ways. First, this spin state is the ground state and separated from other states by a substantial energy gap, of at least the thermal energy kT . On the other hand it is also possible that the different states are exactly degenerate.¹³⁵

When the energy gap between different spin states is small, the magnitude of this gap can be determined. If we consider the equilibration of a triplet with a thermally accessible singlet state, the signal intensity of the triplet does not only depend on the distribution over the spin states (as described by Curie's law), but also on the distribution over S and T. Combination of these two distributions leads to a Bleaney-Bowers-type equation:¹³⁶

$$I = \frac{C'}{T} \frac{1}{3 + \exp(-2J/kT)} \quad (13)$$

C' is an arbitrary constant, and $2J$ is the energy difference, ΔE_{ST} , between singlet and triplet. By fitting the experimental values to equation 13 the magnitude of the energy gap can be estimated. Similar equations can be derived to describe the equilibration of other sets of spin states.^{137, 138}

2.7.2 Magnetization and Magnetic Susceptibility

Paramagnetism is a bulk property of materials made up of molecules with randomly oriented spins in absence of spontaneous magnetization. Upon application of a strong magnetic field at low temperatures the spins may order. The maximal possible magnetization M_{sat} is given by:

$$M_{sat} = Nm = NgS\mu_B \quad (14)$$

N is the number of magnetic dipoles of moment m per unit of volume, S is the spin quantum number of total angular momentum and μ_B is the Bohr magneton. Because of the thermal agitation of the spins at $T > 0$ K, their directions with respect to the magnetic field also fluctuate. The alignment of the spins and consequently the magnetization, is dictated by Boltzmann distributions for all spin sub levels ($S_z = -S, -(S-1), \dots, (S-1), S$), analytically described by the Brillouin function $B(\alpha)$:

$$M = Ng\mu_B B(\alpha) \quad (15)$$

with

$$\alpha = \frac{gS\mu_B H}{kT}$$

and

$$B(\alpha) = \frac{2J+1}{2J} \operatorname{ctnh}\left(\frac{(2J+1)\alpha}{2J}\right) - \frac{1}{2J} \operatorname{ctnh}\left(\frac{\alpha}{2J}\right)$$

The relative magnetization can be plotted against the ratio of magnetic field and temperature (M/M_{sat} vs. H/T). Comparison of experimental results with the theoretical curves based on the Brillouin functions of different S gives insight into the spin state of the species present. Furthermore, this method can be used to estimate the average spin number of inhomogeneous samples.

At high temperatures and/or low magnetic field, M becomes linearly proportional to H/T . Consequently, the paramagnetic susceptibility $\chi (M/H)$ becomes inversely proportional to the temperature T :

$$\chi = \frac{M}{H} = \frac{NgS\mu_B B(\alpha)}{H} \quad (16)$$

for $H/T \ll 1$:

$$B(\alpha) = \frac{g\mu_B HS(S+1)}{3kT} \quad (17)$$

$$\chi = \frac{Ng^2\mu_B^2 S(S+1)}{3kT} = \frac{C}{T} \quad (18)$$

This relation is the exact expression of Curie's law, and the Curie constant C has fixed values for the different spin states, e.g. for $S = \frac{1}{2}$ C has a value of 0.37 K emu/mol and for $S = 1$ $C = 1.0$ K emu/mol. So, in addition to ESR spectroscopy, magnetization measurements can also be used to assess the ground states of high-spin species.

The above statements only apply to assemblies of independent spin systems. Any deviation suggests occurrence of cooperative magnetic phenomena, i.e. intermolecular ferro-, antiferro-, or ferrimagnetic interactions. In that case, the susceptibility at temperatures above the spin ordering temperature T_C is described by the Curie-Weiss law:

$$\chi = \frac{1}{(T - \theta)} \quad (19)$$

The Weiss temperature θ can be either positive or negative, indicating ferromagnetic or antiferromagnetic interactions between the molecules, respectively (Figure 2.9).

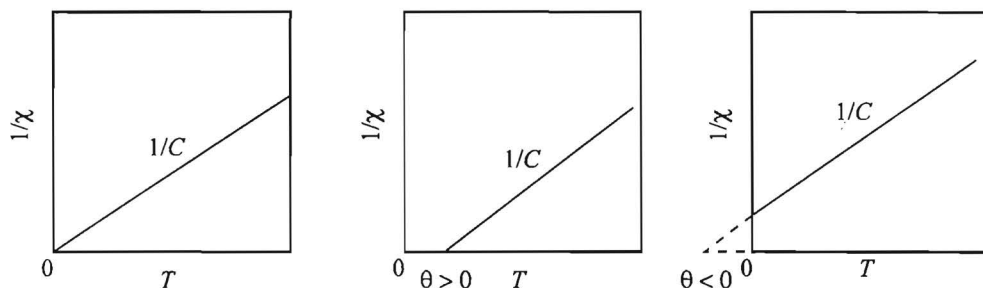


Figure 2.9. Schematic representation of the temperature dependence of the susceptibility of a paramagnetic species. (left): without intermolecular spin-spin coupling. (center): with cooperative ferromagnetic interactions. (right): with cooperative antiferromagnetic interactions.

2.8 Concluding Remarks

Summarizing, two components are necessary for the construction of high-spin molecules: spin-carrying units that provide unpaired electrons and ferromagnetic coupling units that afford a parallel orientation of the corresponding electron spins. Understanding of the mechanisms that govern the intramolecular spin-spin interactions has provided some very effective coupling units. By combination with different organic radicals, various high-spin systems have already been prepared. All known systems, however, are restricted by poor stability of the radical sites, or by weak spin-spin interactions, due to limited spin density at the coupling units. Therefore, intensive research is aimed at the development of new spin-carrying units that can be incorporated in high-spin molecules.

It must be kept in mind, however, that high-spin molecules do not necessarily afford ferromagnetic materials. In order to obtain actual ferromagnetic behavior, a very large number of spins has to be aligned. Therefore, spin coupling between the individual magnetic molecules must also be achieved.

2.9 References

- 1 Magnetic Molecular Materials; Gatteschi, D., Kahn, O., Miller, J. S., Palacio, F., Eds; Kluwer Academic Publishers: Dordrecht, The Netherlands, 1991.
- 2 Chemistry and Physics of Molecular Based Magnetic Materials. Molecular Crystals and Liquid Crystals; Iwamura, H., Miller, J. S., Eds.; Gordon and Breach Publishers: New York, 1993; Vol. 232, pp 1-360.
- 3 Miller, J. S.; Epstein, A. J. *Angew. Chem., Int. Ed. Engl.* **1994**, *33*, 385.
- 4 Rajca, A. *Chem. Rev.* **1994**, *94*, 871.
- 5 Iwamura, H. *Adv. Phys. Org. Chem.* **1990**, *26*, 179.
- 6 Iwamura, H.; Koga, N. *Acc. Chem. Res.* **1993**, *26*, 346.
- 7 Kollmar, C.; Kahn, O. *Acc. Chem. Res.* **1993**, *26*, 259.
- 8 Coulson, C. A.; Longuet-Higgins, H. C. *Proc. R. Soc., Ser A* **1947**, *191*, 39.
- 9 Coulson, C. A.; Rushbrooke, G. S. *Proc. Cambridge Phil. Soc.* **1940**, *36*, 193.
- 10 Longuet-Higgins, H. C. *J. Chem. Phys.* **1950**, *18*, 265.
- 11 Borden, W. T.; Davidson, E. R. *J. Am. Chem. Soc.* **1977**, *99*, 4587.
- 12 Dowd, P. J. *J. Am. Chem. Soc.* **1970**, *92*, 1066.
- 13 Dowd, P. J.; Chang, W.; Paik, Y. H. *J. Am. Chem. Soc.* **1986**, *108*, 7416.
- 14 Nachtigall, P.; Jordan, K. D. *J. Am. Chem. Soc.* **1993**, *115*, 270.
- 15 Snyder, G. J.; Dougherty, D. A. *J. Am. Chem. Soc.* **1989**, *111*, 3927.
- 16 Dewar, M. J. S. *The Molecular Orbital Theory of Organic Chemistry*; McGraw-Hill: New York, 1969; p 232.
- 17 Ovchinnikov, A. A. *Theor. Chim. Acta* **1978**, *47*, 297.

- 18 Klein, D. J. *J. Chem. Phys.* **1982**, *77*, 3098.
- 19 Matsumoto, T.; Ishida, T.; Koga, N.; Iwamura, H. *J. Am. Chem. Soc.* **1992**, *114*, 9952.
- 20 Ling, C.; Minato, M.; Lahti, P. M.; van Willigen, H. *J. Am. Chem. Soc.* **1992**, *114*, 9959.
- 21 McConnell, H. M. *J. Chem. Phys.* **1963**, *39*, 1910.
- 22 Kollmar, C.; Kahn, O. *J. Chem. Phys.* **1993**, *98*, 453.
- 23 Buchachenko, A. L. *Russ. Chem. Rev.* **1990**, *59*, 307.
- 24 Yamaguchi, K.; Fukui, H.; Fueno, T. *Chem. Lett.* **1986**, 625.
- 25 Yamaguchi, K.; Fueno, T.; Nakasuji, K.; Murata, I. *Chem. Lett.* **1986**, 629.
- 26 Yamaguchi, K.; Namimoto, H.; Fueno, T. *Mol. Cryst. Liq. Cryst.* **1989**, *176*, 151.
- 27 McConnell, H. M. *Proc. R. A. Welch Found. Conf. Chem. Res.* **1967**, *11*, 144.
- 28 It was shown later on that this model gives an oversimplified picture, and may not be of the general validity as assumed initially. See: Kollmar, C.; Kahn, O. *J. Am. Chem. Soc.* **1991**, *113*, 7987.
- 29 Breslow, R. *Pure Appl. Chem.* **1982**, *54*, 927.
- 30 Breslow, R.; Juan, B.; Klutz, R. Q.; Xia, C. Z. *Tetrahedron* **1982**, *38*, 863.
- 31 Torrence, J. B.; Oostra, S.; Nazzari, A. *Synth. Met.* **1987**, *19*, 709.
- 32 Dormann, E.; Nowak, M. J.; Williams, K. A.; Angus, R. O. Jr.; Wudl, F. *J. Am. Chem. Soc.* **1987**, *109*, 2594.
- 33 Itoh, K. *Chem. Phys. Lett.* **1967**, *1*, 235.
- 34 Wasserman, E.; Murray, R. W.; Yager, W. A.; Trozzolo, A. M.; Smolinsky, G. *J. Am. Chem. Soc.* **1967**, *89*, 5076.
- 35 Iwamura, H. *Pure Appl. Chem.* **1986**, *58*, 187.
- 36 Iwamura, H. *Pure Appl. Chem.* **1987**, *59*, 1595.
- 37 Mataga, N. *Theoret. Chim. Acta* **1968**, *10*, 372.
- 38 Alexander, S. A.; Klein, D. J. *J. Am. Chem. Soc.* **1988**, *110*, 3401.
- 39 Teki, Y.; Takui, T.; Kinoshita, T.; Yagi, H.; Itoh, K.; Iwamura, H. *J. Chem. Phys.* **1985**, *83*, 539.
- 40 Teki, Y.; Takui, T.; Kinoshita, T.; Ichikawa, S.; Yagi, H.; Itoh, K. *Chem. Phys. Lett.* **1987**, *141*, 201.
- 41 Teki, Y.; Takui, T.; Itoh, K.; Iwamura, H.; Kobayashi, K. *J. Am. Chem. Soc.* **1983**, *105*, 3722.
- 42 Sugawara, T.; Bandow, S.; Kimura, K.; Iwamura, H.; Itoh, K. *J. Am. Chem. Soc.* **1984**, *106*, 6449.
- 43 Sugawara, T.; Bandow, S.; Kimura, K.; Iwamura, H.; Itoh, K. *J. Am. Chem. Soc.* **1986**, *108*, 368.
- 44 Teki, Y.; Takui, T.; Itoh, K.; Iwamura, H.; Kobayashi, K. *J. Am. Chem. Soc.* **1986**, *108*, 2147.
- 45 Fujita, I.; Teki, Y.; Takui, T.; Kinoshita, T.; Itoh, K.; Miko, F.; Sawaki, Y.; Iwamura, H.; Izuoka, A.; Sugawara, T. *J. Am. Chem. Soc.* **1990**, *112*, 4074.
- 46 Nakamura, N.; Inoue, K.; Iwamura, H.; Fujioka, T.; Sawaki, Y. *J. Am. Chem. Soc.* **1992**, *114*, 1484.
- 47 Nakamura, N.; Inoue, K.; Iwamura, H. *Angew. Chem., Int. Ed. Engl.* **1993**, *32*, 872.
- 48 Matsuda, K.; Nakamura, N.; Inoue, K.; Koga, N.; Iwamura, H. *Chem. Eur. J.* **1996**, *2*, 259.
- 49 Matsuda, K.; Nakamura, N.; Inoue, K.; Koga, N.; Iwamura, H. *Bull. Chem. Soc. Jpn.* **1996**, *69*, 1483.
- 50 Izuoka, A.; Murata, S.; Sugawara, T.; Iwamura, H. *J. Am. Chem. Soc.* **1985**, *107*, 1786.
- 51 Izuoka, A.; Murata, S.; Sugawara, T.; Iwamura, H. *J. Am. Chem. Soc.* **1987**, *109*, 2631.
- 52 Leo, M. *Ber.* **1937**, *70*, 1691.

- 53 Schlenk, W.; Brauns, M. *Ber.* **1915**, *48*, 661.
- 54 Luckhurst, G. R.; Pedulli, G. F.; Tiecco, M. *J. Chem. Soc. (B)* **1971**, 329.
- 55 Rajca, A. *J. Am. Chem. Soc.* **1990**, *112*, 5892.
- 56 Rajca, A.; Utamapanya, S.; Thayumanavan, S. *J. Am. Chem. Soc.* **1992**, *114*, 1884.
- 57 Rajca, A.; Utamapanya, S. *J. Am. Chem. Soc.* **1993**, *115*, 2396.
- 58 Utamapanya, S.; Kakegawa, H.; Bryant, L.; Rajca, A. *Chem. Mater.* **1993**, *5*, 1053.
- 59 Rajca, A.; Utamapanya, S. *J. Am. Chem. Soc.* **1993**, *115*, 10688.
- 60 Rajca, A. *Adv. Mater.* **1994**, *6*, 605.
- 61 Raica, A.; Rajca, S.; Padmakumar, R. *Angew. Chem.* **1994**, *106*, 2193.
- 62 Rajca, A.; Rajca, S.; Desai, S. *J. Am. Chem. Soc.* **1995**, *117*, 806.
- 63 Veciana, J.; Rovira, C.; Crespo, M. I.; Armet, O.; Domingo, V. M.; Palacio, F. *J. Am. Chem. Soc.* **1991**, *113*, 2552.
- 64 Veciana, J.; Rovira, C.; Ventosa, N.; Crespo, M. I.; Palacio, F. *J. Am. Chem. Soc.* **1993**, *115*, 57.
- 65 Ventosa, N.; Ruiz, D.; Rovira, C.; Veciana, J. *Mol. Cryst. Liq. Cryst.* **1993**, *232*, 333.
- 66 Berson, J. A. *Acc. Chem. Res.* **1978**, *11*, 446.
- 67 Jacobs, S. J.; Shultz, D. A.; Jain, R.; Novak, J.; Dougherty, D. A. *J. Am. Chem. Soc.* **1993**, *115*, 1744.
- 68 Siverman, S. K.; Dougherty, D. A.; *J. Phys. Chem.* **1993**, *97*, 13273.
- 69 Dougherty, D. A. *Acc. Chem. Res.* **1991**, *24*, 88.
- 70 Novak, J. A.; Jain, R.; Dougherty, D. A. *J. Am. Chem. Soc.* **1989**, *111*, 7618.
- 71 Calder, A.; Forrester, R.; James, P. G.; Luckhurst, G. R. *J. Am. Chem. Soc.* **1969**, *91*, 3724.
- 72 Rassat, A.; Sieveking, H. U. *Angew. Chem.* **1972**, *84*, 353.
- 73 Ishida, T.; Iwamura, H. *J. Am. Chem. Soc.* **1991**, *113*, 4238.
- 74 Kanno, F.; Inoue, K.; Koga, N.; Iwamura, H. *J. Phys. Chem.* **1993**, *97*, 13267.
- 75 Fujita, J.; Tanaka, Suemune, H.; Koga, N.; Matsuda, K.; Iwamura, H. *J. Am. Chem. Soc.* **1996**, *118*, 9347.
- 76 Kanno, F.; Inoue, K.; Koga, N.; Iwamura, H. *J. Am. Chem. Soc.* **1993**, *115*, 847.
- 77 Dvolaitzky, M.; Chiarelli, R.; Rassat, A. *Angew. Chem.* **1992**, *104*, 220.
- 78 Yoshioka, N.; Lahti, P. M.; Kaneko, T.; Kuzumaki, Y.; Tsuchida, E.; Nishide, H. *J. Org. Chem.* **1994**, *59*, 4272.
- 79 Kaneko, T.; Toriu, S.; Nishide, H.; Yamaki, D.; Maruta, G.; Yamaguchi, K. *Chem. Lett.* **1995**, 421.
- 80 Sasaki, S.; Iwamura, H. *Chem. Lett.* **1992**, 1759.
- 81 Ichimura, A. S.; Ochiai, K.; Koga, N.; Iwamura, H. *J. Org. Chem.* **1994**, *59*, 1970.
- 82 Tukada, H.; *J. Chem. Soc., Chem. Commun.* **1994**, 2293.
- 83 Müllen, K.; Baumgarten, M.; Tyutyulkov, N.; Karabunarliev, S. *Synth. Met.* **1991**, *40*, 127.
- 84 Müller, U.; Baumgarten, M. *J. Am. Chem. Soc.* **1995**, *117*, 5840.
- 85 Okada, K.; Imakura, T.; Oda, M.; Murai, H.; Baumgarten, M. *J. Am. Chem. Soc.* **1996**, *118*, 3047.
- 86 Yoshizawa, K.; Ito, A.; Tanaka, K.; Yamabe, T. *Synth. Met.* **1994**, *66*, 81.
- 87 Yoshizawa, K.; Hatanak, M.; Ago, H.; Tanaka, K.; Yamabe, T. *Bull. Chem. Soc. Jpn.* **1996**, *69*, 1417.
- 88 Stickley, K. R.; Blackstock, S. C. *J. Am. Chem. Soc.* **1994**, *116*, 11576.
- 89 Sasaki, S.; Iyoda, M. *Chem. Lett.* **1995**, 1011.

- 90 Ito, A.; Saito, T.; Tanaka, K.; Yamabe, T. *Tetrahedron Lett.* **1995**, *48*, 8890.
- 91 Kamachi, M.; Tamaki, M.; Morishima, Y.; Nozakura, S.; Mori, W.; Kishita, M. *Polymer J.* **1982**, *14*, 363.
- 92 Vlietstra, E. J.; Nolte, R. J. M.; Zwikker, J. W.; Drenth, W.; Meijer, E. W. *Macromolecules*, **1990**, *23*, 946.
- 93 Abdelkader, M.; Drenth, W.; Meijer, E. W. *Chem. Mater.* **1991**, *3*, 598.
- 94 Korshak, Yu. V.; Ovchinnikov, A. A.; Medvedeva, T. V.; Shapiro, A. M.; Spector, V. N. *Pisma Zh. Eksp. Teor. Fiz.* **1986**, *43*, 309.
- 95 Korshak, Yu. V.; Medvedeva, T. V.; Ovchinnikov, A. A.; Spector, V. N. *Nature* **1987**, 326, 370.
- 96 Ovchinnikov, A. A.; Spector, V. N. *Synth. Met.* **1988**, *27*, B615.
- 97 Miller, J. S.; Glatzhofer, D. T.; Laversanne, R.; Chittipeddi, S.; Vaca, P.; Brill, T. B.; Timken, M. D.; O'Conner, C. J.; Zhang, J. H.; Calabrese, J. C.; Epstein, A. J. *Chem. Mater.* **1990**, *2*, 60.
- 98 Zhang, J. H.; Epstein, A. J.; Miller, J. S.; O'Conner, C. J. *Mol. Cryst. Liq. Cryst.* **1989**, *176*, 271.
- 99 Inoue, K.; Koga, N. Iwamura, H. *J. Am. Chem. Soc.* **1991**, *113*, 9803.
- 100 Nishide, H.; Yoshioka, N.; Inagaki, K.; Tsuchida, E. *Macromolecules* **1990**, *23*, 4487.
- 101 Nishide, H.; Yoshioka, N.; Inagaki, K.; Kaku, T.; Tsuchida, E. *Macromolecules* **1992**, *25*, 569.
- 102 Nishide, H.; Yoshioka, N.; Kaneko, T.; Tsuchida, E. *Macromolecules* **1988**, *21*, 3119.
- 103 Yoshioka, N.; Nishide, H.; Kaneko, T.; Yoshiki, H.; Tsuchida, E. *Macromolecules* **1992**, *23*, 3838.
- 104 Fujii, A.; Ishida, T.; Koga, N.; Iwamura, H. *Macromolecules* **1991**, *24*, 1077.
- 105 Miura, Y.; Matsumoto, M.; Ushitani, Y.; Teki, Y.; Takui, T.; Itoh, K. *J. Macromolecules*, **1993**, *26*, 6673.
- 106 Nishide, H.; Kaneko, T.; Nii, T.; Katoh, K.; Tsuchida, E.; Yamaguchi, K. *J. Am. Chem. Soc.* **1995**, *117*, 548.
- 107 Nishide, H. *Adv. Mater.* **1995**, *7*, 937.
- 108 Nishide, H.; Kaneko, T.; Nii, T.; Katoh, K.; Tsuchida, E.; Lahti, P. M. *J. Am. Chem. Soc.* **1996**, *118*, 9695.
- 109 Nishide, H.; Kaneko, T.; Toriu, S.; Kuzumaki, Y.; Tsuchida, E. *Bull. Chem. Soc. Jpn.* **1996**, *69*, 499.
- 110 Fukutome, H.; Takahashi, I.; Ozaki, M. *Chem. Phys. Lett.* **1987**, *133*, 34.
- 111 Kaisaki, D. A.; Chang, W.; Dougherty, D. A. *J. Am. Chem. Soc.* **1991**, *113*, 2764.
- 112 Tanaka, K.; Ago, H.; Yamabe, T. *Synth. Met.* **1995**, *72*, 225.
- 113 Torrence, J. B.; Oostra, S.; Nazzari, A. *Synth. Met.* **1987**, *19*, 709.
- 114 Yoshizawa, K.; Tanaka, K.; Yamabe, T.; Yamauchi, J. *J. Chem. Phys.* **1992**, *96*, 5516.
- 115 Murray, M. M.; Kaszynski, P.; Kaisaki, D. A.; Chang, W.; Dougherty, D. A. *J. Am. Chem. Soc.* **1994**, *116*, 8152.
- 116 Bushby, R. J.; Ng, K. M. *Chem. Commun.* **1996**, 659.
- 117 Awaga, K.; Maruyama, Y. *Chem. Phys. Lett.* **1989**, *158*, 556.
- 118 Awaga, K.; Inabe, T.; Nagashima, U.; Maruyama, Y. *J. Chem. Soc., Chem. Commun.* **1989**, 1617.
- 119 Allemand, P. -M.; Fite, C.; Srdanov, G.; Keder, N.; Wudl, F. *Synth. Met.* **1991**, *41-43*, 3291.
- 120 Tamura, M.; Nakazawa, Y.; Shiomi, D.; Nozawa, K.; Hosokoshi, Y.; Ishikawa, M.; Takahashi, M.; Kinoshita, M. *Chem. Phys. Lett.* **1991**, *186*, 401.

- 121 Takahashi, M.; Turek, P.; Nakazawa, Y.; Tamura, M.; Nozawa, K.; Shiomi, D.; Ishikawa, M.; Kinoshita, M. *Phys. Rev. Lett.* **1991**, *67*, 746.
- 122 Kinoshita, M.; Turek, P.; Tamura, M.; Nozawa, K.; Shiomi, D.; Nakazawa, Y.; Ishikawa, M.; Takahashi, M.; Awaga, K.; Inabe, T.; Maruyama, Y. *Chem. Lett.* **1991**, 1225.
- 123 Cerujeda, J.; Mas, M.; Molins, E.; Lanfranc de Panthou, F.; Laugier, J.; Park, J. G.; Paulsen, C.; Rey, P.; Povira, C.; Veciana, J. *J. Chem. Soc., Chem. Commun.* **1995**, 709.
- 124 Hernández, E.; Mas, M.; Molins, M.; Rovira, C.; Veciana J. *Angew. Chem., Int. Ed. Engl.* **1993**, *32*, 882.
- 125 Lang, A.; Pei, Y.; Ouahab, L.; Kahn, O. *Adv. Mater.* **1996**, *8*, 60.
- 126 Hosokoshi, Y.; Tamura, M.; Kinoshita, M.; Sawa, H.; Kato, H.; Fujiwara, Y.; Ueda, Y. *J. Mater. Chem.* **1995**, *4*, 1219.
- 127 Okuno, T.; Otsuka, T.; Awaga, K. *J. Chem. Soc., Chem. Commun.* **1995**, 827.
- 128 Chiarelli, R.; Rassat, A.; Rey, P. *J. Chem. Soc., Chem. Commun.* **1992**, 1081.
- 129 Chiarelli, R.; Novak, M. A.; Rassat, A.; Tholence, J. L. *Nature* **1993**, *363*, 147.
- 130 Allemand, P. -M.; Khemani, K. C.; Koch, A.; Wudl, F.; Holczer, K.; Donovan, S.; Grüner, G.; Thompson, J. D. *Science* **1991**, *253*, 301.
- 131 Stephens, P. W.; Cox, D.; Jauher, J. W.; Mihaly, L.; Wiley, J. B.; Allemand, P. -M.; Hirsch, A.; Holczer, K.; Li, Q.; Thompson, J. D.; Wudl, F. *Nature* **1992**, *355*, 331.
- 132 Iwamura, H.; Koga, N. *Acc. Chem. Res.* **1993**, *23*, 346.
- 133 Wertz J. E.; Bolton, J. R. *Electron Spin Resonance Elementary Theory and Practical Applications* McGraw-Hill: New York, 1972; p 224.
- 134 Weil, J. A.; Bolton, J. R.; Wertz, J. E. *Electron Paramagnetic Resonance, Elementary Theory and Practical Applications* John Wiley & Sons, New York, 1993; p 179.
- 135 Berson, J. A. In *The Chemistry of Quinoid Compounds*; Patai, S., Rappaport, Z., Eds.; Wiley: 1988; Vol II, Chapter10.
- 136 Bleany, B.; Bowers, D.K. *Proc. R. Soc. London A* **1952**, *214*, 451.
- 137 Murata, S.; Iwamura, H. *J. Am. Chem. Soc.* **1991**, *113*, 5547.
- 138 Ishida, T.; Iwamura, H. *J. Am. Chem. Soc.* **1991**, *113*, 4238.

Chapter 3

Triplet-State Phosphinyl Diradicals

Abstract

The first example of a triplet-state phosphinyl diradical is reported. Photoinduced dissociative electron capture of a meta-phenylene-bis(phosphonous chloride) in a glassy toluene matrix at 110 K using an electron rich olefin, affords the corresponding phosphinyl monoradicals and triplet-state diradicals in a 5:4 ratio. The triplet state ESR spectrum gives zero-field splitting parameters of $D = 260$ MHz, $E \approx 0$ MHz, and $\beta = 90^\circ$. Variable temperature ESR experiments reveal Curie behavior for the $\Delta M_S = \pm 1$ and $\Delta M_S = \pm 2$ ESR signals between 3.8 and 100 K, consistent with a low-energy triplet state that either corresponds to the ground state or is degenerate with a singlet state.

3.1 Introduction

Intramolecular ferromagnetic interaction within di-, oligo-, and polyradicals attracts considerable attention for the design of high-spin organic molecules and molecular ferromagnets.¹⁻⁶ Taking advantage of the topological symmetry and the in-phase periodicity of spin polarization in alternant hydrocarbons, various high-spin molecules have been designed and characterized (see Chapter 2). One particularly successful strategy to construct high-spin molecules is by coupling π - and σ - open-shell centers by a ferromagnetic coupling unit like *m*-phenylene. Although this strategy has been used successfully to align the electron spins of various carbon⁷⁻¹⁰ and nitrogen-centered radicals,¹¹⁻¹³ the use of other central atoms as radical centers has received less attention.¹⁴ The possibility of incorporating heavy elements such as silicon or germanium has recently been suggested,⁶ but experimental examples have not been described so far.

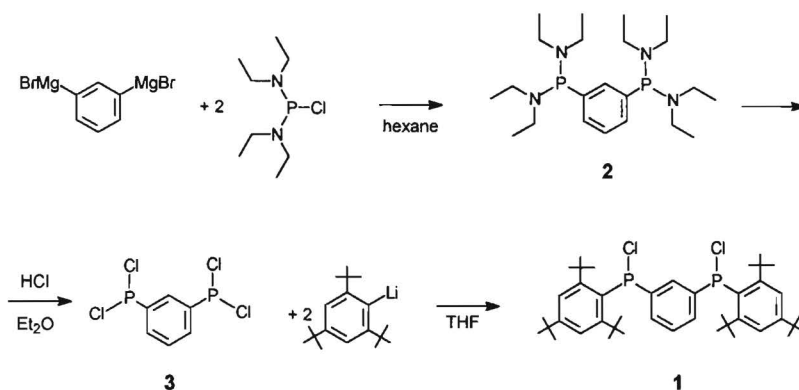
In this chapter, the formation of a novel phosphorus-centered diradical **1**^{2*} is described, in which two phosphinyl radicals (R_2P^\bullet) are coupled via a *m*-phenylene unit. It is expected that

the reduced overlap of the phosphorus valence 3p orbital with the 2p- π -*m*-phenylene orbitals is not beneficial for a high-spin ground state in a phosphinyl diradical. On the other hand, *m*-phenylene is known to be a fairly robust ferromagnetic coupling unit, even for significantly twisted geometries.^{9,10,15} In view of these conflicting arguments, one can speculate on the possibility of achieving a high-spin ground state for phosphinyl diradicals.

The diradicals are obtained in situ from a sterically hindered *m*-phenylene-bis(phosphonous chloride) precursor **1** in the presence of an electron rich olefin (ero) at 110 K via a photoinduced process. In this reaction, UV irradiation of ero in a toluene glass at low temperature produces free electrons which are reactive towards the P-Cl bonds.¹⁶⁻¹⁹ After electron capture, the resulting transient anion radical (with a σ^* three-electron P-Cl bond) dissociates into a phosphinyl radical (R_2P^\bullet) and a chloride anion.

3.2 Synthesis

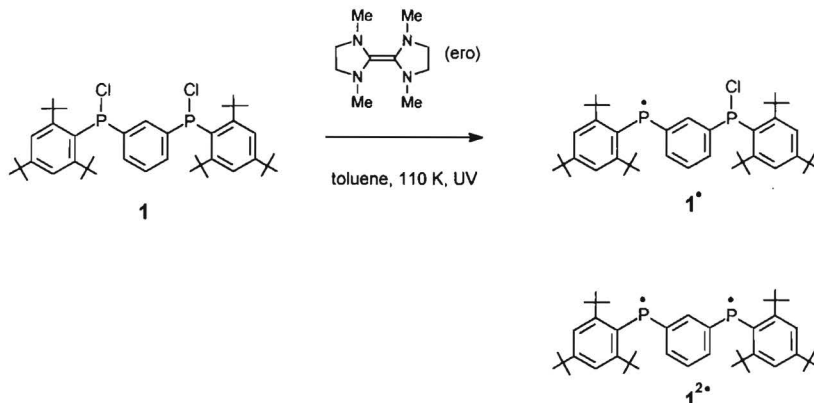
The precursor *P,P'*-bis(2,4,6-tri-*t*-butylphenyl)-1,3-phenylenebis(phosphonous chloride) **1** was prepared starting from 1,3-dibromobenzene (Scheme 3.1). Conversion of the latter to the di-Grignard compound and reaction with tetraethylphosphorodiamidous chloride afforded the tetraamino compound **2**. Reaction with hydrogen chloride in diethyl ether yielded 1,3-phenylene-bis(phosphonous dichloride) **3**. Finally, the bis(phosphonous chloride) precursor **1** was obtained by coupling **3** with two equivalents of 2,4,6-tri-*t*-butylphenyllithium at low temperature in tetrahydrofuran. Characterization using ¹H and ³¹P NMR spectroscopy revealed that the phosphorus atoms are stereocenters, affording **1** as a mixture of *meso* (RS) and *racemic* (RR and SS) diastereoisomers.



Scheme 3.1. Synthesis of bis(phosphonous chloride) precursor.

3.3 ESR Spectroscopy

Phosphinyl radicals are prepared via a dissociative electron-capture reaction of the P-Cl bond (Scheme 3.2). Free electrons are provided by an electron-rich olefin (ero), which is readily oxidized upon UV irradiation, yielding reactive free electrons. In this study a mixture of the appropriate phosphonous chloride precursor and an excess of ero (1,1',3,3'-tetramethyl-2,2'-bi-imidazolidinylidene)²⁰ is used in a frozen toluene matrix with in situ UV irradiation at cryogenic temperatures.



Scheme 3.2. Structures of *P,P'*-bis(2,4,6-tri-*t*-butylphenyl)-1,3-phenylenebis(phosphonous chloride) **1** and the mono- and diradicals observed after a dissociative electron capture reaction, induced by UV irradiation of ero in a toluene matrix.

The ESR spectrum of a 1:5 mixture of **1** and ero in toluene at 110 K, obtained after UV irradiation for several hours, is a complex superposition of at least three different paramagnetic species (Figure 3.1). The strong central line (partially omitted from the spectrum for clarity) is readily assigned to ero cation radicals and trapped free electrons. The two strong signals (marked **1•**) in the lateral regions of the ESR spectrum are attributed to phosphinyl monoradical **1•** and correspond to the $A_{||}$ components of an axially symmetric ³¹P hyperfine tensor. The remaining lines in the spectrum are the $\Delta M_s = \pm 1$ transitions of phosphinyl diradical **1²•** in a triplet state exhibiting both zero-field splitting and ³¹P hyperfine coupling. Unambiguous evidence for the formation of a high spin state in diradical **1²•** is obtained from the ESR spectrum recorded in the $g = 4$ region where the formally forbidden $\Delta M_s = \pm 2$ transition of **1²•** is observed. The $A_{||}$ component in the wings (marked *) of the $\Delta M_s = \pm 2$ spectrum directly relates these transitions to **1²•**. No appreciable decay of phosphinyl monoradicals **1•** or diradicals **1²•** is observed at 110 K in toluene. Above 130 K, their signals disappear irreversibly from the ESR spectrum.

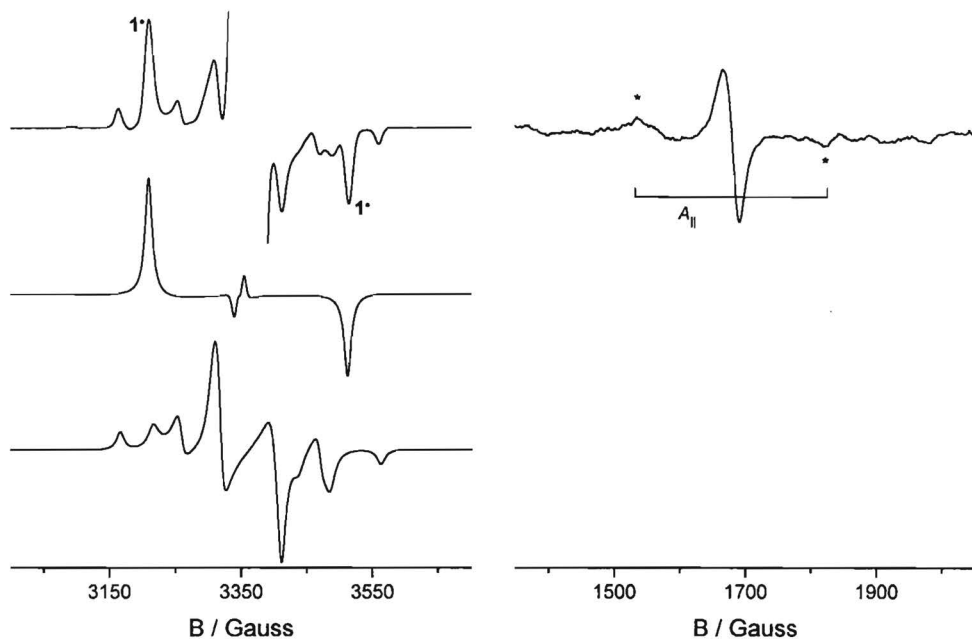


Figure 3.1. ESR spectra of a UV-irradiated mixture of **1** and **ero** in toluene at 110 K. (left, top): Experimental spectrum. (left, center): Simulation of **1**[•]. (left, bottom): Simulation of **1**^{2•}. (right): $\Delta M_s = \pm 2$ transition of experimental spectrum.

The ESR spectrum of monoradical **1**[•] can be simulated using an axially symmetric ³¹P hyperfine coupling tensor with $A_{\parallel} = 850$ MHz and $A_{\perp} = 20$ MHz (Figure 3.1).²¹ The hyperfine coupling tensor of **1**[•] is used to obtain a spectral simulation for **1**^{2•}. The remaining transitions in the ESR spectrum attributed to **1**^{2•} are reproduced very satisfactorily by taking $D = 260$ MHz and $E = 0$ MHz for the zero-field splitting parameters, setting $A_{\parallel} = 425$ MHz and $A_{\perp} = 10$ MHz (half the coupling constants of **1**[•]) for the hyperfine coupling, and using $\beta = 90^\circ$ (Euler angle of D and A_{\parallel}). Double integration and comparison with simulated spectra indicates that the ratio of monoradicals to diradicals is about 5:4.

The zero-field splittings and hyperfine couplings obtained from the spectral simulation can be used to assess the electronic structure of **1**[•] and **1**^{2•} in some detail. From $A_{\parallel} = 850$ MHz and $A_{\perp} = 20$ MHz, the isotropic hyperfine coupling $A_{\text{iso}} = (A_{\parallel} + 2A_{\perp}) / 3 = 297$ MHz and the dipolar hyperfine coupling $2A_{\text{dip}} = A_{\parallel} - A_{\text{iso}} = 553$ MHz can be obtained. These values can be used to approximate the spin density in the phosphorus 3s and 3p orbitals.²² This analysis gives $\rho_{3s} = 0.02$ and $\rho_{3p} = 0.75$, demonstrating that the unpaired electrons are mainly confined to the phosphorus p orbitals. The zero-field splitting of $D = 260$ MHz for **1**^{2•} corresponds within the dipole approximation ($D = 7.8 \times 10^4 d^{-3}$) to a distance d between the radical centers of about 6.7 Å.²³ This approximation is in fair agreement with the distance of 5.5 Å between

the two phosphorus nuclei that has been obtained in the crystallographic X-ray structure of the oxidized form of **1**, as will be discussed in Chapter 4 and in reference 24.

3.4 Determination of the Ground State

The results on phosphinyl diradical **1**^{2•} suggest that spin polarization does occur in the central *m*-phenylene ring, stabilizing a high-spin state. The magnetic interaction within a diradical can be described by the Heisenberg exchange Hamiltonian (see paragraph 2.4.1):

$$\hat{H} = -2 \sum_{i < j} \sum J_{ij} \hat{s}_i \hat{s}_j$$

where $2J$ is the singlet-triplet energy gap. Several techniques have been used to determine J (and hence the multiplicity of the ground state) for di-, oligo- and polyradicals (see paragraph 2.7).^{4,6} Magnetization and magnetic susceptibility measurements cannot be used directly in the present case due to the inhomogeneity of the samples that contain various doublet species in addition to the triplet state diradical of interest. ESR spectroscopy can be used in such a case, but will only give accurate values for J when $|J|$ is in the order of the thermal energy.

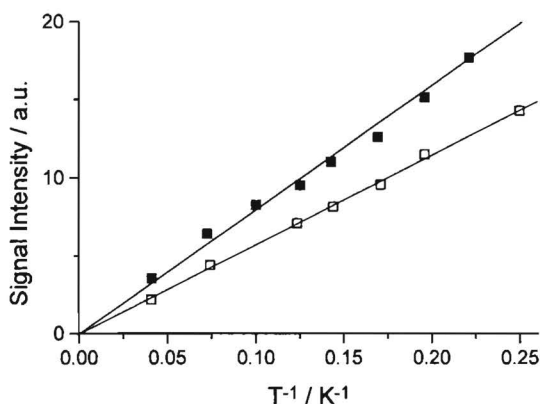


Figure 3.2. Temperature dependence of the ESR signal intensity of the $\Delta M_S = \pm 1$ (■) and $\Delta M_S = \pm 2$ transition (□) of diradical **1**^{2•}. Solid lines are least-square fits to Curie's law.

Variable temperature ESR experiments were carried out in an attempt to assess the ground state multiplicity of diradical **1**^{2•}. The intensity (I) of the $\Delta M_S = \pm 1$ and $\Delta M_S = \pm 2$ signals was measured as function of temperature, between 3.8 and 100 K, with the UV light switched off. Saturation of the ESR signal during variable temperature experiments was avoided by using low microwave powers, well within the range where signal intensity is

proportional to the square root of the microwave power at 4 K.

The temperature dependence of both ESR signals follows Curie's law ($I = C/T$) (Figure 3.2). This thermal behavior is completely reversible in the temperature range examined, indicating that irreversible loss of diradicals is negligible. The fact that Curie behavior is observed has two possible interpretations. Either the high-spin state (triplet) is the ground state and separated from an excited low-spin (singlet) state by a substantial energy gap of a few hundreds of calories per mole, or an extremely small energy gap is present resulting in a (near)degenerate ground state.^{13,25-29} Without additional information, such as magnetization or magnetic susceptibility data, it is not possible to distinguish between either possibility. In principle, a linear variation of the spectral intensity as a function of the reciprocal temperature is also expected when no rapid equilibrium between the various states of different multiplicity occurs. In the present case, however, this criterion is readily met as a result of the relatively high spin-orbit coupling constants of the phosphorus atoms that enhance intersystem crossing rates. Therefore, it can be concluded that the triplet state of diradical 1^{2*} is a low-energy state, either corresponding to the ground state or as part of a degeneracy with a singlet state. This demonstrates the versatility of *m*-phenylene as a ferromagnetic coupling unit, even for phosphorus-centered radicals.

3.5 Conclusion

It is shown that phosphinyl diradical 1^{2*} , coupled via a *m*-phenylene unit, possesses a low-energy triplet state that is either the ground state or degenerate with a singlet state. In combination with the phosphoryl diradicals that will be discussed in Chapter 4, these are the only known examples of molecules in which heavy-atom radical centers are ferromagnetically coupled by a *m*-phenylene unit. The reduced interaction between the unpaired electrons, which is expected for a heavy-atom based radicals, does not rule out ferromagnetic spin coupling. Therefore, this study confirms the effectiveness of *m*-phenylene as ferromagnetic coupling unit. Furthermore, it demonstrates the potential application of second-row atoms as entities for newly designed high-spin molecules.

3.6 Experimental Section

3.6.1 General Methods

Commercial grade reagents were used without further purification. Solvents were purified, dried and degassed following standard procedures. NMR spectra were recorded on a

Bruker AM-400 spectrometer, chemical shifts are given in ppm (δ) relative to TMS for ^1H and ^{13}C -NMR spectra and relative to aqueous 85% H_3PO_4 solution (external standard) for ^{31}P NMR spectra. ESR spectra were recorded on a Bruker ER 200D spectrometer, operating with an X-band standard or TMH cavity, interfaced to a Bruker Aspect 3000 data system. Temperature was controlled by a Bruker ER4111 variable-temperature unit between 100 and 200 K, or by an Oxford 3120 temperature controller combined with an ESR900 continuous flow cryostat in the range 4 - 100 K.

ESR Samples were prepared by adding 100 μL of a 0.25 M solution of 1,1',3,3'-tetramethyl-2,2'-biimidazolidinylidene²⁰ in toluene to 100 μL of a 0.05 M solution of **1** in toluene at room temperature. UV irradiation was performed by focusing the unfiltered light from a 500 W high-pressure mercury lamp (Müller Optik) on a sample in the cavity of the ESR spectrometer. Saturation of the ESR signal during variable temperature experiments was avoided by using low microwave powers, *i.e.* 200 nW for the $\Delta M_s = \pm 1$ transition and 1 mW for the $\Delta M_s = \pm 2$ transition, which is well within the range where signal intensity is proportional to the square root of the microwave power at 4 K.

3.6.2 Synthesis

***N,N,N',N'*-Tetraethyl-*P,P'*-1,3-phenylenebis(phosphonous diamide) 2.** Ca. one fifth of a solution of 1,3-dibromobenzene (29.49 g, 0.125 mol) in THF (100 mL) was added to magnesium (6.08 g, 0.25 mol). Gently heating started the reaction and the remainder of the dibromobenzene was added in a rate sufficient to keep the mixture at reflux. After addition of all dibromobenzene, THF (100 mL) was added and the mixture was boiled under reflux for 18 h. Upon standing at RT for several hours, the white solid settled, and the THF was siphoned off. The Grignard compound was suspended in hexane (100 mL) and tetraethylphosphorodiamidous chloride (38.13 g, 0.25 mol) in hexane (100 mL) was added at ambient temperature. After boiling under reflux for 18 h, the mixture was filtered and all solvents were evaporated. Vacuum distillation of the residue afforded pure **2** (36.9 g, 71%) as a pale yellow oil: bp 176-177 °C (0.005 mmHg); ^{31}P NMR (CDCl_3) δ 97.9; ^1H NMR (CDCl_3) δ 1.06 (12H, t, $J_{\text{HH}} = 7.0$ Hz, CH_3), 3.03 (8H, c, $J_{\text{HH}} = 7.0$ Hz, CH_2), 7.26 (3H, c, H-4, H-5), 7.52 (1H, t, $J_{\text{PH}} = 7.0$ Hz, H-2); ^{13}C NMR (CDCl_3) δ 14.62 (s, CH_3), 42.79 (d, $J_{\text{PC}} = 16.6$ Hz, CH_2), 127.85 (c, C-5), 129.96 (d, $J_{\text{PC}} = 16.8$ Hz, C-4), 133.40 (t, $J_{\text{PC}} = 16.7$ Hz, C-2), 141.42 (c, C-1).

1,3-Phenylenebis(phosphonous dichloride) 3. A solution of HCl (45 mol%) in dry diethyl ether (24.14 g, 120 mmol) was added slowly to a well-stirred solution of **2** (5.55 g, 15 mmol) in hexane (75 mL), while keeping the temperature between 0-10 °C. After subsequent warming to RT, the ammonium salts were filtered off, avoiding any contact with air. The

solvents were evaporated and distillation of the residue afforded pure **3** (3.05g, 73%) as a colorless liquid: bp 97-99 °C (0.004 mmHg); ^{31}P NMR (CDCl_3) δ 157.5; ^1H NMR (CDCl_3) δ 7.69 (1H, tt, $J_{\text{PH}} = 8$ Hz, $J_{\text{HH}} = 2$ Hz, H-5), 8.08 (2H, c, $J_{\text{PH}} = 8$ Hz, H-4) 8.38 (1H, tt, $J_{\text{PH}} = 8$ Hz, $J_{\text{HH}} = 2.5$ Hz, H-2); ^{13}C NMR (CDCl_3) δ 129.94 (t, $J_{\text{PC}} = 9.9$ Hz, C-5), 131.63 (t, $J_{\text{PC}} = 31.4$ Hz, C-2), 134.13 (d, $J_{\text{PC}} = 27.7$ Hz, C-4), 141.78 (dd, $J_{\text{PC}} = 55.3$ Hz, $J_{\text{PC}} = 10.1$ Hz, C-1).

***P,P'*-Bis(2,4,6-tri-*t*-butylphenyl)-1,3-phenylenebis(phosphinous chloride) **1** (mixture of RR, SS, RS).** A solution of 2,4,6-tri-*t*-butylbromobenzene (6.86 g, 21.1 mmol) in THF (25 mL) was stirred at -78 °C and *n*-BuLi (1.6 M in hexane, 13.2 mL, 21.1 mmol) was added slowly. After stirring the reaction mixture at this temperature for 1 hr, a solution of **3** (2.36 g, 8.43 mmol) in THF (50 mL) was added and the mixture was allowed to warm to RT. It was then passed through a thin layer of silica and the solvent was evaporated. Flash chromatography (SiO_2 ; hexane) afforded pure **1** (2.44 g, 42 %) ³⁰ as a white solid: ^{31}P NMR (CDCl_3) δ 75.1, 76.4; ^1H NMR (CDCl_3) δ 1.43, 1.35 (36H, 2 s, *o*-(CH_3)₃C), 1.39, 1.40 (18H, 2 s, *p*-(CH_3)₃C), 6.22 (1H, b s, H-2), 6.42, 6.45 (4H, 2 b s, H-4), 6.84, 6.93 (2H, 2 m, H-5), 7.47, 7.48 (4H, 2 s, H-3').

3.7 References

- 1 *Proceedings of the Symposium on Ferromagnetic and High-Spin Molecular Based Materials*, 197th National Meeting of the American Chemical Society, Dallas, TX, April, 1989; American Chemical Society: Washington, DC. Miller, J. S.; Dougherty, D. A., Eds. *Mol. Cryst. Liq. Cryst.* **1989**, 176, 1-562.
- 2 Gatteschi, D.; Kahn, O.; Miller, J. S.; Palacia, F.; Eds. *Molecular Magnetic Materials*; Kluwer: Dordrecht: 1991.
- 3 *Proceedings of the International Symposium on Chemistry and Physics of Molecular-Based Magnetic Materials*, Iwamura, H.; Miller, J. S., Eds. *Mol. Cryst. Liq. Cryst.* **1993**, 232, 1-360.
- 4 Iwamura, H. *Adv. Phys. Org. Chem.* **1990**, 26, 179.
- 5 Miller, J. S.; Epstein, A. J. *Angew. Chem., Int. Ed. Engl.* **1994**, 33, 385.
- 6 Rajca, A. *Chem. Rev.* **1994**, 94, 871.
- 7 Nakamura, N.; Inoue, K.; Iwamura, H. *Angew. Chem., Int. Ed. Engl.* **1993**, 32, 872.
- 8 Rajca, A.; Rajca, S.; Desai, S. *J. Am. Chem. Soc.* **1995**, 117, 806.
- 9 Veciana, J.; Rovira, C.; Ventosa, N.; Crespo, M. I.; Palacio, F. *J. Am. Chem. Soc.* **1993**, 115, 57.
- 10 Siverman, S. K.; Dougherty, D. A. *J. Phys. Chem.* **1993**, 97, 13273.
- 11 Calder, A.; Forrester, R.; James, P. G.; Luckhurst, G. R. *J. Am. Chem. Soc.* **1969**, 91, 3724.
- 12 Ishida, T.; Iwamura, H. *J. Am. Chem. Soc.* **1991**, 113, 4238.
- 13 Minato, M.; Lahti, P. M.; van Willigen, H. *J. Am. Chem. Soc.* **1993**, 115, 4532.
- 14 Rajca, A.; Rajca S.; Besui, S. R. *J. Chem. Soc., Chem. Commun.* **1995**, 1957.
- 15 Racja, A.; Utamapanya, S. *J. Am. Chem. Soc.* **1993**, 115, 2396.

- 16 Gynane, M. J. S.; Hudson, A.; Lappert, M. F.; Power, P. P. *J. Chem. Soc., Chem. Commun.* **1976**, 623.
- 17 Gynane, M. J. S.; Hudson, A.; Lappert, M. F.; Power, P. P.; Goldwhite, H. *J. Chem. Soc., Dalton Trans.* **1980**, 2428.
- 18 Cetinkaya, B.; Hudson, A.; Lappert, M. F.; Goldwhite, J. *J. Chem. Soc., Chem. Commun.* **1982**, 609.
- 19 Cowley, A. H.; Kemp, R. A. *Inorg. Chem.* **1983**, 22, 547.
- 20 Winberg, H. E. *US Patent*, 3,239,519, 1966
- 21 Geoffroy, M.; Lucken, E. A. C.; Mazeline, C. *Mol. Phys.* **1974**, 28, 839.
- 22 Morton, J. R.; Preston, K. F.; *J. Magn. Reson.* **1978**, 30, 577.
- 23 Weil, J. A.; Bolton, J. R.; Wertz, J. E. *Electron Paramagnetic Resonance, Elementary Theory and Practical Applications* John Wiley & Sons, New York, 1993; p 179.
- 24 Wienk, M. M.; Janssen, R. A. J.; Meijer, E. W. *J. Phys. Chem.* **1995**, 99, 9331.
- 25 Ling, C.; Lahti, P. M. *J. Am. Chem. Soc.* **1994**, 116, 8784.
- 26 Doi, T.; Ichimura, A. S.; Koga, N.; Iwamura, H. *J. Am. Chem. Soc.* **1993**, 115, 8928.
- 27 Matsumoto, T.; Ishida, T.; Koga, N.; Iwamura, H. *J. Am. Chem. Soc.* **1992**, 114, 9952.
- 28 Kanno, F.; Inoue, K.; Koga, N.; Iwamura, H. *J. Phys. Chem.* **1993**, 97, 13267.
- 29 Berson, J. A. In *The Chemistry of Quinoid Compounds*: Patai, S., Rappaport, Z., Eds.; Wiley: New York, 1988; p 462.
- 30 A significant part of the product is lost during chromatography.

Chapter 4

Triplet-State Phosphoryl Diradicals

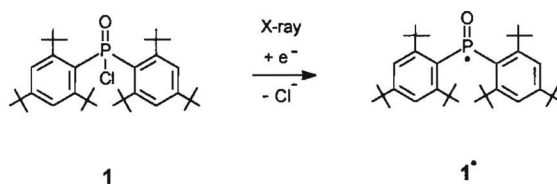
Abstract

*The first example of triplet-state phosphoryl diradicals is reported. Photoinduced dissociative electron capture of two diastereoisomeric *m*-phenylenebis(phosphinic chloride)s in a glassy toluene matrix at 130 K using an electron rich olefin, affords the corresponding phosphoryl monoradicals and triplet-state diradicals in a 5:2 ratio. The triplet state ESR spectrum is characterized by zero-field parameters of $D = 360$ MHz, $E = 45$ MHz, and $\beta = 90^\circ$. Variable temperature ESR experiments reveal Curie behavior for the $\Delta M_S = \pm 2$ ESR signals between 3.8 and 100 K, consistent with a low-energy triplet state which either corresponds to the ground state or is degenerate with a singlet state. For the corresponding *p*-phenylene diastereoisomers, no triplet-state diradicals can be detected under identical experimental conditions and the ESR spectra only reveal phosphoryl monoradicals and their protonated forms, as secondary species. Attempts to use acylphosphine oxides as more efficient precursors for phosphoryl radicals were not successful.*

4.1 Introduction

In the previous chapter, phosphinyl diradicals have been discussed, as an example of high-spin molecules in which ferromagnetic spin coupling is achieved between second-row atom centered radicals via *m*-phenylene.¹ Due to the in-phase periodicity of the spin polarization in *m*-phenylene, a parallel orientation of the electron spins is favored, resulting in a triplet ground state. In this chapter, phosphoryl radicals ($R_2P^{\bullet}O$) will be addressed as another example of a phosphorus-centered radical which can be used to investigate the spin-coupling between heavy-atom spin-carrying substituents.

Phosphoryl radicals are closely related to nitroxide radicals ($R_2N^{\bullet}O$), having the same number of valence electrons. In contrast to nitroxide radicals, for which single or shallow double-well potential energy surfaces are found for out-of-plane distortions,²⁻⁴ there is no doubt that phosphoryl radicals are non-planar.⁵ The pyramidal geometry of phosphoryl radicals can give rise to stereoisomerism; X-irradiation of single crystals of phosphinic chloride **1** at 77 K produces the corresponding phosphoryl radical **1[•]** (Scheme 4.1) which exhibits an enantioselective stereoinversion after annealing to 120 K.⁶ The large isotropic (A_{iso}) and dipolar (A_{dip}) hyperfine couplings observed for **1[•]** indicate that more than half of the spin density is localized on phosphorus in a valence sp^x hybridized molecular orbital with a p/s ratio of about 6. The remaining spin density is predominantly confined to the phosphoryl oxygen.⁶

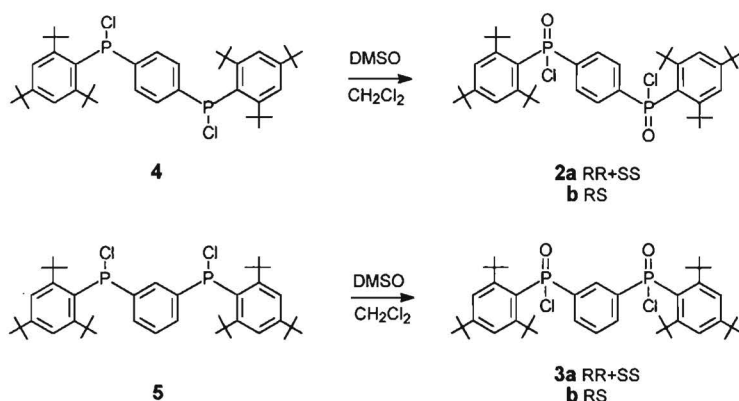


Scheme 4.1. Structure of monophosphinic chloride **1** and radical **1[•]** observed after dissociative electron capture reaction of **1**.

Because of the delocalization of spin, phosphoryl radicals are expected to be somewhat more stable than corresponding phosphinyl analogues. On the other hand, the spin delocalization onto the phosphoryl oxygen and the pyramidal geometry will further reduce the spin coupling as compared to that of the phosphinyl radicals, and it is of interest to investigate whether *m*-phenylene is still capable to provide sufficient spin-spin interactions to achieve high-spin ground states. In order to test this possibility, *m*-phenylenebis(phosphinic chloride)s **3a** and **3b** have been prepared and their conversion to the corresponding phosphoryl diradicals by P-Cl bond fission has been studied. For comparison *p*-phenylene isomers **2a** and **2b** have been investigated as well. All precursors possess two phosphorus stereocenters, resulting in three possible stereoisomers (RR, SS, RS). Compounds **2a** and **2b** (as well as **3a** and **3b**) represent the racemic mixture (RR + SS) and the meso (RS) compound, respectively. Using these precursors, spectral evidence of heavy-atom high-spin diradicals linked via *m*-phenylene has been obtained. Furthermore, in an attempt to improve the efficiency of the generation of radicals, acylphosphine oxides have been investigated as potential precursor molecules for phosphoryl oligoradicals.

4.2 Synthesis

The precursor molecules **2** and **3** were synthesized from the corresponding bis(phosphonous chloride)s **4** and **5** (Scheme 4.2). The synthesis of the *meta* compound **5** is described in the previous chapter and the *para*-substituted isomer **4** was prepared analogously, starting from 1,4-dibromobenzene. Oxidation of the bis(phosphonous chloride)s with DMSO in dichloromethane afforded the bis(phosphinic chloride)s as a mixture of three stereoisomers, which were separated by column chromatography into the racemic mixture (RR+SS: **2a**, **3a**) and the meso form (RS: **2b**, **3b**).



Scheme 4.2 Synthesis of bis(phosphinic chloride)s.

4.3 X-ray Analysis

Crystallization from a mixture of acetonitrile and dichloromethane, provided crystals of **2b**, **3a**, and **3b** suitable for X-ray diffraction analysis. These studies revealed that for both **2** and **3**, the fraction with the highest retention on silica is the racemic mixture (RR+SS: **2a**, **3a**).⁷

Compound **2b** crystallizes in a monoclinic spacegroup ($P2_1/c$ (No. 14)): $a = 10.0259$ (7) Å, $b = 20.189$ (1) Å, $c = 11.371$ (1) Å, $\beta = 110.342$ (8)°, $V = 2158.1$ (3) Å³, and $Z = 2$. The structure of this *para* substituted compound reveals a *Z*-like conformation. (Figure 4.1). The two phosphoryl oxygen atoms are in the plane of the central ring, and due to steric hindrance, the outer rings have a twisted, non-planar structure. The P-P distance is 6.40 Å.

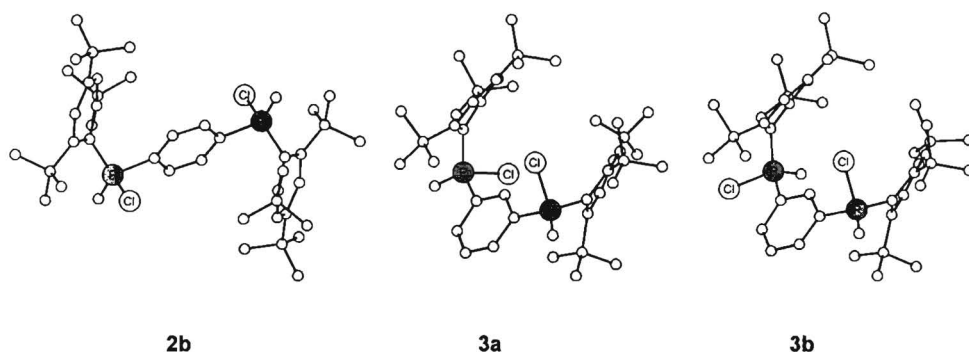


Figure 4.1. Molecular structures of **2b**, **3a**, and **3b** as determined by X-ray crystallography. Hydrogen atoms are left out for clarity reasons.

Compound **3a** crystallizes in a triclinic spacegroup ($P\bar{1}$ (No. 2)): $a = 10.905$ (2) Å, $b = 12.1204$ (8) Å, $c = 16.742$ (2) Å, $\alpha = 86.297$ (8)°, $\beta = 85.864$ (11)°, $\gamma = 76.885$ (8)°, $V = 2146.8$ (5) Å³, and $Z = 2$. The molecule adopts a cleft-like conformation in which the two outer phenylene rings are facing each other. The two phosphoryl oxygens are in the plane of the central phenyl ring. The P-P distance is 5.62 Å.

Compound **3b** crystallizes in a monoclinic spacegroup ($P2_1/c$ (No. 14)): $a = 11.9363$ (4) Å, $b = 18.7967$ (6) Å, $c = 119.4507$ (5) Å, $\beta = 96.984$ (2)°, $V = 4331.6$ (2) Å³, and $Z = 4$. The structure is very similar to the structure of **3a**, the only difference being the configuration around one of the phosphorus atoms, where the chlorine and oxygen atoms have swapped places. The P-P distance in this compound is 5.51 Å.

4.4 NMR Analysis

At room temperature, the ¹H NMR spectra of all precursor molecules display a number of very broad transitions, pointing to the existence of different conformers, presumably as a result of rotational barriers caused by the bulky *t*-butyl groups. X-ray analysis shows that in the solid-state, the molecules have a preference for a conformation in which the phosphoryl oxygens are in the plane of the central phenylene ring. With this in mind, two conformers may be expected in solution, one in which the phosphoryl moieties have a *syn* orientation and one in which they are *anti*.

For compound **2a** all proton signals start to decoalesce at -20 °C. The two *t*-butyl groups on the *ortho* positions become non-equivalent, indicating restricted rotation around the bonds between phosphorus and the outer phenyl rings. The same non-equivalence can be

noticed for the 3'-hydrogens. Because of the restricted rotation around the bonds between phosphorus and the central phenylene ring, the protons on the central phenylene ring –on either side of the phosphorus– also become non-equivalent. One is shielded by the outer phenyl ring, the other deshielded by the phosphoryl oxygen. Two conformers can be distinguished, which differ with respect to the orientation of the phosphoryl moieties. The *syn* conformation, with the phosphoryl oxygens oriented in the same direction, is expected to give rise to the greater shielding and deshielding effects, and seems to be favored in this isomer. The ^{31}P NMR spectrum consists of a single transition over the whole temperature range under investigation.

Similar effects occur for diastereoisomer **2b**. The major difference being the observed ratio of the two different conformers. A 5:1 ratio, in favor of the structure in which the phosphoryl moieties are oriented in an *anti* fashion, is found. This conformation is actually found in the crystal structure as well.

For compound **3a**, no conformers are observed upon lowering the temperature. The ^1H -NMR spectrum only changes with respect to the signals of the *t*-butyl groups and 3'-hydrogens, similar to the effects observed for **2a** and **2b**. The ^{31}P NMR does not change. The chemical shift values of the 4- and 2-hydrogens on the central ring are remarkably far apart. As is the case in the crystal structure, the 2-hydrogen is sandwiched between the two outer phenyl rings, leading to a large shielding effect and a large up-field shift. The 4-hydrogens, on the other hand, experience a large deshielding effect of the phosphoryl group.

Upon cooling, the ^1H NMR spectrum of isomer **2b** becomes very complicated, due to a number of asymmetric conformations. This is also reflected in the ^{31}P NMR, which displays four doublets at $-80\text{ }^\circ\text{C}$, indicative of the presence of two different conformers, both with two non-equivalent phosphorus atoms.

4.5 ESR Spectroscopy

Phosphoryl radicals are prepared via a dissociative electron-capture reaction of the P-Cl bond, the electrons being provided by an electron-rich olefin (ero), which readily yields reactive free electrons upon UV irradiation.⁸⁻¹⁰ In this study, a mixture of the appropriate phosphinic chloride precursor and an excess of ero (1,1',3,3'-tetramethyl-2,2'-biimidazolidinylidene)¹¹ is used in a frozen solvent matrix of either toluene or 2MeTHF in combination with in situ UV irradiation at cryogenic temperatures.

Monophosphinic chloride 1. UV irradiation of a 5:1 mixture of ero and bis(2,4,6-*t*-butylphenylphosphinic chloride) **1** in 2MeTHF at 77 K for 30 min and recording the ESR spectrum at 110 K affords an anisotropic ^{31}P doublet spectrum attributed to $\text{Ar}_2\text{P}^\bullet\text{O}$ ($\mathbf{1}^\bullet$, $\text{Ar} = 2,4,6\text{-tri-}t\text{-butylphenyl}$), featuring well-resolved parallel ($A_{\parallel} = 1390\text{ MHz}$) and

perpendicular ($A_{\perp} = 868$ MHz) transitions (Figure 4.2). The isotropic and dipolar contributions to the hyperfine coupling tensor $A_{\text{iso}} = (A_{\parallel} + 2A_{\perp})/3 = 1042$ MHz and $2A_{\text{dip}} = A_{\parallel} - A_{\text{iso}} = 348$ MHz are in good accordance with the values previously reported for radiogenically generated $\mathbf{1}^{\bullet}$ in glassy toluene as well as in single crystals (see Table 4.1).⁶

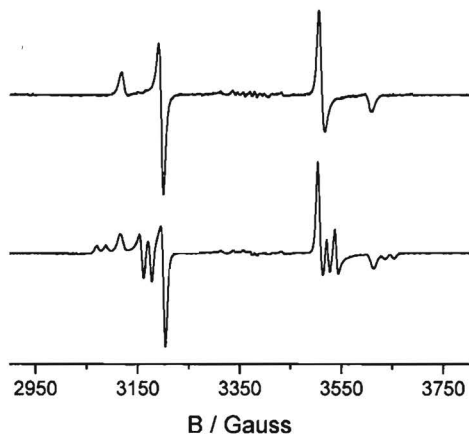
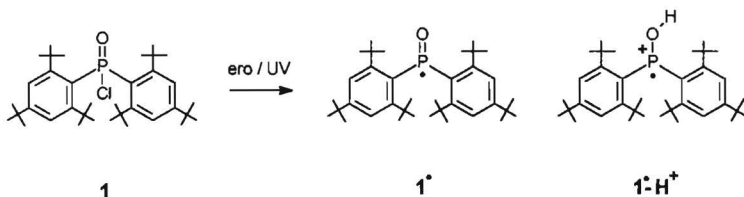


Figure 4.2. ESR spectra recorded at 110 K (top) and 120 K (bottom) of a mixture of monophosphinic chloride **1** and ero in 2MeTHF UV-irradiated at 77 K.

Gradual warming of the sample to 120 K produces a secondary phosphorus-centered radical $\mathbf{1}^{\bullet}\text{-H}^+$. The ESR spectrum of $\mathbf{1}^{\bullet}\text{-H}^+$ exhibits a large ^{31}P hyperfine coupling ($A_{\text{iso}} = 1210$ MHz), together with an additional splitting of about 50 MHz by one $I = 1/2$ nucleus (Figure 4.2). A similar additional hyperfine coupling has been observed for $\text{PhP}^+(\text{O})\text{OH}$ radicals, and we tentatively assign $\mathbf{1}^{\bullet}\text{-H}^+$ to the $\text{Ar}_2\text{P}^+\text{OH}^{\bullet}$ radical (Scheme 4.3).¹² This anisotropic double doublet ESR spectrum disappears irreversibly at 130 K, leaving the original doublet spectrum of $\text{Ar}_2\text{P}^+\text{O}$, which remains up to the melting temperature of the host matrix.



Scheme 4.3. Reaction of monophosphinic chloride **1**, induced by UV irradiation of ero in a 2MeTHF matrix.

Racemic 1,4-phenylenebis(phosphinic chloride) 2a. Radicals were generated by UV irradiation of a 5:1 mixture of *ero* and **2a** in toluene at temperatures around 130 - 135 K for several hours. The transitions in the $\Delta M_S = \pm 1$ region of the resulting ESR spectrum show a strong resemblance to those obtained by irradiation of the monophosphinic chloride **1** (Figure 4.3). Accordingly, they are attributed to a monoradical **2a \cdot** , resulting from cleavage of only one of both P-Cl bonds in the precursor molecule (Scheme 4.4). The central line is due to photo-oxidized *ero* and is slightly more persistent in frozen toluene than in 2MeTHF at the temperature at which the UV irradiation is performed. No signals are observed in the $\Delta M_S = \pm 1$ or $\Delta M_S = \pm 2$ regions at various different temperatures and/or irradiation times, that can be attributed to a triplet state.

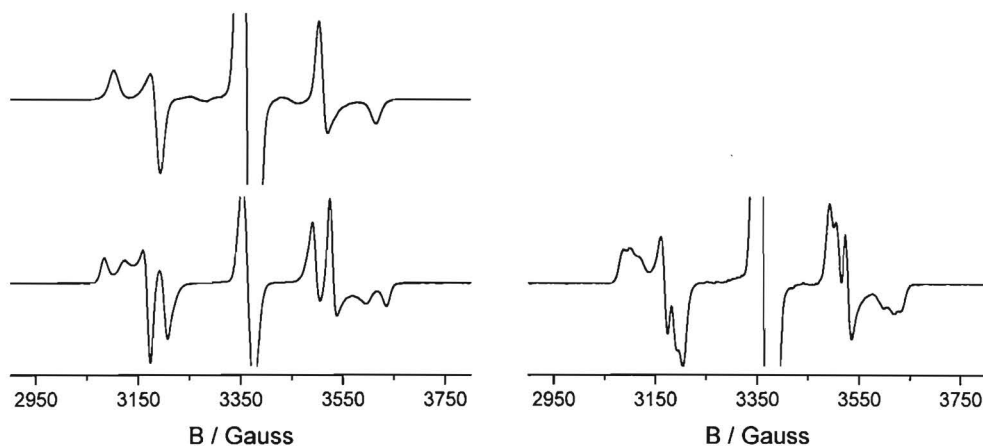
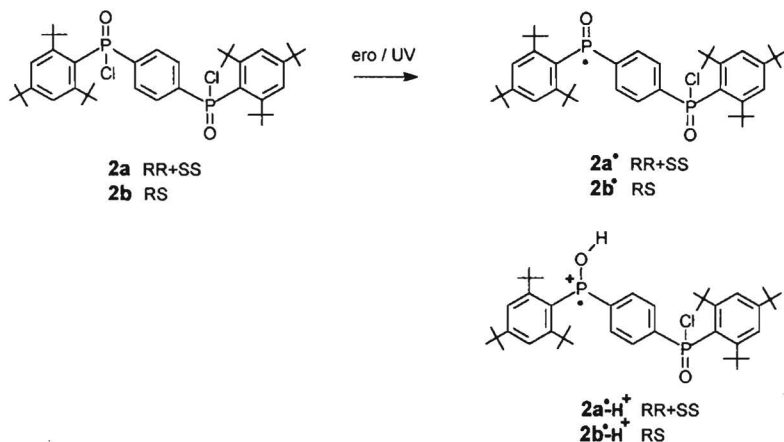


Figure 4.3. (left): ESR spectra of a UV-irradiated mixture of bis(phosphinic chloride) **2a** and *ero* in toluene, recorded at 110 K (top) and 130 K (bottom). (right): ESR spectrum of a UV-irradiated mixture of bis(phosphinic chloride) **2b** and *ero* in toluene, recorded at 110 K.

Slight annealing results in a complete conversion of phosphoryl radical **2a \cdot** to a secondary phosphorus-centered radical **2a \cdot -H $^+$** , exhibiting an additional hyperfine splitting. The ^{31}P hyperfine splitting of **2a \cdot -H $^+$** is similar to that of primary radical **2 \cdot** . This behavior is similar to the formation of **1 \cdot -H $^+$** from **1 \cdot** in monophosphinic chloride **1**. In this case, however, the extra hyperfine splitting is significantly larger: 110 MHz for **2a \cdot -H $^+$** vs 50 MHz for **1 \cdot -H $^+$** .

The absence of a triplet state for **2a** does not necessarily imply that no diradicals are formed, since the radical centers may couple antiferromagnetically to a singlet state ($J \ll 0$) which is not detected by ESR. In fact, this is to be expected when spin polarization does occur in the *p*-phenylene ring because the topology favors antiferromagnetic interaction by the out-of-phase periodicity of the spin polarization at the 1,4 positions.



Scheme 4.4. Structures of *para* isomers **2a** and **2b** and the radicals observed after a dissociative electron capture reaction induced by UV irradiation of *ero* in a toluene matrix.

Meso 1,4-phenylenebis(phosphinic chloride) 2b. No triplet state can be observed after UV irradiation of a 5:1 mixture of *ero* and **2b** in toluene (Figure 4.3). The ESR spectrum recorded at 110 K exhibits signals of $\text{Ar}_2\text{P}^\bullet\text{O}$ (**2b** $^\bullet$) and $\text{Ar}_2\text{P}^\bullet\text{OH}^+$ (**2b** $^\bullet\text{-H}^+$) monoradicals. Analogous to UV irradiation of **2a**, no conclusive evidence can be obtained whether diradicals are formed in **2b**.

Racemic 1,3-phenylenebis(phosphinic chloride) 3a. After UV irradiation of a 5:1 mixture of *ero* and **3a** in toluene at temperatures around 130 - 135 K for several hours, the major transitions in the $\Delta M_S = \pm 1$ region of the ESR spectrum are attributed to monoradical (**3a** $^\bullet$), resulting from cleavage of only one of both P-Cl bonds in the precursor molecule (Figure 4.4). The most interesting features in the ESR spectrum are two pairs of transitions in the outermost low- and high-field regions. These lines are assigned to a triplet-state phosphoryl diradical (**3a** $^{2\bullet}$), formed by two successive dissociative electron capture reactions of both P-Cl bonds of the bis(phosphinic chloride) precursor (Scheme 4.5). Direct spectral evidence for the existence of a triplet species is obtained from the spectrum in the $\Delta M_S = \pm 2$ region, featuring a number of well-resolved transitions, which can only be attributed to a triplet state. Diradical **3a** $^{2\bullet}$ is stable in the toluene matrix up to the melting point of toluene. Surprisingly, no signals attributable to a secondary radical like **1** $^\bullet\text{-H}^+$ are observed.

By using the isotropic and dipolar hyperfine couplings of $\text{Ar}_2\text{P}^\bullet\text{O}$, a spectral simulation of the $\Delta M_S = \pm 2$ signal has been obtained, which is in excellent agreement with the experimental spectrum.¹³ The fact that hyperfine coupling with two identical ^{31}P nuclei is observed while the isotropic and dipolar hyperfine coupling constants are halved, indicates that the phosphoryl radicals are strongly coupled in **3a** $^{2\bullet}$, i.e. $|J| \gg |A_{\parallel}|$, where $A_{\parallel} \approx 1500$ MHz. The zero-field splitting of triplet diradical **3a** $^{2\bullet}$ is characterized by $D = 360$ MHz, $E = 45$

MHz, and $\beta = 90^\circ$ (Euler angle of D and $A_{||}$). The $\Delta M_S = \pm 1$ region of the spectrum is reproduced adequately by combining the simulations of mono- and diradicals in a 5:2 ratio. This implies a significant concentration of diradicals as compared to monoradicals, possibly indicating that the second P-Cl bond within the same molecule is cleaved at a higher rate than the first.

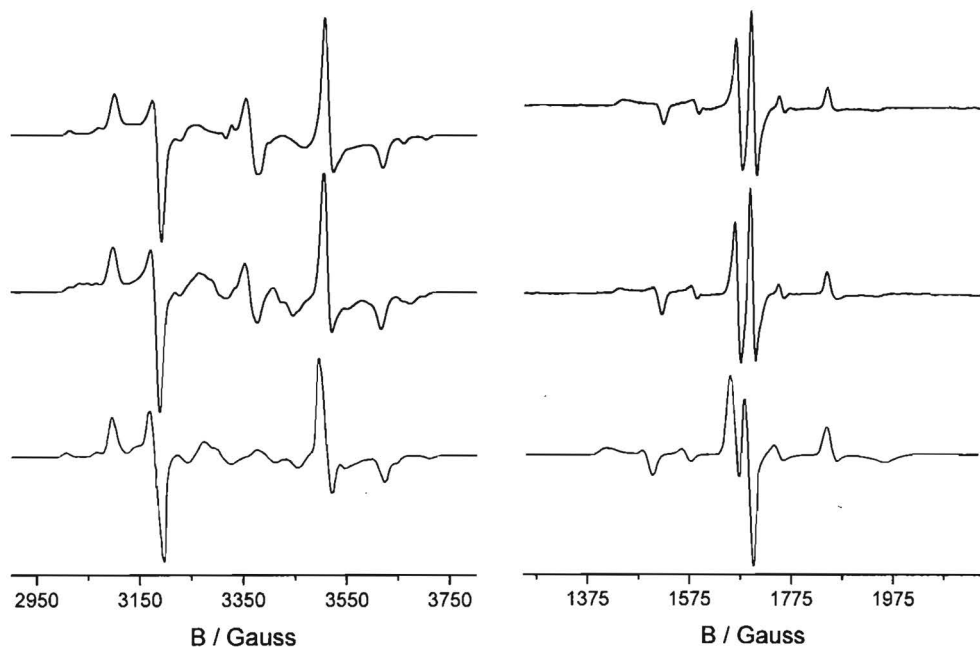
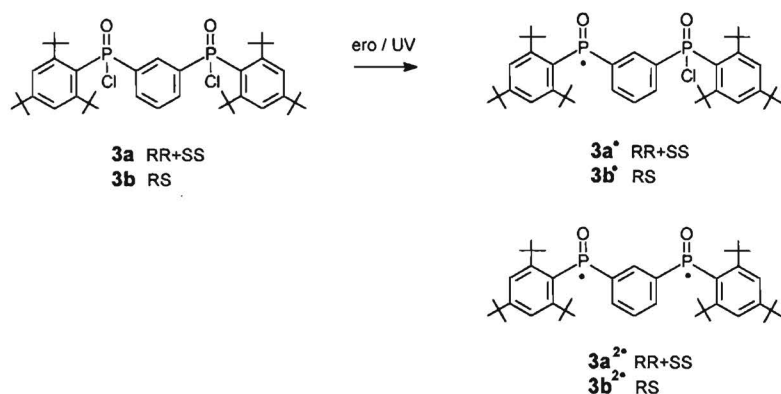


Figure 4.4. $\Delta M_S = \pm 1$ (left side) and $\Delta M_S = \pm 2$ region (right side) of ESR spectra of a UV-irradiated mixture of *ero* and bis(phosphinic chloride) **2a** (top) or **3b** (center) in toluene, recorded at 130 K. (bottom): Simulations of 5:2 mixture of mono- and diradical.

Meso 1,3-phenylenebis(phosphinic chloride) 3b. UV irradiation of meso isomer **3b** reveals essentially the same behavior as compared to racemic form **3a**. We conclude that monoradicals **3a[•]** and diradicals **3a^{2•}** are formed. The $\Delta M_S = \pm 2$ part of the ESR spectrum of **3a^{2•}** is identical to that of the racemic form (Figure 4.4). The $\Delta M_S = \pm 1$ ESR spectrum, however, is somewhat different and reveals a total of eight lines in the outermost regions of the spectrum, in contrast to the ESR spectrum of **3b^{2•}** that exhibits only four lines in this section. These eight transitions are likely to arise from two different conformations of the diradical, originating from the two conformers of the precursor that exist at low temperatures, as inferred from variable temperature NMR spectroscopy studies. Also for this precursor no protonated secondary radicals are obtained.



Scheme 4.5. Structures of meta isomers **3a** and **3b** and the radicals observed after a dissociative electron capture reaction induced by UV irradiation of *ero* in a toluene matrix.

Table 4.1. Isotropic and Dipolar Hyperfine Couplings for Phosphoryl Mono- and Diradicals^a

Radical	host	<i>T</i> (K)	<i>A</i> _{iso} (MHz)	2 <i>A</i> _{dip}
1[•]	2MeTHF	110	³¹ P 1042	348
1[•]-H⁺	2MeTHF	120	³¹ P 1210 ¹ H ≈ 50	371
2a[•]	toluene	110	³¹ P 1095	338
2a[•]-H⁺	toluene	130	³¹ P 1068 ¹ H ≈ 110	364
2b[•]	toluene	110	³¹ P 1099	349
2b[•]-H⁺	toluene	110	³¹ P 1099 ¹ H ≈ 110	332
3a[•]	toluene	130	³¹ P 1123	346
3a^{2•}	toluene	77	³¹ P 535 ^b	186 ^b
3b[•]	toluene	130	³¹ P 1112	339
3b^{2•}	toluene	77	³¹ P 535 ^b	186 ^b

^a Isotropic and dipolar hyperfine couplings are corrected up to second-order. ^b For diradical in the triplet state.

4.6 Determination of Ground States

The results on phosphoryl radical formation in **2** and **3** suggest that spin polarization does occur in the central phenylene ring, stabilizing a high-spin state for *meta* and possibly destabilizing it for *para* isomers. In the present case, magnetization and magnetic susceptibility measurements cannot be used for the assessment of the ground state multiplicity of diradicals **3a**^{2*} and **3b**^{2*}, due to the inhomogeneity of the samples. Therefore, variable temperature ESR experiments were performed. The intensity (*I*) of the $\Delta M_S = \pm 2$ signal was measured as function of temperature, between 3.8 and 100 K, with the UV light switched off.

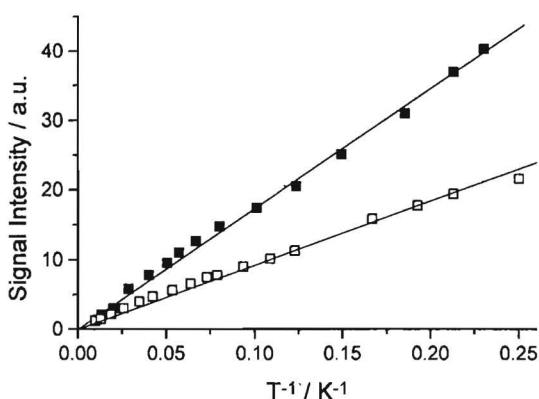


Figure 4.5. Temperature dependence of the $\Delta M_S = \pm 2$ ESR signal intensity of diradicals **3a**^{2*} (\blacksquare) and **3b**^{2*} (\square). Solid lines are least-square fits to Curie's law.

The temperature dependence of the $\Delta M_S = \pm 2$ ESR signals of **2a** and **3a** follows Curie's law ($I = C/T$) (Figure 4.5). This thermal behavior is completely reversible in the temperature range examined, indicating that irreversible loss of diradicals is negligible. The observed Curie behavior implies that no thermal population or depopulation of the triplet state occurs. This can be interpreted in two ways: either the triplet state is the ground state and separated from an excited singlet state by a substantial energy gap of a few hundreds of calories per mole, or an extremely small energy gap is present resulting in a (near) degenerate ground state.¹⁴⁻¹⁸ Therefore, we conclude that the triplet states of diradicals **3a**^{2*} and **3b**^{2*} are low-energy states, either corresponding to the ground state or as part of a degeneracy with a singlet state.

4.7 Structure Assignment of Diradicals

The distance $d(\text{\AA})$ between the two radical sites in $3\mathbf{a}^{2\bullet}$ and $3\mathbf{b}^{2\bullet}$ can be estimated from the zero-field splitting by $D = 7.8 \times 10^4 d^{-3}$ under a point dipole approximation.¹⁹ The observed D value of 360 MHz corresponds to a distance of about 6.0 \AA , which is somewhat larger than the actual P-P distance of 5.6 and 5.5 \AA for precursors $3\mathbf{a}$ and $3\mathbf{b}$, respectively, as determined by X-ray analysis. This small deviation is likely to result from delocalization of the unpaired electrons onto the phosphoryl oxygens and the terminal phenyl rings. Similarly, one can estimate the zero-field splitting of a hypothetical diradical derived from $2\mathbf{a}$ or $2\mathbf{b}$ using the P-P distance of 6.40 \AA given by the X-ray structure of $2\mathbf{b}$. The expected separation of the two radical centers would be 6.40 + 0.50 \AA and gives $D = 237$ MHz. The absence of corresponding signals in the $\Delta M_S = \pm 1$ region, gives unambiguous evidence for the absence of triplet-state diradicals for $2\mathbf{a}$ and $2\mathbf{b}$.

Although the spin density distribution on phosphorus indicates a pyramidal geometry, there is no conclusive evidence of stereoisomerism between diradicals $3\mathbf{a}^{2\bullet}$ and $3\mathbf{b}^{2\bullet}$, formed from the racemic and meso precursors, respectively. It is well established that in a frozen solvent matrix at cryogenic temperatures, intramolecular motional freedom of free radicals is sufficient to allow for monomolecular reactivity. Hence, it is very well possible that stereoinversion takes place, though not being observed experimentally in the randomly oriented matrix employed in this study. If this is the case, both $3\mathbf{a}^{2\bullet}$ and $3\mathbf{b}^{2\bullet}$ are the energetically favored diastereoisomer, and thus identical.

The additional pairs of lines observed in the spectrum of $3\mathbf{b}^{2\bullet}$, are likely to arise from a different conformation of precursor $3\mathbf{b}$, based on low-temperature NMR studies. The conformational diversity of $3\mathbf{b}$ is a result of the sterically crowded 2,4,6-tri-*t*-butylphenyl substituents and involves *syn* and *anti* conformations of the two phosphoryl bonds with respect to the central phenylene ring. A stereochemical effect as discussed above, however, cannot be excluded to explain the two triplet ESR spectra in the $\Delta M_S = \pm 1$ region.

4.8 Discussion

It is shown that phosphoryl diradicals $3\mathbf{a}^{2\bullet}$ and $3\mathbf{b}^{2\bullet}$, coupled via a *m*-phenylene unit, possess a low-energy triplet state. Apparently, despite the spin diffusion onto the phosphoryl oxygen spin and the pyramidal geometry of the radical sites, spin coupling does still occur. The triplet-singlet energy gap can not be determined, but most likely, this energy difference is at least a few hundred calories per mole in favor of the triplet, though formally, the possibility that the energy difference is zero can not be excluded. For nitroxyl diradicals, cases have been reported that display much smaller energy gaps or even low-spin ground states. However,

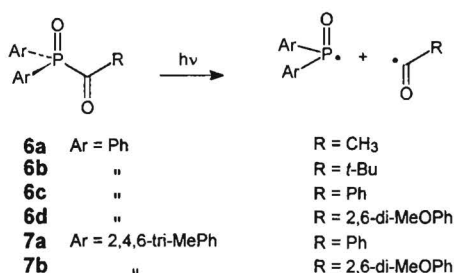
because **3a**^{2•} and **3b**^{2•} are the only known examples of triplet-state phosphoryl diradicals, no definite conclusion can be drawn from this comparison. As expected for more delocalized radicals, the phosphoryl diradicals are more persistent than the corresponding phosphinyl diradicals, but the improvement is not spectacular. Whereas the phosphinyl diradicals decompose at temperatures above 130 K, the phosphoryl diradicals are stable up to the melting point of the toluene matrix at 180 K. No insight is gained into the relative magnitude of the spin coupling in both systems, because the temperature dependence of the ESR signals is identical.

One of the major drawbacks of both phosphoryl and phosphinyl radicals is the inefficient generation of these species. Due to the nature of the dissociative electron capture process, it is difficult to drive the spin-generating reaction to completion. Though diradicals have actually been prepared this way, extension to larger spin systems will be very difficult. Therefore, other precursors have to be considered and attempts into that direction are presented below.

4.9 Acylphosphine Oxides Precursors

4.9.1 Introduction

In order to increase the yield of the phosphoryl radicals, acylphosphine oxides have been investigated as precursors. These compounds have been developed as photoinitiators for the photocuring of polymer resins.²⁰⁻²⁴ UV irradiation results in a homolytical dissociation of the bond between the phosphoryl and carbonyl moiety, affording a phosphoryl radical and an acyl radical (Scheme 4.6). Especially in solution, this is a very efficient process with quantum yields of 50 -70%.²⁵

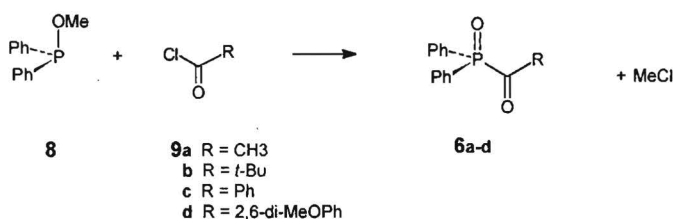


Scheme 4.6. Structure of acylphosphine oxide precursors and reaction products after homolytical dissociation.

Research was focused on monofunctional compounds, to test whether it is possible to obtain phosphoryl radicals which are sufficiently stable. Therefore, in addition to acyldiphenylphosphine oxides **6a-d** (Scheme 4.6; Ar = phenyl), precursors with sterically crowded aryl groups on the phosphoryl moiety, **7a,b** (Ar = 2,4,6-trimethylphenyl) have been prepared, in order to stabilize the phosphoryl radicals that result from irradiation

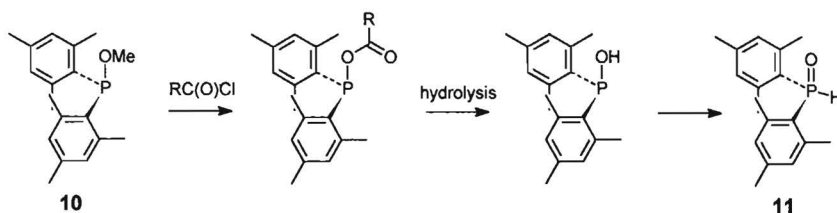
4.9.2 Synthesis

Acyldiphenylphosphine oxide precursors **6a-d** were prepared by an Arbuzov-like reaction between methyl diphenylphosphinite **8** and the appropriate acid chloride **9** (Scheme 4.7).^{20,22,26}



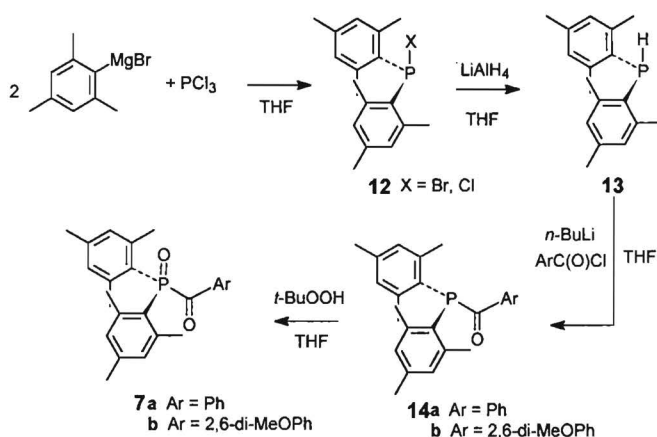
Scheme 4.7. Synthesis of acyldiphenylphosphine oxide precursors.

The same reaction could not be used for the synthesis of sterically hindered acylphosphine oxides. When methyl bis(2,4,6-trimethylphenyl)phosphinite **10** was treated with an acid chloride, the reaction did not take place at the phosphorus atom due to steric hindrance. Instead, the acid chloride reacted at the oxygen atom, yielding an ester, which ultimately afforded bis(2,4,6-trimethylphenyl)phosphine oxide **11** (Scheme 4.8).



Scheme 4.8. Reaction between acid chlorides and sterically hindered methyl phosphinite.

An alternative route towards acylbis(2,4,6-trimethylphenyl)phosphine oxides **7a,b** started with the Grignard reagent of 2,4,6-trimethylbromobenzene (Scheme 4.9). Reaction with 0.5 equiv of PCl_3 afforded not only bis(2,4,6-trimethylphenyl)phosphonous chloride, but also a significant amount of the corresponding phosphonous bromide, as a result of halogen exchange. Reduction of this mixture afforded bis(2,4,6-trimethylphenyl)phosphine **13** as the single product. Deprotonation by *n*-butyllithium, and subsequent reaction with a suitable acid chloride provided the acylphosphine **14**. Acetyl chloride could not be used in this reaction, because of its acidic protons, which readily react with the anion of **13**, which is a strong base. Reactions with benzoyl chlorides were not hampered by this side reaction. The resulting benzoylphosphines were oxidized to the corresponding benzoylphosphine oxides using *t*-butylhydroperoxide.



Scheme 4.9. Alternative route to benzoyl bis(2,4,6-trimethylphenyl)phosphine oxides.

4.9.3 ESR Spectroscopy

Radicals were generated in situ by continuous UV irradiation of a 0.1 M solution of the appropriate precursor in degassed toluene. Spectra were recorded with the UV light source switched on.

At room temperature, irradiation of acyldiphenylphosphine oxide precursors **6a-d**, only results in signals corresponding to secondary radicals. The exact nature of these secondary radicals is not clear. When the irradiation of the precursors is carried out in a frozen solution at 110 K, again no signals of phosphoryl radicals are obtained. This can either be due to an insufficient reactivity at this temperature, or to fast recombination of the geminal radical pairs in the solid matrix.

Photolysis of benzoylbis(2,4,6-trimethylphenyl)phosphine oxide **7a** at room temperature affords weak signals of the phosphoryl radical **15** (doublet; $A_{\text{iso}} = 1024$ MHz) and benzoyl radical **16** (singlet) (Figure 4.6). These signals can only be observed under continuous irradiation. This implies that the radicals are not persistent at this temperature. No secondary radicals are obtained. At 110 K, irradiation affords anisotropic ESR signals of the bis(2,4,6-trimethylphenyl)phosphoryl radical **15** ($A_{\text{iso}} = (A_{\parallel} + 2A_{\perp})/3 = 1040$ MHz and $A_{\text{dip}} = A_{\parallel} - A_{\text{iso}} = 333$ MHz).²⁷ The spectrum however, is dominated by a doublet, characterized by a significantly smaller hyperfine coupling. The magnitude of this coupling ($A_{\text{iso}} = 63$ MHz) suggests that this does not concern a phosphorus-centered radical, and therefore, the signal is tentatively attributed to a secondary radical **17**, resulting from the reaction between benzoyl radical **16** and the precursor benzoyl phosphinoyl **7a** (Scheme 4.10).²⁸

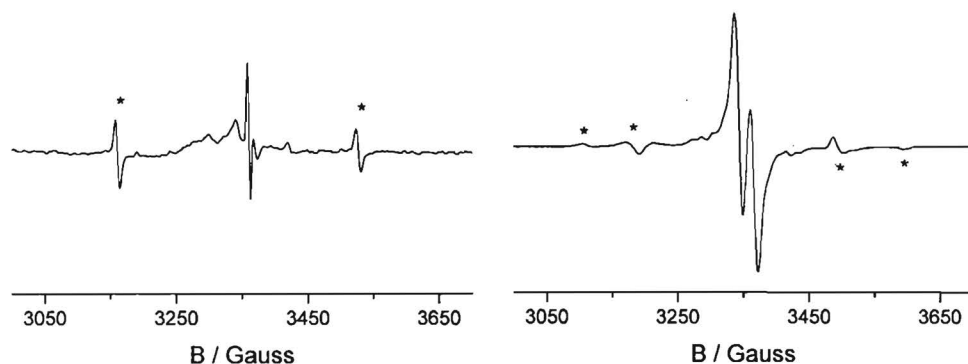
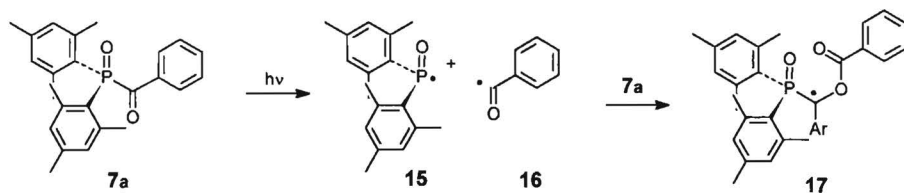


Figure 4.6. ESR spectra after photolysis of benzoylphosphine oxide **7a** in toluene at RT (left) and at 110 K (right). Transitions attributed to phosphoryl radical **15** are marked (*).



Scheme 4.10. Proposed reaction upon photolysis of benzoylphosphine oxide **7a**.

Similarly, photolysis of 2,6-dimethoxybenzoylphosphine oxide **7b**, affords carbon-centered secondary radical **19** ($A_{\text{iso}} = 77$ MHz) as the only open-shell species, irrespective of the temperature at which the irradiation is performed (Figure 4.7).

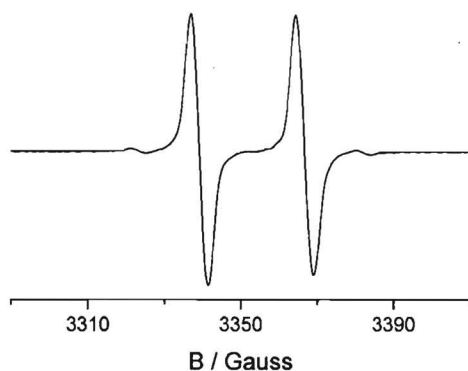


Figure 4.7. ESR spectrum after photolysis of 2,6-dimethoxybenzoylphosphine oxide **7b** in toluene at room temperature. ^{13}C -satellite peaks can be distinguished.

Upon irradiation at room temperature, the signal intensity of this radical levels off rapidly (Figure 4.8). Surprisingly, when at that point the UV-light source is switched off, the signal intensity increases, whereas the signal intensity decreases again when the light source is switched back on. This process can be repeated, but the amount of **19** decreases as a result of depletion of starting material.

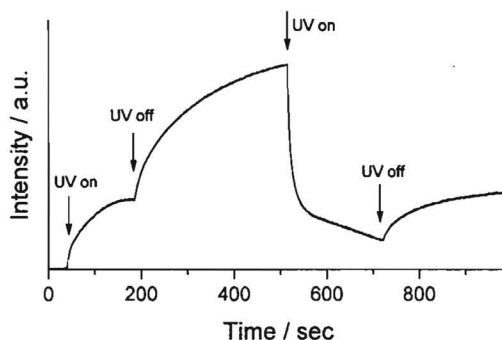
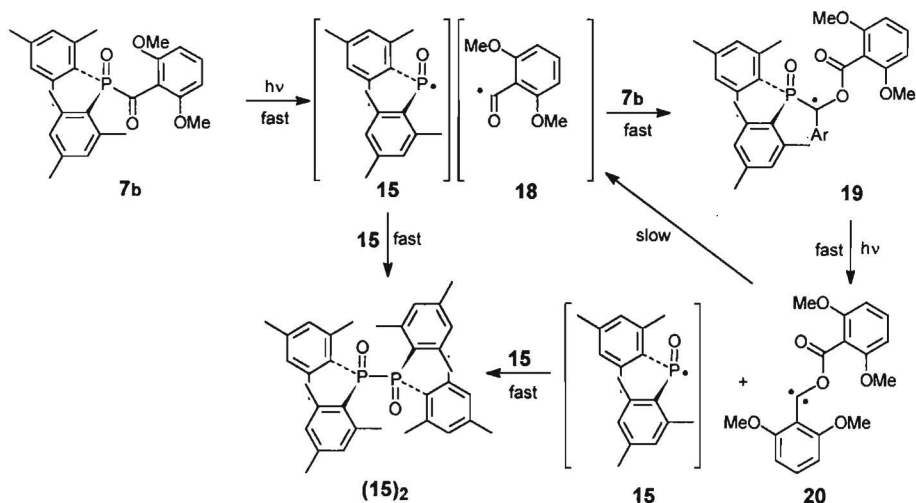


Figure 4.8. ESR signal intensity of secondary radical **19** vs time, as a function of the UV irradiation.

Apparently, the UV light not only initiates the formation of the secondary radical, but it also accelerates its degradation. One of the products of this photodegradation somehow accounts for the increasing concentration of **19**, when no irradiation takes place. This species has to be ESR silent, because it is not observed in the spectrum, and via a relatively slow

process it affords benzoyl radicals, which react with the starting material to give **19**. Based on these considerations, a hypothetical mechanism is proposed, that accounts for all the observed phenomena (Scheme 4.11).



Scheme 4.11. Proposed mechanism for the photochemical behavior of 2,6-dimethoxybenzoylbis(2,4,6-trimethylphenyl)phosphine oxide **7b**.

The fact that no phosphoryl radicals are observed is attributed to a facile dimerization of this species. This presumption is supported by ^{31}P NMR analysis of the products of the photolysis of **7b**, which reveals that diphosphine oxide $(15)_2$ is the major phosphorus-containing product. The proposed intermediate **20** is a carbene, which slowly dissociates into two benzoyl radicals. Carbenes readily react with alkenes, and when the photolysis of **7b** is carried out in cyclohexene, the additional generation of **19** in the dark is largely suppressed, indicating that a carbene may indeed be involved in the mechanism.

4.10 Conclusion

Phosphoryl diradicals **3a** $^{2\bullet}$ and **3b** $^{2\bullet}$, possess a low-energy triplet state, which is most likely the ground state, though strictly, the possibility of a ground state degeneracy can not be excluded. Together with the phosphinyl diradicals discussed in Chapter 3, these are the only known examples of heavy-atom radical centers, ferromagnetically coupled by *m*-phenylene. Though the spin coupling is expected to be weaker than in the case of phosphinyl diradicals, this is not reflected in the variable temperature ESR measurements. Therefore, this study

confirms the effectiveness of radicals of second-row atoms as spin carrying units in high-spin molecules as well as the versatility of *m*-phenylene as a ferromagnetic coupling unit.

Finally, it can be concluded that acylphosphine oxides are not suitable as precursors for the generation of phosphoryl radicals which can be incorporated in polyradicals, due to instability of the phosphoryl radicals at the temperature at which they are generated and the reactivity of the acyl radicals, leading to secondary products

4.11 Experimental Section

4.11.1 General Methods

For general procedures see Chapter 3. For X-ray crystal structure determination,⁷ data collection was performed at room temperature on a Enraf-Nonius CAD4F diffractometer with Zr-filtered Mo $K\alpha$ radiation, using the ω -2 Θ scan mode and $2\Theta_{\max} = 55^\circ$. Lattice parameters were obtained by least-square refinement of the setting angles of 25 reflections. Intensities were corrected for Lp effects, but not for absorption. The structures were solved by direct methods with SHELX86,²⁹ and the refinements were performed with SHELX76.³⁰ The non-H atoms were refined anisotropically, and the H-atoms were placed at calculated positions (C-H 1.00 Å) and refined riding on their bonded atoms with general isotropic thermal parameters. The refinement weights were calculated as $w = 1/\sigma^2(F_o)$. The scattering factors were those of Cromer and Mann³¹ and the anomalous-dispersion terms are from Cromer and Lieberman.³² The program package EUCLID was used for the calculation of geometries.³³ All calculations were carried out on an ULTRIX DEC system-5000.

UV irradiation was carried out using a 500 W high-pressure mercury lamp (either Müller Optik or Philips SP 500 W). Elemental analyses were performed on a Perkin Elmer Element Analyzer Model 240.

4.11.2 Synthesis

The synthesis of *P,P'*-Bis(2,4,6-tri-*t*-butylphenyl)-1,3-phenylenebis(phosphinous chloride), **5**, has been described in the previous chapter. The preparation of the *para* substituted isomer **4** has been carried out analogously and the spectral data of all intermediates are presented below.

Bis(2,4,6-tri-*t*-butylphenyl)phosphinic chloride 1 was synthesized from bromo-2,4,6-tri-*t*-butylphenyllithium and phosphoryl chloride according to a literature procedure.³⁴

***N,N,N',N'*-Tetraethyl-*P,P'*-1,4-phenylenebis(phosphonous diamide)**. Synthesis was carried out as described for **2** in paragraph 3.6.2, starting with 1,4-dibromobenzene. Recrystallization from hexane afforded pure product (43.2 g, 83%) as white, needle-shaped crystals: mp 101 °C; ^{31}P NMR (CDCl_3) δ 97.7; ^1H NMR (CDCl_3) δ 1.06 (12H, t, $J_{\text{HH}} = 7.1$ Hz, CH_3), 3.03 (8H, c, $J_{\text{HH}} = 7.1$ Hz, CH_2), 7.34 (4H, t, $J_{\text{PH}} = 4.0$ Hz, H-2); ^{13}C NMR (CDCl_3) δ 14.53 (s, CH_3), 42.71 (c, $J_{\text{PC}} = 16.6$ Hz, CH_2), 130.66 (c, $J_{\text{PC}} = 18.7$ Hz, C-2), 140.72 (c, C-1).

1,4-Phenylenebis(phosphonous dichloride). A procedure carried out as described for **3** in paragraph 3.6.2, afforded the product (3.6 g, 86%) from the bis(phosphonous diamide), as a white crystalline solid, pure enough to be used in the next reaction step without further purification: ^{31}P NMR (CDCl_3) δ 157.3; ^1H NMR (CDCl_3) δ 8.01 (4H, dd, $J_{\text{PH}} = 6.0$ Hz, $J_{\text{PH}} = 3.9$ Hz); ^{13}C NMR (CDCl_3) δ 130.29 (dd, $J_{\text{PC}} = 30.6$ Hz, $J_{\text{PC}} = 7.1$ Hz, C-2), 144.78 (d, $J_{\text{PC}} = 54.9$ Hz, C-1).

P,P'*-Bis(2,4,6-tri-*t*-butylphenyl)-1,4-phenylenebis(phosphinous chloride) **4*. The compound was prepared according to the procedure as described for **1** in paragraph 3.6.2, yielding a white solid (5.9 g, 102%³⁵). ^{31}P NMR (CDCl_3): δ 75.4, 76.3.

P,P'*-Bis(2,4,6-tri-*t*-butylphenyl)-1,4-phenylenebis(phosphinic chloride) **2a** and **2b*. Crude **4**³⁶ (obtained from 8.43 mmol 1,4-phenylenebis(phosphonous dichloride)) was dissolved in CH_2Cl_2 (75 mL), DMSO (4 mL) was added, and the mixture was heated under reflux overnight. The solvent was removed and the diastereoisomers (RS; RR + SS) were separated by flash chromatography (SiO_2 ; hexane/EtOAc 5:1). Finally, **2a** and **2b** were recrystallized from $\text{CH}_2\text{Cl}_2/\text{CH}_3\text{CN}$.

Racemic (RR + SS) **2a**: yield 1.56 g (25%, calculated from bis(phosphonous dichloride)): mp 251-253 °C; ^{31}P NMR (CD_2Cl_2) δ 43.3; ^1H NMR (CD_2Cl_2) δ 1.30 (36H, s, *o*-(CH_3)₃C), 1.34 (18H, s, *p*-(CH_3)₃C), 7.30 (4H, b s, H-2), 7.35 (4H, d, $J_{\text{PH}} = 5.4$ Hz, H-3'); ^{13}C NMR (CD_2Cl_2) δ 31.08 (s, *p*-(CH_3)₃C), 33.27 (s, *o*-(CH_3)₃C), 35.12 (s, *p*-(CH_3)₃C), 41.20 (s, *o*-(CH_3)₃C), 124.10 (c, $J_{\text{PC}} = 16.9$ Hz, C-3'), 124.93 (d, $J_{\text{PC}} = 134.2$ Hz, C-1'), 130.88 (t, $J_{\text{PC}} = 12.1$ Hz, C-2), 145.63 (dd, $J_{\text{PC}} = 123.6$, $J_{\text{PC}} = 2.5$ Hz, C-1), 154.58 (s, C-4'), 160.04 (d, $J_{\text{PC}} = 9.7$ Hz, C-2'). Anal. Calcd for $\text{C}_{42}\text{H}_{62}\text{Cl}_2\text{O}_2\text{P}_2$: C, 69.01; H, 8.56. Found: C, 68.87; H, 8.48.

Meso (RS) **2b**: yield 1.97 g (32% from bis(phosphonous dichloride)): subl. 260 °C; ^{31}P NMR (CD_2Cl_2) δ 43.3; ^1H NMR (CD_2Cl_2) δ 1.27 (36H, s, *o*-(CH_3)₃C), 1.35 (18H, s, *p*-(CH_3)₃C), 7.27 (4H, b s, H-2), 7.35 (4H, d, $J_{\text{PH}} = 5.3$ Hz, H-3'); ^{13}C NMR (CD_2Cl_2) δ 31.09 (s, *p*-(CH_3)₃C), 33.18 (s, *o*-(CH_3)₃C), 35.13 (s, *p*-(CH_3)₃C), 41.12 (s, *o*-(CH_3)₃C), 124.06 (c, $J_{\text{PC}} = 17.0$ Hz, C-3'), 124.91 (d, $J_{\text{PC}} = 130.9$ Hz, C-1'), 130.96 (t, $J_{\text{PC}} = 12.1$ Hz, C-2), 145.55

(dd, $J_{PC} = 123.6$, $J_{PC} = 2.5$ Hz, C-1), 154.63, (s, C-4'), 160.05 (d, $J_{PC} = 10.3$ Hz, C-2'). Anal. Calcd for $C_{42}H_{62}Cl_2O_2P_2$: C, 69.01; H, 8.56. Found: C, 68.87; H, 8.92.

***P,P'*-Bis(2,4,6-tri-*t*-butylphenyl)-1,3-phenylenebis(phosphinic chloride) 3a and 3b.**

Prepared from crude 1,3-phenylenebis(phosphonous chloride) **1** (paragraph 3.6.2)³⁶ by a procedure as described for the synthesis of **3a** and **3b**.

Racemic (RR + SS) 3a: yield 2.16 g (35%, calculated from **3** (2.5.2)): subl 260 °C; ^{31}P NMR (CD_2Cl_2) δ 43.6; 1H NMR (CD_2Cl_2) δ 1.20 (36H, b s, *o*-(CH_3)₃C), 1.24 (18H, s, *p*-(CH_3)₃C), 5.93 (1H, b s, H-2), 7.12 (4H, b s, H-3'), 7.60 (1H, tt, $J_{PH} = 17.2$ Hz, $J_{HH} = 8.9$ Hz, H-5), 8.20 (2H, b s, H-4); ^{13}C NMR (CD_2Cl_2) δ 31.29 (s, *p*-(CH_3)₃C), 33.09 (s, *o*-(CH_3)₃C), 34.98 (s, *p*-(CH_3)₃C), 41.12 (b s, *o*-(CH_3)₃C), 123.92 (c, $J_{PC} = 17.1$ Hz, C-3'), 125.95 (d, $J_{PC} = 132.4$ Hz, C-1'), 127.29 (t, $J_{PC} = 13.0$ Hz, C-5), 135.01 (c, C-4), 136.98 (b s, C-2), 141.91 (dd, $J_{PC} = 124.3$, $J_{PC} = 13.0$ Hz, C-1), 153.60, (s, C-4'), 160.08 (b s, C-2'). Anal. Calcd for $C_{42}H_{62}Cl_2O_2P_2$: C, 69.01; H, 8.56. Found: C, 68.90; H, 8.78.

Meso (RS) 3b: yield 1.42 g (23%, calculated from **3** (2.5.2)): mp 210-212 °C; ^{31}P NMR (CD_2Cl_2) δ 43.1; 1H NMR (CD_2Cl_2) δ 1.22 (36H, b s, *o*-(CH_3)₃C), 1.33 (18H, s, *p*-(CH_3)₃C), 6.93 (1H, b s, H-2), 7.29 (4H, d, $J_{PH} = 1.4$ Hz, H-3'), 7.40 (1H, c, H-5), 7.53 (2H, b s, H-4); ^{13}C NMR (CD_2Cl_2) δ 31.15 (s, *p*-(CH_3)₃C), 33.22 (s, *o*-(CH_3)₃C), 35.07 (s, *p*-(CH_3)₃C), 41.07 (b s, *o*-(CH_3)₃C), 124.12 (c, $J_{PC} = 17.1$ Hz, C-3'), 125.44 (d, $J_{PC} = 131.2$ Hz, C-1'), 127.73 (t, $J_{PC} = 13.3$ Hz, C-5), 134.54 (d, $J_{PC} = 8.5$ Hz, C-4), 135.13 (b s, C-2), 141.93 (dd, $J_{PC} = 125.1$, $J_{PC} = 12.3$ Hz, C-1), 154.31, (d, $J_{PC} = 4.2$ Hz, C-4'), 160.70 (b s, C-2'). Anal. Calcd for $C_{42}H_{62}Cl_2O_2P_2$: C, 69.01; H, 8.56. Found: C, 68.46; H, 8.54.

Acylidiphenylphosphine oxides **6a-d** were prepared according to known procedures.^{21,22,26}

Benzoyl-bis(2,4,6-trimethylphenyl)phosphine 14a. To a solution of dimesitylphosphine, **13**,³⁷ (0.27 g, 1.0 mmol) in THF (10 mL) at room temperature was added 1.6 M *n*-BuLi in hexane (0.65 mL, 1.05 mmol), and the mixture was boiled under reflux for 1 h. Benzoyl chloride (0.16 g, 1.12 mmol) was added and the mixture was refluxed for 1 h. After cooling to room temperature, ca. 10 mL of water was added. The THF was removed under reduced pressure, another 10 mL of water was added and the mixture was extracted with hexane. The organic phase was dried over $MgSO_4$ and the hexane was evaporated. Flash chromatography of the residue (SiO_2 ; hexane / EtOAc 9:1) afforded pure **14a** (0.21 g, 56%) as a yellow solid. ^{31}P NMR ($CDCl_3$) δ -1.31; 1H NMR ($CDCl_3$) δ 2.23 (12H, s, *o*- CH_3), 2.24 (6H, s, *p*- CH_3), 6.83 (4H, d, $J_{PH} = 3.2$ Hz, H-3), 7.31 (2H, t, $J_{HH} = 7.8$ Hz, H-3'), 7.43 (1H, t, $J_{HH} = 7.4$ Hz, H-4'), 7.88 (2H, m, H-2).

2,6-Dimethoxybenzoylbis(2,4,6-trimethylphenyl)phosphine 14b. The title compound was prepared from **13** and 2,6-dimethoxybenzoyl chloride using the same procedure as for the synthesis of **14a**. Yield 60 % : ^{31}P NMR (CDCl_3) δ 5.47; ^1H NMR (CDCl_3) δ 2.15 (12H, s, *o*- CH_3), 2.24 (6H, s, *p*- CH_3), 3.51 (6H, s, OCH_3), 6.31 (2H, d, $J_{\text{HH}} = 7.9$ Hz, H-3'), 6.77 (4H, d, $J_{\text{PH}} = 2.8$ Hz, H-3), 7.11 (1H, t, $J_{\text{HH}} = 8.4$ Hz, H-4'); ^{13}C NMR (CDCl_3) δ 20.83 (s, *p*- CH_3), 23.28 (d, $J_{\text{PC}} = 12$ Hz, *o*- CH_3), 55.30 (s, OCH_3), 103.32 (s, C-3'), 121.19 (d, $J_{\text{PC}} = 41$ Hz, C-1), 126.82 (d, $J_{\text{PC}} = 12$ Hz, C-1'), 129.02 (s, C-3), 130.60 (s, C-4'), 138.26 (s, C-4), 143.34 (d, $J_{\text{PC}} = 14$ Hz, C-2), 157.03 (s, C-2'), 210.56 (d, $J_{\text{PC}} = 39$ Hz, CO).

Benzoyl-bis(2,4,6-trimethylphenyl)phosphine oxide 7a. To a solution of **14a** (0.217 g, 0.5 mmol) in THF (5 mL) *t*-butylhydroperoxide (0.12 g 80% in di-*t*-butylperoxide, 1.0 mmol) was added. After stirring at RT for 30 min the solvent were evaporated. Flash chromatography of the residue (SiO_2 ; hexane / EtOAc 7:3) afforded pure **7a** (0.162 g, 72%) as a white solid: mp 143 °C; ^{31}P NMR (CDCl_3) δ 31.3; ^1H NMR (CDCl_3) δ 2.26 (6H, s, *p*- CH_3), 2.32 (12H, s, *o*- CH_3), 6.86 (4H, d, $J_{\text{PH}} = 3.8$ Hz, H-3), 7.43 (2H, t, $J_{\text{HH}} = 7.6$ Hz, H-3'), 7.54 (1H, t, $J_{\text{HH}} = 7.4$ Hz, H-4'), 8.45 (2H, d, $J_{\text{HH}} = 7.4$ Hz, H-2'); ^{13}C NMR δ 20.95 (s, *p*- CH_3), 23.29 (s, *o*- CH_3), 127.82 (d, $J_{\text{PC}} = 91$ Hz, C-1), 128.58 (s, C-3'), 130.10 (s, C-2'), 130.97 (d, $J_{\text{PC}} = 11$ Hz, C-3), 133.98 (s, C-4'), 136.77 (d, $J_{\text{PC}} = 48$ Hz, C-1'), 141.66 (s, C-4), 142.24 (d, $J_{\text{PC}} = 10$ Hz, C-2), 205.22 (d, $J_{\text{PC}} = 77$ Hz, CO).

2,6-Dimethoxybenzoylbis(2,4,6-trimethylphenyl)phosphine oxide 7b. The title compound was prepared from **14b**, using same procedure as described for the synthesis of **7a**. Yield 58%: mp 168 °C; ^{31}P NMR (CDCl_3) δ 31.3; ^1H NMR (CDCl_3) δ 2.27 (s, 6H, *p*- CH_3), 2.28 (s, 12H, *o*- CH_3), 6.55 (2H, d, $J_{\text{HH}} = 8.5$ Hz, H-3'), 6.83 (4H, d, $J_{\text{PC}} = 5.4$ Hz, H-3), 7.36 (1H, t, $J_{\text{HH}} = 8.4$ Hz, H-4'); ^{13}C NMR δ 20.96 (s, *p*- CH_3), 23.39 (s, *o*- CH_3), 55.74 (s, OCH_3), 104.23 (s, C-3'), 117.38 (d, $J_{\text{PC}} = 50$ Hz, C-1'), 129.16 (d, $J_{\text{PC}} = 90$ Hz, C-1), 130.51 (d, $J_{\text{PC}} = 11$ Hz, C-3), 133.48 (s, C-4'), 140.78 (s, C-4), 142.64 (d, $J_{\text{PC}} = 10$ Hz, C-2), 159.12 (s, C-2'), 210.32 (d, $J_{\text{PC}} = 80$ Hz, CO).

4.12 References

- 1 Wienk, M. M.; Janssen, R. A. J. *Chem. Commun.* **1996**, 1919.
- 2 Barone, V.; Grand, A.; Michino, C.; Subra, R. *J. Phys. Chem.* **1993**, *97*, 6355.
- 3 Puzat, F.; Girtli, H.; Ellinger, Y.; Subra, R. *J. Phys. Chem.* **1984**, *88*, 4581.
- 4 Mikami, H.; Saito, S.; Yamamoto, S. *J. Chem. Phys.* **1991**, *94*, 3415.
- 5 Nguyen, M. T.; Ha, T.-K., *Chem. Phys.* **1989**, *131*, 245.
- 6 de Waal, B. F. M.; Aagaard, O. M.; Janssen, R. A. J. *J. Am. Chem. Soc.* **1991**, *113*, 9471.
- 7 X-ray studies were performed by Dr. A. Schouten and Dr. J. A. Kanters (Bijvoet Center for Biomolecular Research, University of Utrecht, The Netherlands).

- 8 Ayant, Y.; Theveland, A.; Werbelow, L.; Tordo, P. *J. Magn. Reson.* **1987**, *72*, 251.
- 9 Winter, N. J.; Fossey, J.; Beccard, B.; Berchadsky, Y.; Villa, F.; Werbelow, L.; Tordo, P. *J. Phys. Chem.* **1986**, *90*, 6749.
- 10 Cetinkaya, B.; Hudson, A.; Lappert, M. F.; Goldwhite, J. *J. Chem. Soc., Chem. Commun.* **1982**, 609.
- 11 Winberg, H. E. *US Patent*, 3,239,519, 1966.
- 12 Geoffroy, M.; Lucken, E. A. C. *Mol. Phys.* **1972**, *24*, 335.
- 13 Spectral simulations were performed by Dr. E. Reijerse (University of Nijmegen, The Netherlands).
- 14 Ling, C.; Lahti, P. M. *J. Am. Chem. Soc.* **1994**, *116*, 8784.
- 15 Doi, T.; Ichimura, A. S.; Koga, N.; Iwamura, H. *J. Am. Chem. Soc.* **1993**, *115*, 8928.
- 16 Matsumoto, T.; Ishida, T.; Koga, N.; Iwamura, H. *J. Am. Chem. Soc.* **1992**, *114*, 9952.
- 17 Kanno, F.; Inoue, K.; Koga, N.; Iwamura, H. *J. Phys. Chem.* **1993**, *97*, 13267.
- 18 Berson, J. A. In *The Chemistry of Quinoid Compounds*: Patai, S., Rappaport, Z., Eds.; Wiley: New York, 1988; p 462.
- 19 Weil, J. A.; Bolton, J. R.; Wertz, J. E. *Electron Paramagnetic Resonance, Elementary Theory and Practical Applications* John Wiley & Sons, New York, 1993; p 179.
- 20 Dankowski M. In *The chemistry of organophosphorus compounds*; Hartly, F. R.; Patai, S., Eds.; John Wiley & Sons, Chichester, 1992; Vol 2, Chapter 4.
- 21 Lechtken, P.; Buethe, I.; Henne, A. DOS 28 30 927, **1980**.
- 22 Lechtken, P.; Buethe, I.; Jacobi, M. Trimborn, W. DOS 2909 994, **1980**.
- 23 Kamachi, M.; Ushio, Y.; Nozakura, S.; Ueda, F. *Polym. Prepr. Jpn.* **1987**, *36*, 113.
- 24 Kajiwara, A.; Konishi, Y.; Morishama, Y.; Schnabel, W.; Kuwata, K.; Kamachi, M. *Macromolecules* **1993**, *26*, 1656.
- 25 Sumiyoshi, T.; Schnabel, W.; Henne, A.; Lechtken, P. *Polymer* **1985**, *26*, 141.
- 26 Miller, A. J.; Stewart, D. *J. Chem. Soc., Perkin Trans.* **1977**, 1898.
- 27 The coupling constants are identical to those obtained for the bis(2,4,6-trimethylphenyl)-phosphoryl radical, prepared from the corresponding phosphinic chloride, using an electron rich olefin in combination with UV irradiation.
- 28 A different carbon-centered radical has been observed after photolysis of 2,4,6-trimethylbenzoyldiphenylphosphine oxide, resulting from the addition of the phosphoryl radical to the precursor. Kamachi, M.; Kuwata, K.; Sumiyoshi, T.; Schnabel, W. *J. Chem. Soc., Perkin Trans. 2* **1988**, 961.
- 29 Sheldrick, G. M., SHELX86, program for the solution of crystal structures, University of Göttingen, Germany, 1986.
- 30 Sheldrick, G. M., SHELX76, program for the solution of crystal structures, University of Cambridge, 1976.
- 31 Cromer, D. T.; Mann, J. B. *Acta Crystallogr., Sect A* **1968**, *24*, 321.
- 32 Cromer, D.T.; Liberman, J. *J. Chem. Phys.* **1970**, *53*, 1891.
- 33 Spek, A. L.; Sayre, D.; Eds *The EUCLID package in Computational Crystallography*, Clarendon Press, Oxford, 1982, p 528.
- 34 Yoshifuji, M.; Shima, I.; Inamota, N. *Tetrahedron Lett.* **1979**, 3963.
- 35 Contaminated, mainly by 1,3,5-tri-*t*-butylbenzene.
- 36 To improve the overall yield, no purification of this intermediate was carried out.
- 37 Bartlett, R. A.; Olmstead, M. M.; Power, P. P.; Sigel, G. A. *Inorg. Chem.* **1987**, *26*, 1941.

Chapter 5

High-Spin Cation Radicals of Methylene Phosphoranes

Abstract

*Novel di(cation radical)s and tri(cation radical)s are prepared by oxidation of 1,3-phenylenebis{[(4-*t*-butylphenyl)methylene]-triphenyl phosphorane} and 1,3,5-benzenetriyltris{[(4-*t*-butylphenyl)methylene]triphenyl phosphorane} precursors. The oligo(cation radical)s are investigated in frozen solutions using ESR spectroscopy. The di(cation radical) has a triplet state as evidenced from a $\Delta M_s = \pm 2$ ESR transition exhibiting hyperfine coupling to two identical phosphorus nuclei and is characterized by zero-field splitting parameters $D = 350$ MHz and $E = 0$ MHz. The corresponding tri(cation radical) possesses a quartet state with $D = 262$ MHz and $E = 0$ MHz, and exhibits a $\Delta M_s = \pm 3$ transition. Temperature dependent studies (4 - 100 K) reveal that the ESR intensities follow Curie's law, consistent with high-spin ground states. The stability of these oligo(cation radical)s is assessed via cyclic voltammetry at room temperature in THF solution. In addition, sterically crowded bis and trisphosphines have been synthesized as precursors for phosphine cation radicals, but electrochemical oxidation of these molecules affords species, which are not stable enough to be measured by ESR spectroscopy.*

5.1 Introduction

For the design of high-spin molecules, the nature of the radical center is an important aspect, since it determines the chemical stability and the spin density at the coupling unit. For effective spin alignment, the spin density at the coupling unit must be high, whereas the stability usually increases with the extension of the delocalization of the unpaired electron. In Chapters 3 and 4, phosphinyl and phosphoryl diradicals have been discussed, as examples of heavy-atom based radicals, which can be ferromagnetically coupled, when *m*-phenylene is

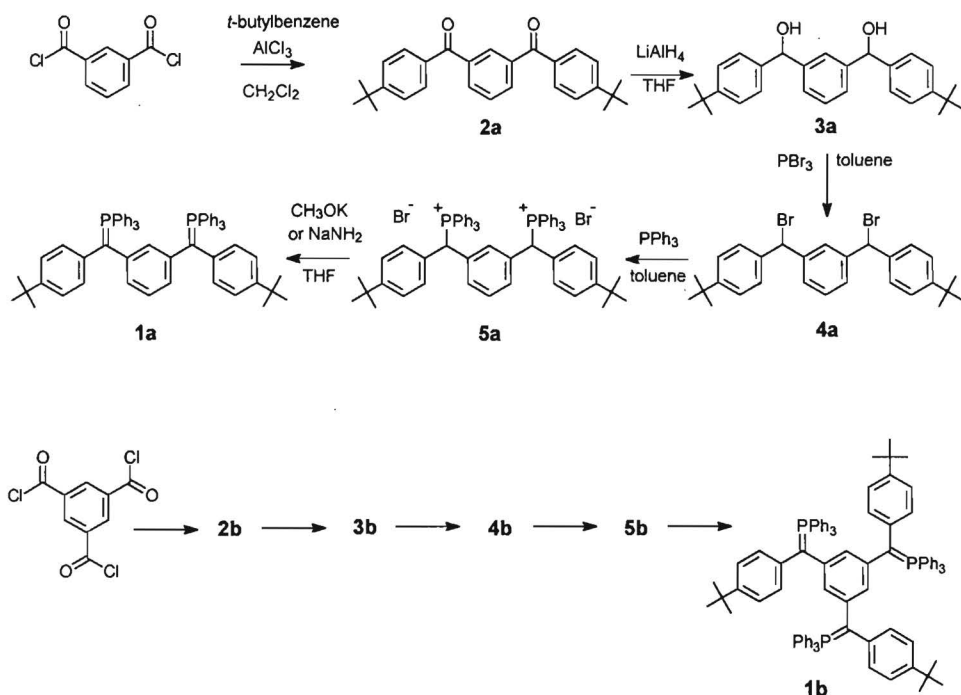
used as coupling unit.^{1,2} It was shown, that –in spite of the geometry at phosphorus and the limited overlap of the phosphorus valence 3p orbital with the 2p- π -*m*-phenylene orbitals–parallel spin alignment occurs between the unpaired electrons. One of the disadvantages of these radicals, however, remains their inherent instability. Therefore, other more stable spin-carrying units have been pursued.

Diphenylmethylene phosphorane cation radicals ($\text{Ph}_2\text{C}^+\text{PPh}_3^+$) form a class of radicals, which are more stable than phosphinyl and phosphoryl radicals. Compared to the well-known triarylmethyl radicals,³⁻⁶ substituted diphenylmethylene ($\text{Ph}_2\text{C}^+\text{X}$) radicals may provide a higher spin density at the methylene carbon atom directly linked to the 1,3-phenylene ring, which may be beneficial for a stronger exchange interaction. For example, ketyl radicals ($\text{Ph}_2\text{C}^+\text{O}^-$), which are isoelectronic with nitroxyl radicals ($\text{R}_2\text{N}^+\text{O}^-$), have recently been used for the preparation of high-spin molecules.^{7,8} While appealing for their stability, ketyl radicals and nitroxyl radicals exhibit an appreciable delocalization of the spin density onto the oxygen nucleus, which is estimated to be on the order of 50% for nitroxyl radicals.⁹ Diphenylmethylene phosphorane cation radicals ($\text{Ph}_2\text{C}^+\text{PPh}_3^+$) can be expected to give a higher spin density at the methylene carbon atom, because almost no direct delocalization of electron spin occurs onto the phosphorus nucleus.¹⁰⁻¹³ These open-shell molecules can be prepared by chemical oxidation of neutral precursors, affording the methylene phosphorane cation radicals as the only spin-carrying species. In this chapter, the formation and characterization of two novel high-spin molecules (**1a**²⁺²⁺ and **1b**³⁺³⁺) is described, which contain methylene phosphorane cation radicals as spin centers, linked via *m*-phenylene and 1,3,5-benzenetriyl coupling units, respectively.

Phosphine cation radicals ($\text{R}_3\text{P}^{+\cdot}$) form a second class of charged phosphorus-related radicals. These open-shell molecules can be generated by removing one electron from the phosphorus non-bonding orbital of a neutral phosphine. Triaryl phosphine cation radicals ($\text{Ar}_3\text{P}^{+\cdot}$) may even be stable at ambient temperature if the 2- and 6-positions of the aryl groups are substituted. This indicates that in this case the stability results from steric crowding around the radical center and not from the delocalization of the unpaired electron.^{14,15} With this in mind, two precursor molecules have been designed, in which sterically crowded diarylphosphinyl groups are linked via a *m*-phenylene ring and a 1,3,5-triazinetriyl ring, respectively. A two-electron oxidation of bisphosphine **7** is expected to afford the di(cation radical), in which two phosphorus-centered radicals are ferromagnetically linked via *m*-phenylene. Theoretical studies have indicated that the 1,3,5-triazine ring also acts as a ferromagnetic coupling unit.¹⁶ Hence, three-electron oxidation of trisphosphine **8** is expected to afford the corresponding tri(cation radical), in which three unpaired electrons are ferromagnetically coupled. 2,4,6-Trimethylphenyl rings were chosen as additional bulky substituents on the phosphorus atoms, in order to stabilize the cation radicals.

5.2 Synthesis of Methylene Phosphoranes

The synthesis of linear **1a** and star-shaped **1b** is outlined in Scheme 5.1. Isophthaloyl chloride or 1,3,5-benzenetricarbonyl trichloride were reacted with *t*-butylbenzene in a Friedel-Crafts acylation to afford 1,3-phenylene diketone (**2a**) and 1,3,5-benzenetriyl triketone (**2b**), respectively. Reduction to the corresponding diol (**3a**) and triol (**3b**) was accomplished with lithium aluminum hydride in THF and subsequent conversion to the corresponding bromides **4a** and **4b** was carried out using phosphorus tribromide in toluene. Reaction of **4a** and **4b**, respectively with triphenylphosphine provided the bis(phosphonium bromide) **5a** and tris(phosphonium bromide) **5b**. ^{31}P NMR and electrospray mass spectrometry confirm the proposed structure. Deprotonation with potassium methoxide or sodium amide in THF afforded the methylene phosphoranes **1a** and **1b**. These precursor compounds are stable at $-20\text{ }^\circ\text{C}$, but slowly decompose at room temperature.



Scheme 5.1. Synthesis of bis and tris(methylene phosphorane)s **1a** and **1b**.

5.3 Cyclic Voltammetry

Cyclic voltammetry in THF solution containing 0.1 M tetrabutylammonium hexafluorophosphate (TBAH) was used to assess the stability of the different redox states of the methylene phosphoranes. The cyclic voltammogram of the parent (diphenylmethylene)-triphenyl phosphorane (**6**, Scheme 5.2) displays a quasi-reversible one-electron oxidation at 0.18 V vs SCE, which is associated with the formation of a diphenylmethylene phosphorane cation radical (Figure 5.1). This cation radical has a limited stability and in a second scan an additional oxidation wave is observed at -0.08 V vs SCE. This secondary product is identified by ESR spectroscopy as 4,4'-biphenylenebis(methylene triphenyl phosphorane), formed by coupling of the cation radical with a second molecule of **6** via the *para* positions (Scheme 5.2).

The cyclic voltammogram of **1a** recorded at ambient temperature reveals two quasi-reversible one-electron oxidation waves at -0.14 and 0.23 V vs SCE (Figure 5.1). The quasi-reversible wave indicates that the doubly oxidized state of bis(methylene phosphorane) **1a** is moderately stable at room temperature. In this case, however, coupling reactions as observed for **6**, are effectively suppressed by the *para* *t*-butyl substituents on terminal phenyl rings. In a similar experiment, one-electron oxidations of the tris(methylene phosphorane) **1b** occurred at -0.29, -0.01, and 0.27 V vs SCE (Figure 5.1).

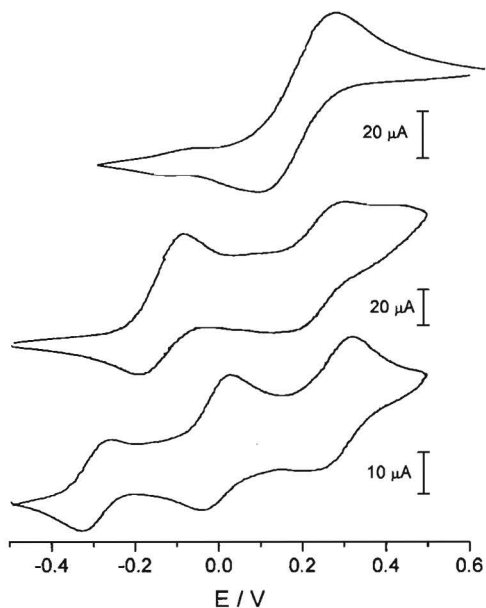
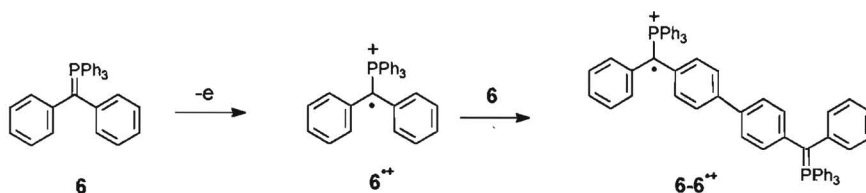


Figure 5.1. Cyclic voltammogram of methylene phosphoranes recorded at RT in THF/TBAH (0.1 M), scan rate 100 mV/s. (top): Parent methylene phosphorane **6**. (center): Bis(methylene phosphorane) **1a**. (bottom): Tris(methylene phosphorane) **1b**. Potential vs SCE calibrated against Fc/Fc^+ (0.47 V).



Scheme 5.2. Oxidation of methylene phosphorane **6**.

The electrochemical experiments demonstrate that the first oxidation potential decreases by nearly 0.5 V when the number of methylene phosphoranes linked to the central benzene unit increases from one to three. This decrease results from the increasing repulsive Coulombic interaction of the negative charges at the methylene carbon atoms. The effect of conjugation on the oxidation potential is likely to be small as a result of the non-resonant *meta* substitution pattern at the central ring. The final oxidation step for **6**, **1a**, and **1b** occurs at almost the same potential (0.18 - 0.27 V vs SCE). Similar effects have been described for perchlorotriarylmethyl anions.¹⁷

5.4 ESR Spectroscopy

Chemical oxidation of **6** at room temperature in THF –using iodine or AgBF_4 – produces the cation radical $6^{\bullet+}$, which exhibits a well-resolved ESR spectrum due to hyperfine coupling with a phosphorus nucleus ($A(\text{P}) = 74.5$ MHz) and the protons of the diphenylmethylene moiety ($A(\text{H}-1) = 7.60$ MHz, $A(\text{H}-2) = 3.28$ MHz, and $A(\text{H}) = 8.32$ MHz) (Figure 5.2).¹⁸ Under these conditions the cation radical is moderately stable.

When prepared via in situ electrochemical oxidation, the ESR spectrum initially indicates the formation of $6^{\bullet+}$, which under these conditions, however, rapidly couples oxidatively with a second molecule of **6** at the *para* positions to the adduct cation radical $6-6^{\bullet+}$ (Scheme 5.2). The ESR spectrum of $6-6^{\bullet+}$ (Figure 5.2) features a triplet of pentuplets resulting from hyperfine coupling with two identical ^{31}P nuclei ($A(\text{P}) = 32.82$ MHz) and four identical ^1H nuclei ($A(\text{H}) = 4.96$ MHz, at 3, 3', 5, and 5'-positions), identical to the ESR spectrum obtained after oxidation of 4,4'-biphenylenebis[phenylmethylenetriphenyl phosphorane] (**6-6**).¹⁹ When electrochemical oxidation is carried out at 240 K, the coupling reaction is suppressed.

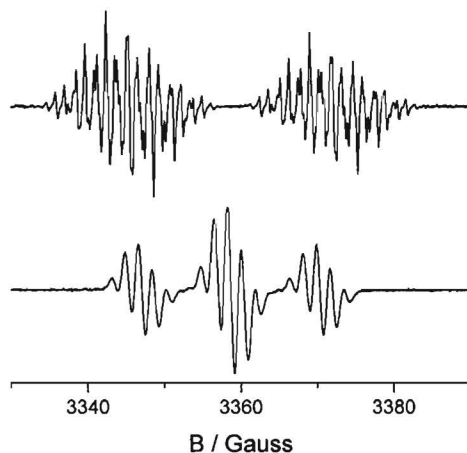
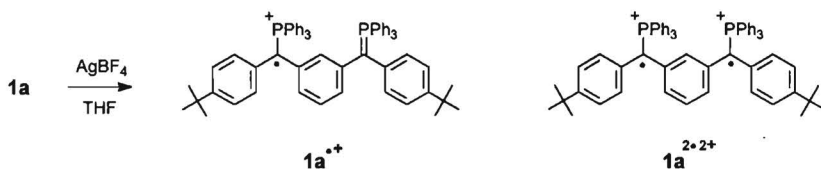


Figure 5.2. ESR spectra. (top): cation radical $6^{+\cdot}$ obtained via iodine-oxidation of **6** in THF. (bottom): the adduct cation radical $6-6^{+\cdot}$, prepared via electrochemical oxidation of **6** in THF/TBAH (0.1 M). Hyperfine parameters are described in the text.

To prevent side reactions, chemical oxidation of the bis and tris(methylene phosphoranes) **1a** and **1b** was carried out at 195 K (Scheme 5.3). At that temperature chemical oxidation of **1a** with AgBF_4 in THF initially produces the corresponding mono(cation radical) $1a^{+\cdot}$, which is characterized by a partially resolved ESR spectrum. Hyperfine interactions with one ^{31}P nucleus ($A(\text{P}) = 72.5$ MHz) and three different sets of two equivalent ^1H nuclei ($A(\text{H}) = 11.5, 3.75,$ and 2.75 MHz) indicate appreciable spin delocalization over both the terminal and central benzene rings. Further oxidation of $1a^{+\cdot}$ produces $1a^{2\cdot 2+}$. An excess of oxidant has to be avoided, because each singly oxidized methylene phosphorane can be further oxidized to the dication state, thereby losing the open-shell character.



Scheme 5.3. Oxidation of bis(methylene phosphorane) **1a**.

The anisotropic ESR spectrum recorded in frozen THF at 120 K reveals a superposition of the spectra of the mono(cation radical) and the triplet di(cation radical) (Figure 5.3). The two strong central transitions are attributed to the mono(cation radical) $1a^{+\cdot}$, possessing an essentially isotropic ^{31}P hyperfine coupling. The broad lines in the lateral

regions of the spectrum are the $\Delta M_s = \pm 1$ transitions of the di(cation radical) $1a^{2+2+}$, exhibiting a zero-field splitting characteristic of a triplet state. No ^{31}P hyperfine coupling is resolved in the ESR spectrum of $1a^{2+2+}$. Further evidence for the formation of di(cation radical) $1a^{2+2+}$ in a triplet state is obtained from the ESR spectrum recorded in $g = 4$ region, where the formally forbidden $\Delta M_s = \pm 2$ transition of $1a^{2+2+}$ is observed (Figure 5.3). The $\Delta M_s = \pm 2$ ESR spectrum exhibits a well-resolved 1:2:1 three-line pattern, resulting from hyperfine interaction of the $S = 1$ spin with two equivalent ^{31}P nuclei, which exhibit half the hyperfine coupling constant observed for mono(cation radical) $1a^{+}$. The identical hyperfine coupling with two ^{31}P nuclei directly relates the spectrum to the proposed structure of $1a^{2+2+}$.

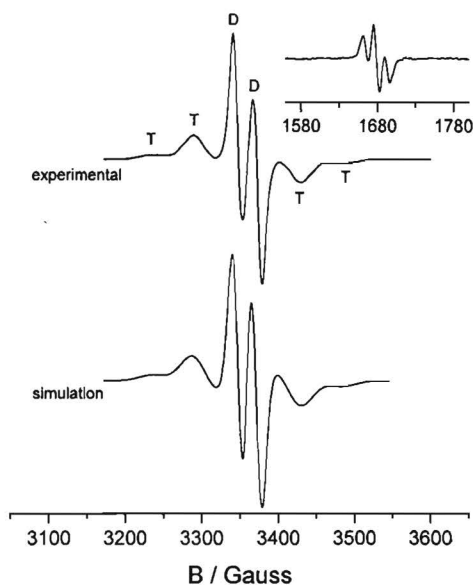
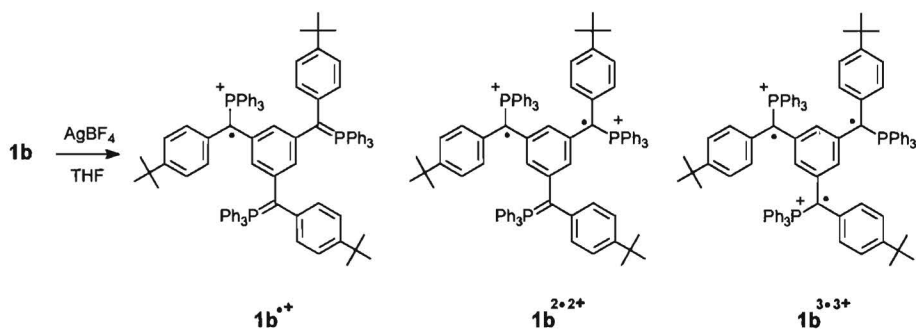


Figure 5.3. ESR spectra after oxidation of $1a$ with AgBF_4 , recorded in THF at 120 K. (top): Experimental spectrum showing the transitions assigned to $1a^{+}$ (D) and $1a^{2+2+}$ (T). The inset shows the $\Delta M_s = \pm 2$ ESR spectrum of $1a^{2+2+}$. (bottom): Simulated spectrum is a 2:5 superposition of the spectra of mono(cation radical) $1a^{+}$ and di(cation radical) $1a^{2+2+}$.

The ESR spectrum of mono(cation radical) $1a^{+}$ can be simulated, assuming an isotropic ^{31}P hyperfine coupling constant of $A(\text{P}) = 65$ MHz and a Gaussian line width of 45 MHz. The hyperfine coupling constant of $1a^{+}$ was used as starting point to obtain a spectral simulation for $1a^{2+2+}$. The remaining transitions in the ESR spectrum, attributed to $1a^{2+2+}$ are reproduced satisfactorily by taking $D = 350$ MHz and $E = 0$ MHz for the zero-field splitting parameters, an isotropic hyperfine constant of $A(\text{P}) = 32.5$ MHz (i.e. half the coupling constant of $1a^{+}$), and a Gaussian line width of 85 MHz (Figure 5.3). The increased line width

of $1\mathbf{a}^{2+}$ as compared to $1\mathbf{a}^{+}$ explains the loss of hyperfine structure in the $\Delta M_s = \pm 1$ triplet spectrum. Adding the simulated spectra of $1\mathbf{a}^{+}$ and $1\mathbf{a}^{2+}$ in a 2:5 ratio provides a good agreement with the experimental spectrum (Figure 5.3) and demonstrates the fairly efficient production of di(cation radical)s.

The zero-field splittings and hyperfine couplings obtained from the spectral simulation can be used to assess the electronic structure of $1\mathbf{a}^{+}$ and $1\mathbf{a}^{2+}$ in some detail. The isotropic hyperfine coupling $A(P) = 65$ MHz of $1\mathbf{a}^{+}$ suggests that the spin density at the methylene carbon is about 57%, when compared to $A(P) = 114$ MHz of the methylenetriphenyl phosphorane cation radical ($\text{Ph}_3\text{PCH}_2^{+}$), for which unit spin density on carbon can be assumed.¹¹ The zero-field splitting of $D = 350$ MHz for $1\mathbf{a}^{2+}$ corresponds within the point-dipole approximation to a distance between the radical centers of about 6.1 Å. Standard bond lengths suggest a distance of only 4.85 Å between the two methylene carbon nuclei. The increase is attributed to delocalization of spin density into the terminal 4-*t*-butylphenyl rings.



Scheme 5.4. Oxidation of tris(methylene phosphorane) $1\mathbf{b}$.

The ESR spectrum of $1\mathbf{b}$ recorded at 150 K after oxidation with AgBF_4 in THF at 195 K (Scheme 5.4), reveals the presence of the corresponding mono(cation radical), di(cation radical), and tri(cation radical) (Figure 5.4). In the central region of the ESR spectrum, the strong partially-resolved ^{31}P doublet of $1\mathbf{b}^{+}$ is observed, accompanied on each side by the transitions of triplet-state $1\mathbf{b}^{2+2+}$ showing some poorly resolved hyperfine structure. The broad lines in the outer parts are attributed to the $\Delta M_s = \pm 1$ transitions of $1\mathbf{b}^{3+3+}$ in a quartet state. The presence of high spin states can further be inferred from the ESR spectra at lower fields. In the $g = 4$ region (Figure 5.4), the 1:2:1 three-line pattern of the $\Delta M_s = \pm 2$ transition of $1\mathbf{b}^{2+2+}$ is observed, resulting from a triplet state with a hyperfine coupling to two identical ^{31}P nuclei with a coupling constant of about 33 MHz. In the outer regions of the half-field spectrum a weak pattern can be discerned, which is attributed to the $\Delta M_s = \pm 2$ of $1\mathbf{b}^{3+3+}$ in a quartet state. The $\Delta M_s = \pm 2$ spectrum of a quartet state is expected to exhibit four lines with a spacing of $D/2$, D , and $D/2$ respectively.²⁰⁻²² Experimentally, the two inner lines appear as clear

shoulders on the $\Delta M_s = \pm 2$ transition of $1b^{2+2+}$, while the outer two lines could not be identified with certainty. The seemingly weak intensity of the $\Delta M_s = \pm 2$ transition of $1b^{3+3+}$ compared to the $\Delta M_s = \pm 2$ transition of $1b^{2+2+}$ is a result of the increased spectral width. Direct spectral evidence of a quartet state for $1b^{3+3+}$ is obtained in the $g = 6$ region, where the $\Delta M_s = \pm 3$ transition is observed. This leaves no doubt on the formation of a quartet state. In literature only few organic polyradicals have been reported that exhibit a $\Delta M_s = \pm 3$ transition in the ESR spectrum.^{7,21-24}

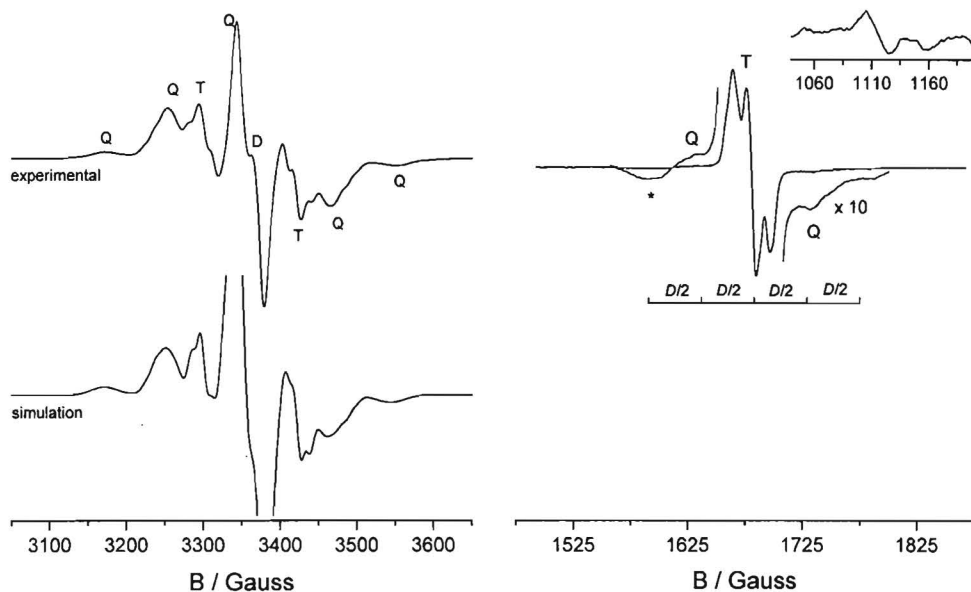


Figure 5.4. (left): $\Delta M_s = \pm 1$ ESR spectrum after oxidation of $1b$ with $AgBF_4$, recorded in THF at 120 K, showing the transitions assigned to $1b^{+}$ (D), $1b^{2+2+}$ (T), and $1b^{3+3+}$ (Q). The simulation is a 1:6:14 superposition of the spectra of mono(cation radical) $1b^{+}$, di(cation radical) $1b^{2+2+}$, and tri(cation radical) $1b^{3+3+}$. (right): $\Delta M_s = \pm 2$ ESR spectrum of di(cation radical) $1b^{2+2+}$ (T) and tri(cation radical) $1b^{3+3+}$ (Q). The signal marked with an asterisk is a background signal. The inset shows the $\Delta M_s = \pm 3$ ESR spectrum of $1b^{3+3+}$.

The spectral simulation of the $g = 2$ region of the mixture of the three oxidation states $1b^{+}$, $1b^{2+2+}$, and $1b^{3+3+}$ is shown in Figure 5.4. For this simulation the hyperfine and zero-field parameters of $1b^{+}$ ($S = 1/2$, $A(P) = 65$ MHz, Gaussian line width of 16 MHz) and $1b^{2+2+}$ ($S = 1$, $D = 350$, $E = 0$, $A(P) = 32.5$ MHz, Gaussian line width of 11.5 MHz) are identical to those of $1a^{+}$ and $1a^{2+2+}$, except for the $A(P)$ value of $1b^{2+2+}$ which is now used explicitly as a parameter to explain the partially resolved hyperfine coupling in the triplet spectrum. For $1b^{3+3+}$ the experimental spectrum can be simulated by taking $S = 3/2$, $D = 262$ MHz, $E = 0$

MHz and a Gaussian line width of 35 MHz (no ^{31}P hyperfine coupling was used in this case). By adding the spectra of $1\mathbf{b}^{2+}$, $1\mathbf{b}^{2+2+}$, and $1\mathbf{b}^{3+3+}$ in a 1:6:14 ratio, an acceptable correspondence was obtained with the experimental spectrum. The decreased zero-field splitting for $1\mathbf{b}^{3+3+}$ ($D = 262$ MHz) compared to $1\mathbf{a}^{2+2+}$ and $1\mathbf{b}^{2+2+}$ ($D = 350$ MHz) indicates a small increase in the distance between the unpaired electrons. Within a point-dipole approximation, the average distance increases from 6.1 Å to 6.7 Å.

5.5 Determination of Ground States

Variable temperature experiments in the range from $T = 4$ to 100 K on the $\Delta M_S = \pm 1$ and $\Delta M_S = \pm 2$ ESR transitions of $1\mathbf{a}^{2+2+}$ reveal Curie behavior ($I = C/T$), indicating that the population of the triplet state is independent of temperature (Figure 5.5). Hence, the triplet state is separated from the corresponding singlet state by either a very large or a very small energy gap.²⁵ Although it is not possible to resolve this ambiguity using ESR, it can be concluded that in either case the triplet state corresponds to a low-energy state.

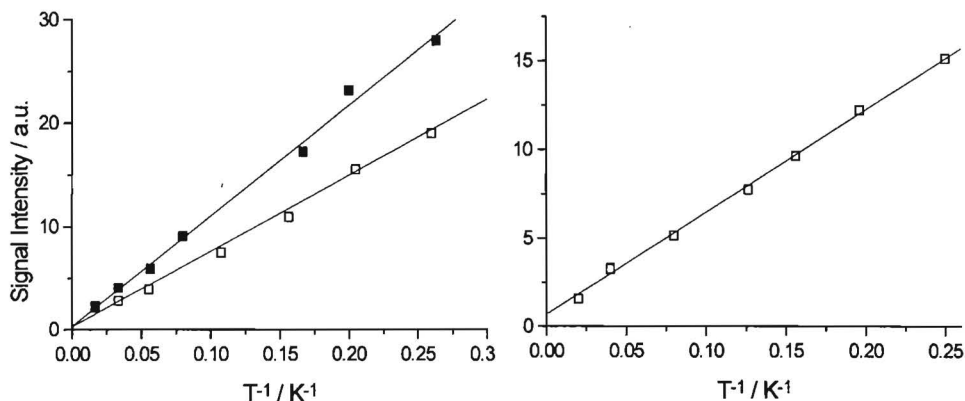
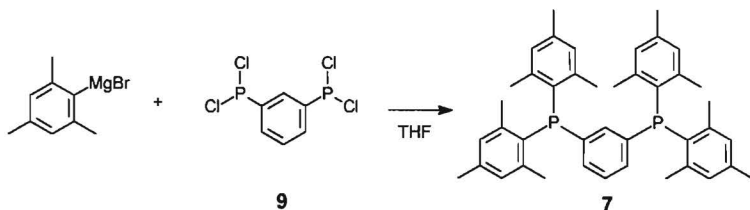


Figure 5.5. Temperature dependence of the ESR signal intensity. (left): $\Delta M_S = \pm 1$ (■) and $\Delta M_S = \pm 2$ signal (□) of di(cation radical) $1\mathbf{a}^{2+2+}$. (right): $\Delta M_S = \pm 1$ of tri(cation radical) $1\mathbf{b}^{3+3+}$. Solid lines are least-square fits to Curie's law.

The signals at $g = 4$ and $g = 6$ of $1\mathbf{b}^{3+3+}$ were too weak to be measured accurately at temperatures above 4 K, but the $\Delta M_S = \pm 1$ transitions follow Curie's law, when changing the temperature in the range from $T = 3.8$ to 100 K. It is therefore concluded that the triplet state of $1\mathbf{b}^{3+3+}$ is the ground state, although a near degeneracy with the corresponding doublet state cannot be excluded from this experiment.

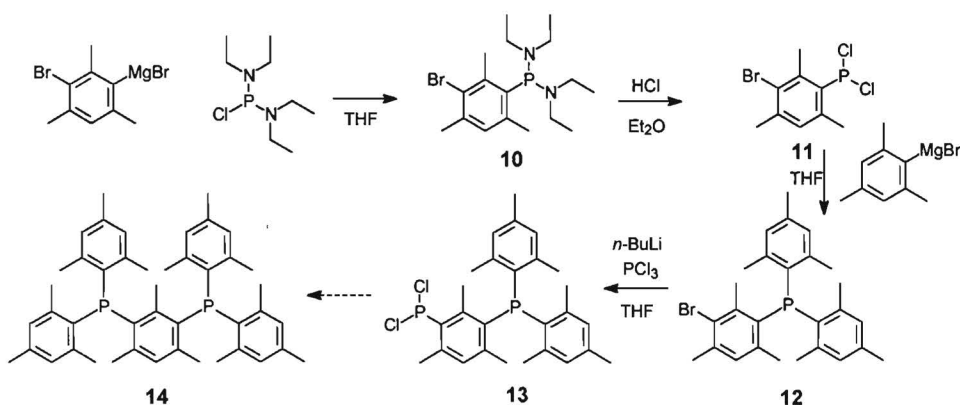
5.6 Synthesis of Bis and Triphosphines

1,3-Phenylenebis[bis(2,4,6-trimethylphenyl)phosphine] **7** was synthesized from 1,3-phenylenebis(phosphonous dichloride) **9** (Chapter 3), which was reacted with 4 equiv of the Grignard compound of 2,4,6-trimethylbromobenzene (Scheme 5.5). Purification of the product was the major difficulty, because the bisphosphine readily oxidized. Eventually, pure material was obtained by column chromatography, carried out in a glove box.



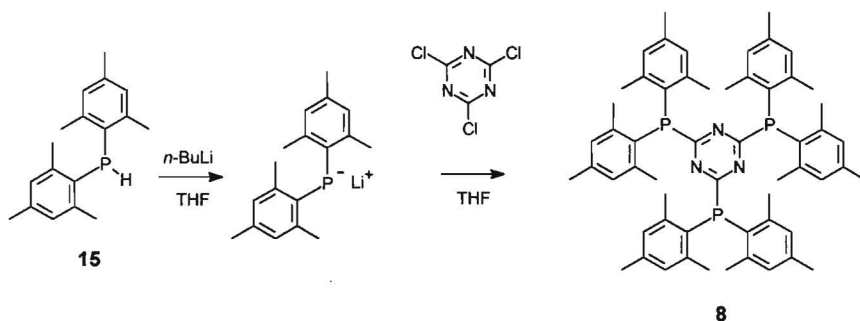
Scheme 5.5. Synthesis of bisphosphine **7**.

Additional methyl substituents at the 2, 4, and 6-positions of the central *m*-phenylene ring are expected to give rise to more stable cation radicals after oxidation. The synthesis of compound **14**, however, could not be achieved (Scheme 5.6). Compound **12** has been prepared, but the final two reaction steps were seriously hampered by poor yields and instability of the reaction products.



Scheme 5.6. Attempted synthesis of 2,4,6-trimethylphenylene linked bisphosphine **14**.

1,3,5-Triazinetriyl linked trisphosphine **8** was prepared in a single reaction step from bis(2,4,6-trimethylphenyl)phosphine (Scheme 5.7). Deprotonation with *n*-butyllithium and reaction with cyanuric chloride afforded **8**, which was isolated by column chromatography.



Scheme 5.7. Synthesis of trisphosphine **8**.

5.7 Cyclic Voltammetry

To examine the redox behavior of compounds **7** and **8**, and determine the stability of the different redox states, cyclic voltammetry measurements were performed. Measurements were carried out at ambient temperature in dichloromethane, containing 0.1 M tetrabutylammonium hexafluorophosphate (TBAH) as supporting electrolyte. The cyclic voltammogram of bisphosphine **7** reveals an oxidation wave at 0.79 V vs SCE (Figure 5.6). The corresponding reduction wave is significantly smaller, indicating that this oxidation step is only partially reversible. When the potential is increased, a second oxidation wave appears at 1.13 V vs SCE, which is nearly completely irreversible. In addition, the reduction wave of the first oxidation step further decreases. From these measurements it can be concluded that at room temperature the singly oxidized radical cation $7^{+\bullet}$ is only moderately stable and that the di(cation radical) is unstable under these circumstances.

ESR experiments with a combined ESR/electrochemical cell between 220 and 290 K fail to produce any signal that can be attributed to either mono or di(cation radical)s of compound **7**.²⁶ Because of the limited stability of the open-shell species, no further attempts have been made to generate the cation radicals by other methods. Introduction of methyl groups on the central phenylene ring is expected to give rise to more stable cation radicals, but the synthesis of such a compound turned out to be too complicated.

The cyclic voltammogram of compound **8** reveals two irreversible oxidation waves at significantly higher potential, due to the electron-withdrawing property of the central triazine ring (Figure 5.4). The absence of reduction waves indicates that at room temperature no stable cation radicals can be generated from this precursor. Therefore, no efforts were made to oxidize compound **8** by other methods, nor to measure the resulting cation radicals by ESR spectroscopy.

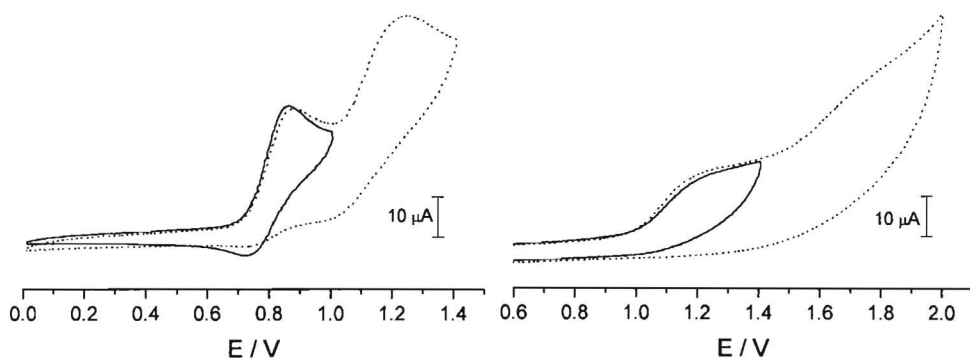


Figure 5.6. Cyclic voltammograms recorded at RT in $\text{CH}_2\text{Cl}_2/\text{TBAH}$ (0.1 M), scan rate 100 mV/s. (left): Bisphosphine **7**. (right): Trisphosphine **8**. Potential vs SCE, calibrated using Fc/Fc^+ (0.40 V).

5.8 Conclusion

Novel oligo(cation radical)s **1a**^{2•2+} and **1b**^{3•3+} have been prepared by chemical oxidation of the corresponding oligo(methylene phosphoranes). Using this method, the conversion of each methylene phosphorane moiety to the singly oxidized state is efficient, affording the desired di- and tri(cation radical)s in reasonable yields. This method of preparation of the open-shell moieties is much more effective than the in situ generation of phosphinyl and phosphoryl radicals described in Chapters 3 and 4. Moreover, the methylene phosphorane oligo(cation radical)s, are persistent in cold solution up to 200 K, which is also a significant improvement. The stability of triarylmethyl radicals or ketyl radicals—some of which are stable at room temperature—is not matched.^{3,7} Di- and tri(cation radical)s **1a**^{2•2+} and **1b**^{3•3+} have been fully characterized using ESR spectroscopy and possess a triplet and quartet ground state, respectively, as a consequence of the *meta* substitution pattern at the central benzene ring. Hence, it can be concluded that the spin coupling between the radical sites in these systems is sufficient. Because no deviation from Curie behavior is observed between 4 and 100 K, no magnitude for the triplet-singlet energy gap is obtained.

Bis and trisphosphines **7** and **8** have been prepared as precursors for phosphine di- and tri(cation radical)s. However, oxidation of these species leads to cation radicals which are not persistent enough to be measured by ESR, even though oxidation of similar monophosphines affords cation radicals, which are stable at ambient temperature.

5.9 Experimental Section

5.9.1 General Methods

For general procedures and equipment see Chapter 3. Electrochemical measurements were carried out with 0.1 M tetrabutylammonium hexafluorophosphate as supporting electrolyte using a Potentiostat Wenking POS73 potentiostat. The working electrode was a platinum disc (0.2 cm²), the counter electrode was a platinum plate (0.5 cm²), and a saturated calomel electrode was used as reference electrode, calibrated against a Fc/Fc⁺ couple. Electrospray mass spectra were recorded using a API 300 MS/MS mass spectrometer (PE-Sciex). The sample solutions were delivered directly to the ES-MS by a syringe pump (Harvard Apparatus) at a flow rate of 5 μ L/min.

5.9.2 Synthesis

1,3-Phenylenebis[(4-*t*-butylphenyl)methanone] 2a. Isophthaloyl chloride (10.15 g, 0.05 mol) in CH₂Cl₂ (20 mL) was added slowly to a suspension of AlCl₃ (16.0 g, 0.12 mol) in CH₂Cl₂ (50 mL) with stirring and cooling in an ice bath. Then *t*-butylbenzene (16.1 g, 0.12 mol) was added keeping the temperature at 20 °C. After stirring for 18 h at RT the mixture was poured onto ice. The organic phase was separated and the aqueous phase was extracted with CH₂Cl₂. The combined organic fractions were consecutively washed with dilute NaOH solution and water and dried over MgSO₄. Evaporation of the solvent and recrystallization from ethanol afforded pure **2** (14.6 g, 74%) as a white crystalline material: mp 153 °C; ¹H NMR (CDCl₃) δ 1.36 (18H, s, CH₃), 7.51 (4H, d, J = 8.6 Hz, H-2'), 7.62 (1H, t, J = 7.7 Hz, H-5), 7.78 (4H, d, J = 8.6 Hz, H-3'), 8.02 (2H, dd, J = 7.7 Hz and 1.8 Hz, H-4), 8.17 (1H, t, J = 1.8 Hz, H-2); ¹³C NMR (CDCl₃): δ 31.10 (CH₃), 35.16 (CCH₃), 125.44 (C-3'), 128.41 (C-5), 130.17 (C-2'), 131.13 (C-2), 133.21 (C-4), 134.26 (C-1), 138.01 (C-1'), 156.67 (C-4'), 195.63 (CO).

1,3,5-Benzenetriyltris[(4-*t*-butylphenyl)methanone] 2b. Compound **2b** was prepared from 1,3,5-benzenetricarbonyl trichloride using the same procedure as described for **2a**. Yield (3.52 g, 63%) as white crystals (2.65 g, 10 mmol): mp 181 °C; ¹H NMR (CDCl₃) δ 1.36 (27H, s, CH₃), 7.53 (6H, d, J = 8.4 Hz, H-2'), 7.81 (6H, d, J = 8.4 Hz, H-3'), 8.39 (3H, s, H-2); ¹³C NMR (CDCl₃): δ 31.03 (CH₃), 35.14 (CCH₃), 125.56 (C-3'), 130.16 (C-2'), 133.80 (C-1 + C-2), 138.36 (C-1'), 157.03 (C-4'), 194.67 (CO).

α,α' -Bis(4-*t*-butylphenyl)-1,3-benzenedimethanol 3a. A solution of compound **2a** (9.96 g, 25 mmol) in THF (50 mL) was added slowly to a suspension of LiAlH₄ (1.9 g, 50

mmol) in THF (50 mL) with stirring and cooling in an ice bath. After completion of the addition, the ice bath was removed and the mixture was stirred at RT for 30 min. Then water was added carefully to quench the excess of LiAlH_4 , whereafter the mixture was concentrated and extracted with diethyl ether. The collected organic fractions were washed with water, dried with MgSO_4 and concentrated to afford **3a** (9.73 g, 97%) as a white solid: ^1H NMR (CDCl_3) δ 1.29 (18H, s, CH_3), 2.15 (2H, b s, OH), 5.77 (2H, 2 s, CHOH), 7.24 - 7.34 (11H, m, H-4, H-5, H-2', H-3'), 7.47, 7.49 (1H, 2 s, H-2); ^{13}C NMR (CDCl_3): δ 31.32 (CH_3), 34.48 (CCH_3), 76.00 (COH), 124.59, 124.62 (C-2), 125.39 (C-3'), 125.55, 125.65 (C-4), 126.30, 126.35 (C-2'), 128.53 (C-5), 140.76 (C-1'), 144.02, 144.08 (C-1), 150.51 (C-4').

α,α',α'' -Tris(4-*t*-butylphenyl)-1,3,5-benzenetrimethanol 3b. The title compound was prepared from **2b** (2.24 g, 4 mmol), using the same procedure as described for **3a**, affording **3b** as a white solid. Yield (2.16 g, 96%): ^1H NMR (CDCl_3) δ 1.29 (27H, s, CH_3), 3.2 (3H, 2 b s, OH) 5.67 (3H, m, CHOH), 7.24 - 7.34 (15H, m, H-2, H-2', H-3'); ^{13}C NMR (CDCl_3): δ 31.27 (CH_3), 34.39 (CCH_3), 75.76, 75.80 (COH), 123.83 (C-2), 125.22 (C-3'), 126.34, 126.36 (C-2'), 140.63 (C-1'), 144.21, 144.27 (C-1), 150.22 (C-4').

1,3-Bis[bromo(4-*t*-butylphenyl)methyl]benzene 4a. PBr_3 (5.41 g, 20 mmol) in toluene (40 mL) was added slowly to a stirred suspension of **3a** (4.02 g, 10 mmol) in toluene (20 mL) at RT. The solution became clear and was stirred for 1 h. The mixture was poured onto ice and extracted two times with toluene. The combined organic layers were washed with water, dried over MgSO_4 and the solvent was evaporated affording **4a** (4.91 g, 93%) as a light yellow solid: ^1H NMR (CDCl_3) δ 1.30 (18H, s, CH_3), 6.25 (2H, 2 s, CHBr), 7.2 - 7.4 (11H, m, H-4, H-5, H-2', H-3'), 7.62 (1H, s, H-2); ^{13}C NMR (CDCl_3): δ 31.23 (CH_3), 34.57 (CCH_3), 54.96 (CBr), 125.54 (C-3'), 128.09 (C-2'), 128.15 (C-4), 128.58, 128.70 (C-2, C-5), 137.74, 137.81 (C-1'), 141.27, 141.39 (C-1), 151.22 (C-4').

1,3,5-Tris[bromo(4-*t*-butylphenyl)methyl]benzene 4b. The title compound was prepared from **3b** (1.69 g, 3 mmol), using the same procedure as described for **4a**, affording **4b** as a light brown solid. Yield (2.05 g, 91%): ^1H NMR (CDCl_3) δ 1.29 (27H, s, CH_3), 6.22 (3H, m, CHBr), 7.2 - 7.4 (15H, m, H-2', H-3'), 7.55 (3H, m, H-2); ^{13}C NMR (CDCl_3): δ 31.22 (CH_3), 34.58 (CCH_3), 54.45 (CBr), 125.60 (C-3'), 129.09 (C-2'), 128.35 (C-2), 137.43, 137.53, 137.63 (C-1'), 141.46, 141.59, 141.75 (C-1), 151.35 (C-4').

1,3-Phenylenebis{[(4-*t*-butylphenyl)methyl]triphenylphosphonium bromide} 5a. A solution of **4a** (1.06 g, 2 mmol) and triphenylphosphine (1.31 g, 5 mmol) was heated under reflux for 24 h. After cooling, the solvent was evaporated. Column chromatography of the residue (SiO_2 , $\text{CHCl}_3/\text{MeOH}$ 95:5 - 9:1) afforded **5a** (0.90g, 43%) as a white solid. ^{31}P NMR

(CDCl₃) δ 23.14, 23.18.²⁷ ES-MS m/z (M-Br⁻) calcd 971.4, obsd 971.3.

1,3,5-Benzenetriyltris{[(4-*t*-butylphenyl)methyl]triphenylphosphonium bromide} 5b. The title compound was prepared from **4b** (0.75 g, 1 mmol) using the same procedure as described for **5a**, affording **5b** as a white solid. Yield (0.60 g, 41%): ³¹P NMR(CDCl₃) δ 23.34, 23.78, 24.08.²⁸ ES-MS m/z (M-Br⁻) calcd 1457.5, obsd 1457.5.

1,3-Phenylenebis{[(4-*t*-butylphenyl)methylene]triphenyl phosphorane} 1a. NaNH₂ (4.0 mg, 0.1 mmol) was added to a suspension of **5a** (21 mg, 0.02 mmol) in THF (2 mL) at RT. The reaction mixture quickly turned deep red. After stirring at RT for 1 h, the conversion was complete as evidenced by NMR spectroscopy, using a small aliquot of the reaction mixture: ³¹P NMR (THF)²⁹ δ 6.39; ¹H NMR (THF)²⁹ δ 6.25 (2H, d, J = 8.0 Hz, H-4), 6.31 (4H, d, J = 8.6 Hz, H-2'), 6.36 (1H, t, J = 8.0 Hz, H-5), 6.61 (4H, d, J = 8.6 Hz, H-3'), 6.73 (1H, s, H-2), 7.23-7.30 (12 H, m, H-3''), 7.33-7.39 (6H, m, H-4''), 7.41-7.48 (12H, m, H-3'').

1,3,5-Benzenetriyltris{[(4-*t*-butylphenyl)methylene]triphenyl phosphorane} 1b. The title compound was prepared from **5b** (0.75 g, 1 mmol), according to the procedure described for **1a**: ³¹P NMR (THF)²⁹ δ 5.80; ¹H NMR (THF)²⁹ δ 6.06 (6H, d, J = 8.3 Hz, H-2'), 6.33 (3H, s, H-2), 6.54 (6H, d, J = 8.3 Hz, H-3'), 7.21-7.26 (18 H, m, H-3''), 7.29-7.45 (27H, m, H-2'' + H-4'').

Oxidation of bis(methylene phosphorane) 1a. A freshly prepared solution of phosphorane **1a** (0.02 mmol) in THF (2 mL) was cooled to -78 °C in a Schlenk vessel and a solution of AgBF₄ (0.5 mL, 0.08 M in THF) was added slowly by syringe. After stirring at -78 °C for 30 min., the mixture was transferred as quickly as possible into a pre-cooled ESR tube equipped with a ground-glass joint. After sealing, the sample was cooled to 77 K using liquid nitrogen.

Oxidation of tris(methylene phosphorane) 1b. Freshly prepared **1b** (0.02 mmol) in THF (2 mL) was reacted with AgBF₄ (0.75 mL, 0.08 M in THF), using the same procedure as described for the oxidation of **1a**.

1,3-Phenylenebis[bis(2,4,6-trimethylphenyl)phosphine] 7. Ca. one tenth of a solution of 2,4,6-trimethyl-bromobenzene (2.0 g, 10 mmol) in THF (20 mL) was added to magnesium (0.24 g, 10 mmol), and the mixture was heated carefully until an exothermic reaction started. The heating was removed and the remaining 2,4,6-trimethyl-bromobenzene solution was added at a rate sufficient to keep the solvent boiling. When the addition was complete the reaction mixture was heated under reflux for 1 hr. After cooling, the mixture was

decanted –preventing contact with air– in order to remove the remaining magnesium. Subsequently, tetrachloride **9**³⁰ (0.56 g, 2 mmol) in THF (10 mL) was added slowly and the mixture was stirred at RT for 4h. The THF was evaporated, diethyl ether was added and the mixture was washed with aqueous NH₄Cl and water. After drying over MgSO₄, the solvent was evaporated. Column chromatography of the residue (SiO₂; hexane / EtOAc 4:1), performed under a nitrogen atmosphere, afforded pure **7** (0.42 g, 34%) as a white solid:³¹H NMR (CDCl₃) δ 1.93 (24H, s, *o*-CH₃), 2.24 (12H, s, *p*-CH₃), 6.70 (8H, d, *J*_{PH} = 2.7 Hz, H-3'), 7.09 (1H, b t, *J*_{PH} = 5.5 Hz, H-2), 7.22 (1H, t t, *J*_{HH} = 7.5 Hz, *J*_{PH} = 2.2 Hz, H-5), 7.43 (2H, b t, *J* = 8.2 Hz, H-2); ¹³C NMR (CDCl₃) δ 22.67 (s, *p*-CH₃), 22.85 (d, *J*_{PC} = 15 Hz, *o*-CH₃), 127.71 (t, *J*_{PC} = 20 Hz, C-5), 19.91 (s, C-3'), 130.14 (d, *J*_{PC} = 19 Hz, C-1'), 134.45 (d, *J*_{PC} = 34 Hz, C-4), 137.34 (d d, *J*_{PC} = 13 Hz, *J*_{PC} = 3 Hz, C-1), 137.77 (s, C-4'), 138.24 (t, *J*_{PC} = 20 Hz, C-2), 142.44 (d, *J*_{PC} = 15 Hz, C-2').

2,4,6-Tris[bis(2,4,6-trimethylphenyl)phosphino]-1,3,5-triazine 8. To a solution of dimesitylphosphine **15**,³² (0.54 g, 2.0 mmol) in THF (25 mL) was added *n*-BuLi (1.3 mL, 1.6 M in hexane, 2.1 mmol) at RT, and subsequently, the mixture was boiled under reflux for 1 hr. After cooling to RT, cyanuric chloride (0.09 g, 0.5 mmol) was added and the mixture was boiled under reflux overnight. After cooling, the THF was evaporated and diethyl ether (50 mL) was added. The organic phase was washed with aqueous NH₄Cl solution and water, dried over MgSO₄ and the solvents were evaporated. Column chromatography (SiO₂, hexane / CHCl₃ 1:1) afforded pure **8** (0.30 g, 67%) as a yellow solid: mp 199 °C; ³¹P NMR (CDCl₃) δ -15.5; ¹H NMR (CDCl₃) δ 1.98 (36H, s, *o*-CH₃), 2.25 (18H, s, *p*-CH₃), 6.66 (12H, d, *J*_{PH} = 2.7 Hz, H-3'); ¹³C NMR (CDCl₃) δ 20.96 (s, *p*-CH₃), 23.10 (d, *J*_{PC} = 15 Hz, *o*-CH₃), 127.88 (d, *J*_{PC} = 12 Hz, C-1'), 129.34 (d, *J*_{PC} = 4 Hz, C-3'), 138.08 (s, C-4'), 143.18 (d, *J*_{PC} = 16 Hz, C-2'), 183.94 (d t, *J*_{PC} = 6 Hz, *J*_{PC} = 5 Hz, C-1).

5.10 References

- 1 Wienk, M. M.; Janssen, R. A. J.; Meijer, E. W. *J. Phys. Chem.* **1995**, *99*, 9331.
- 2 Wienk, M. M.; Janssen, R. A. J. *Chem. Commun.* **1996**, 1919.
- 3 Rajca, A. *Chem. Rev.* **1994**, *94*, 871.
- 4 Leo, M. *Ber.* **1937**, *70*, 1691.
- 5 Schlenk, W.; Brauns, M. *Ber.* **1915**, *48*, 661.
- 6 Luckhurst, G. R.; Pedulli, G. F.; Tiecco, M. *J. Chem. Soc. (B)* **1971**, 329.
- 7 Baumgarten, M. *Mol. Cryst. Liq. Cryst.* **1995**, *272*, 109.
- 8 Jang, S.-H.; Mitchell, C.; Jackson, J. E.; Kahr, B. *Mol. Cryst. Liq. Cryst.* **1995**, *272*, 147.
- 9 Forrester, A. R.; Hay, J. M.; Thomson, R. H. *Organic Chemistry of Stable Free Radicals*; Academic Press: London, 1968.

- 10 Lucken, E. A. C.; Mazeline, C. *J. Chem. Soc. A.* **1966**, 1074.
- 11 Lucken, E. A. C.; Mazeline, C. *J. Chem. Soc. A.* **1967**, 439.
- 12 Begum, A.; Lyons, A. R.; Symons, M. C. R. *J. Chem. Soc. A*, **1971**, 2388.
- 13 Lyons, A. R.; Neilson, G. W.; Symons, M. C. R. *J. Chem. Soc., Faraday Trans. 2* **1992**, 68, 807.
- 14 Culcasi, M.; Berchadsky, Y.; Grochi, G.; Tordo, P. *J. Org. Chem.* **1991**, 56, 3537.
- 15 Palau, C.; Berchadsky, Y.; Chalier, F.; Finet, J.-P.; Grochi, G.; Tordo, P. *J. Phys. Chem.* **1995**, 99, 158.
- 16 Ito, A.; Miyajima, H.; Yoshizawa, K.; Tanaka, K.; Yamabe, T. *Proceedings of the International Conference on Synthetic Metals*, Salt Lake City, Aug. 1996; to be published in *Synth. Met.*
- 17 Veciana, J.; Rovira, C.; Ventosa, N.; Crespo, N. I.; Palacio, F. *J. Am. Chem. Soc.* **1993**, 115, 57.
- 18 Buck, H. M.; Huizer, A. H.; Oldenburg, S. J.; Schipper, P. *Recl. Trav. Chim.* **1970**, 89, 1085.
- 19 Kooistra, C.; van Dijk, J. M. F.; van Lier, P. M.; Buck, H. M. *Recl. Trav. Chim.* **1973**, 92, 961.
- 20 Brickmann, J.; Kothe, G. *J. Chem. Phys.* **1973**, 59, 2807.
- 21 Rajca, A.; Utamapanya, S. *J. Am. Chem. Soc.* **1993**, 115, 2396.
- 22 Rajca, A.; Rajca, S.; Desai, S. R. *J. Am. Chem. Soc.* **1995**, 117, 806.
- 23 Weissman, S. I.; Kothe, G. *J. Am. Chem. Soc.* **1975**, 97, 2537.
- 24 Müller, U.; Baumgarten, M. *J. Am. Chem. Soc.* **1995**, 117, 5840.
- 25 Berson, J. A. In *The Chemistry of Quinoid Compounds*; Patai, S., Rappaport, Z. Eds.; Wiley: 1988; Vol II, Chapter 10.
- 26 Combined electrochemical ESR measurements were performed by Uwe Segelbacher, University of Stuttgart, Germany.
- 27 Different signals arise from diastereoisomeric *RS* and *RR + SS* isomers.
- 28 One signal arises from *RRR + SSS* isomers, the other two from the *RRS* and *SSR* isomers which contain two inequivalent phosphorus nuclei.
- 29 Non-deuterated THF was used in combination with an internal lock tube filled with deuterated acetone.
- 30 For the synthesis see Chapter 3 (compound 3).
- 31 Because the solid is a glass, no clear melting point could be observed.
- 32 Bartlett, R. A.; Olmstead, M. M.; Power, P. P.; Sigel, G. A. *Inorg. Chem.* **1987**, 26, 1941.

Chapter 6

Stable High-Spin Cation Radicals of *m-p-N*-Phenylaniline Oligomers

Abstract

*A series of linear and branched high-spin di- and tri(cation radical)s (1^{2+2+} , 3^{3+3+} , and 4^{3+3+}) has been prepared by oxidation of the corresponding oligo(meta-para-N-phenylaniline)s. These oligo(cation radical)s are stable under ambient conditions. The formation and properties of the cation radicals has been studied in detail by cyclic voltammetry and UV/visible/nearIR spectroscopy. ESR spectroscopy has provided the zero-field splittings, which are consistent with the topology of the molecules and the localization of the unpaired electrons. Variable temperature ESR measurements reveal that the high-spin states correspond to the lowest energy state. The stability of the high-spin *m-p*-aniline oligomers, and the possibility to extend these systems demonstrate that alternating meta and para aniline oligomers are promising building blocks for future polaronic ferromagnets.*

6.1 Introduction

In the previous chapters, different phosphorus-related radical centers have been evaluated as spin-carrying moieties in high-spin molecules. Using *m*-phenylene as ferromagnetic coupling unit, high-spin states were indeed observed, but the limited stability of the radical sites is a major drawback of these systems.

A particularly interesting alternative method to generate spin carrying units in an organic molecule or material is the oxidative or reductive doping of neutral π -conjugated segments, as put forward by Fukutome.¹ When these segments are linked via a ferromagnetic

coupling unit, doping of such a polymer may result in polaronic (radical ion) units, which are ferromagnetically coupled, yielding a high-spin polaronic polyradical (Figure 6.1).^{2,3} Preliminary results suggest that this concept may work, but poor characterization and low doping levels are the most serious problems encountered so far.⁴⁻⁶

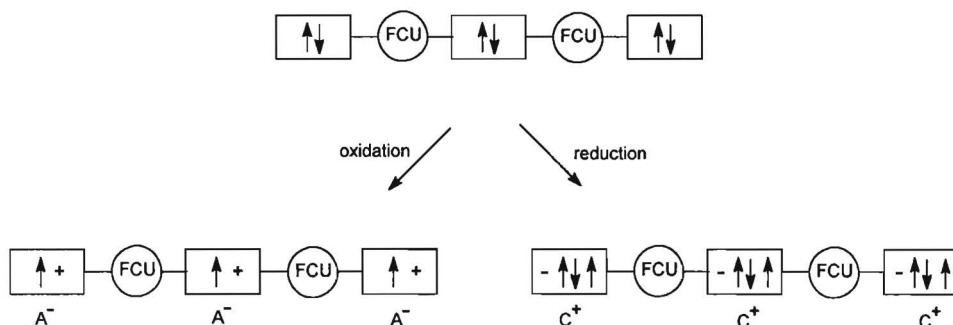
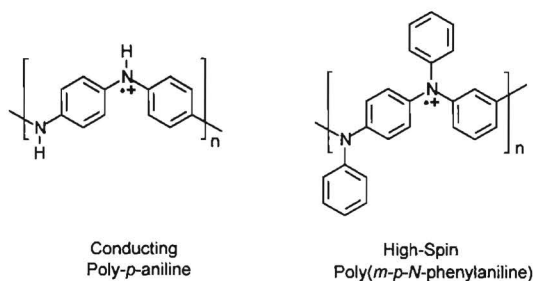


Figure 6.1. Schematic representation of a polaronic ferromagnetic chain. Oxidative or reductive doping of neutral π -conjugated segments creates unpaired electrons, which are aligned via a ferromagnetic coupling unit.

The doping of π -conjugated polymers is well known and leads to conducting materials. At high doping levels, however, most conjugated polymers have a low spin density, due to the formation of spinless bipolarons or π -dimers.⁷⁻⁹ One noticeable exception is the emeraldine salt of polyaniline, in which polarons are favored over the bipolaronic structure, resulting in a conducting polymer with considerable spin density. The repeat unit of the emeraldine salt comprises one polaron, effectively stabilized by delocalization of the unpaired electron and positive charge within two aniline units.^{10,11}

Moreover, nitrogen cation radicals have previously been incorporated in several high-spin oligoradicals as well, but the systems reported until now suffer from irreproducibility,⁴ insufficient doping,⁶ poor stability,¹²⁻¹⁶ or they cannot easily be extended to larger systems.^{17,18}

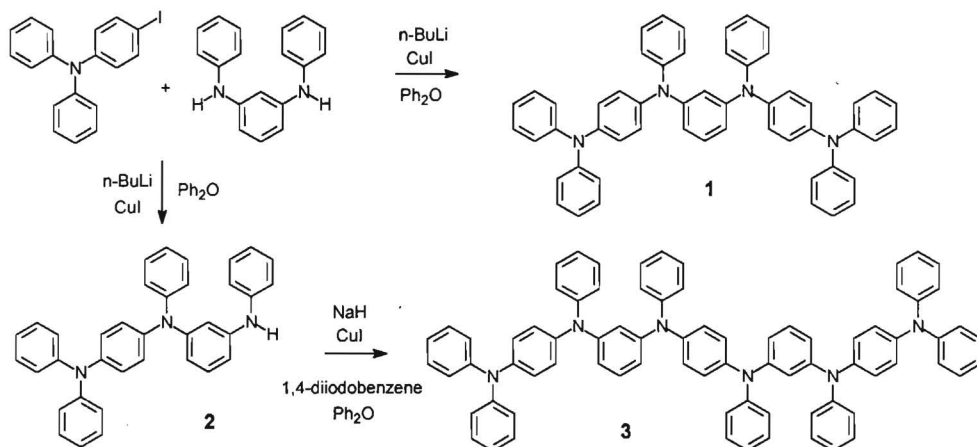
With this in mind, poly(*meta-para-N*-phenylaniline) has been designed as a candidate for a polaronic ferromagnetic chain. This polymer comprises an alternating sequence of *meta* and *para* substituted phenylene rings in the main chain. Upon oxidation to an intermediate oxidation state—in which one electron per two aniline units is removed—each *p*-phenylenediamine unit is expected to stabilize the unpaired electron, whereas the *meta* substituted phenylene ring will give rise to ferromagnetic coupling between the individual spins.



To verify this concept, linear and branched oligomers **1**, **3**, and **4** have been prepared. Oxidation of these precursor aniline oligomers to the intermediate oxidation state, results in ground-state high-spin molecules with a remarkable chemical stability.

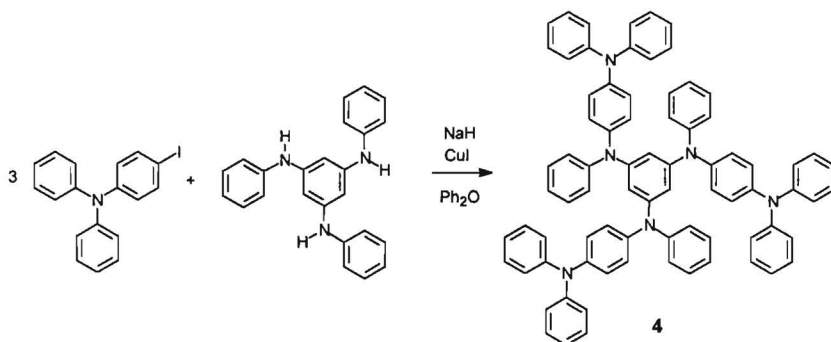
6.2 Synthesis

Tetra(amine) **1** was synthesized from *N,N'*-diphenyl-1,3-benzenediamine and 2 equiv of 4-iodo-*N,N'*-diphenylaniline in diphenyl ether at 200 °C, using *n*-butyllithium and copper(I) iodide as a catalyst (Scheme 6.1). The product was isolated by flash column chromatography and recrystallization from benzene.



Scheme 6.1. Synthesis of linear oligomers

When only 1 equiv of 4-iodo-*N,N*-diphenylaniline was used, a mixture of **1** and the singly coupled product **2**, as well as some unreacted *N,N'*-diphenyl-1,3-benzenediamine was obtained. These were separated by flash column chromatography. Reaction of **2** with 0.5 equiv of 1,4-diiodobenzene afforded hexa(amine) **3**. Star-shaped hexa(amine) **4** was synthesized from *N,N',N''*-triphenyl-1,3,5-benzenetriamine and 4-iodo-*N,N*-diphenylaniline (Scheme 6.2).



Scheme 6.2. Synthesis of star-shaped oligomer

6.3 Cyclic Voltammetry

Electrochemical studies on *N*-phenyl substituted oligomers **1**, **3**, and **4** were carried out in dichloromethane with 0.1 M tetrabutylammonium hexafluorophosphate (TBAH) as supporting electrolyte to investigate the redox behavior and the stability of the different redox states. The results are summarized in Table 6.1.

The cyclic voltammogram of **1** reveals four consecutive one-electron oxidation waves (Figure 6.2). The anodic and cathodic waves are separated by 62 - 65 mV, independent of the scan rate between 50 and 200 mV/s. These measurements demonstrate that at room temperature, oxidation of **1** is a chemically reversible process, in which up to four electrons can be removed, illustrating the outstanding stability of the generated cation radicals. The first two waves that occur at a potential of ca. 0.6 V, are due to the removal of one electron from each of the two *p*-phenylenediamine moieties present in the molecule. At a potential of ca. 1.1 V, both units are oxidized for a second time, giving rise to a third and fourth wave. The first and second set of oxidation waves occur at potentials comparable to the first and second oxidation wave of *N,N,N',N''*-tetraphenyl-1,4-benzenediamine (TPBD) (Figure 6.2). Comparison of the oxidation potentials of **1** with the values reported for the corresponding all-*para*-substituted isomer (0.42, 0.68, 1.15 and 1.31 V)¹⁹ reveals that E_2^0 and E_3^0 are identical, whereas E_1^0 and E_4^0 of **1** are higher and lower, respectively. The decreased separation between E_1^0 and E_2^0 , as well as between E_3^0 and E_4^0 , is consistent with the non-resonant nature of the central *meta*-phenylene unit.

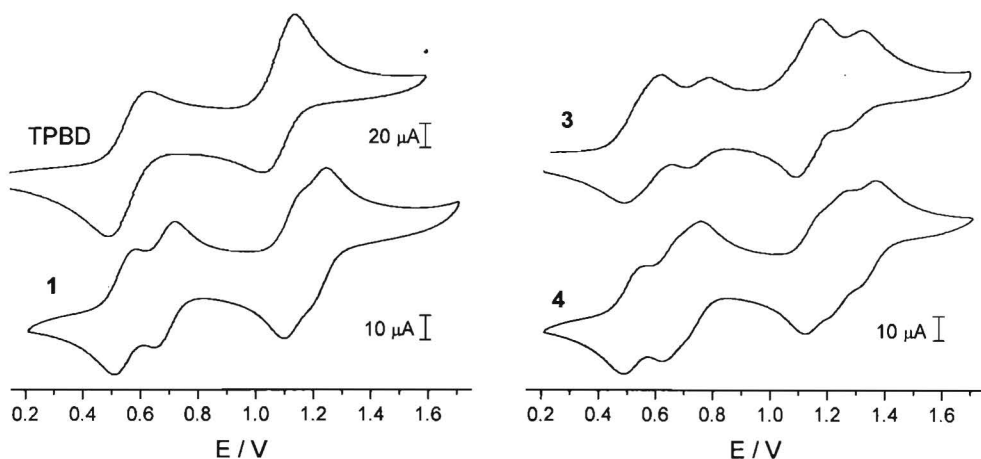


Figure 6.2. Cyclic voltammogram of oligo(*N*-phenylaniline)s recorded at RT in $\text{CH}_2\text{Cl}_2/\text{TBAH}$ (0.1 M), scan rate 100 mV/s. (top, left): TPBD. (bottom, left): Tetra(amine) **1**. (top, right): Linear hexa(amine) **3**. (bottom, right): Branched hexa(amine) **4**. Potential vs SCE, calibrated against Fc/Fc^+ (0.47 V)

The cyclic voltammogram of **3** also reveals four reversible redox waves, but the currents associated with the first and third wave are twice as large as for the second and the fourth wave (Figure 6.2). Hence, the first and third waves correspond to two-electron oxidations, while the second and fourth waves are one-electron oxidations. The peak-to-peak separations of the first and third wave (ca. 120 and 90 mV) are significantly larger than the theoretical value of 59 mV, while the second and fourth waves have peak-to-peak separations of 65 and 68 mV, respectively. This behavior can be rationalized, assuming that electrostatic repulsion favors the localization of the first two charges in the two outer *p*-phenylenediamine units. In this view, the third oxidation wave corresponds to the removal of an electron from the central unit, and occurs at significantly higher potential as a result of the charges in the two adjacent units. Similar effects occur at higher potential, when a second electron is removed from each unit.

In the cyclic voltammogram of **4** (Figure 6.2), six reversible oxidation waves of equal magnitude can be distinguished. Some of these transitions only show up as shoulders and it is not possible to determine the peak-to-peak separation accurately. However, for all six waves it is close to the theoretical value of 59 mV. In contrast to the linear hexamer **3**, the star-shaped isomer **4**, contains three equivalent *p*-phenylenediamine units. As a consequence, the charges in the dication cannot keep away from each other and six separate oxidation/reduction waves are observed.

Table 6.1. Redox Potentials of Oligomers vs SCE ^a

	E^0 (V)	E^0 (V)	E^0 (V)	E^0 (V)	E^0 (V)	E^0 (V)
TPBD	0.55			1.08		
1	0.54	0.68	-	1.13	1.22	-
3	0.56 ^b	0.56 ^b	0.75	1.14 ^b	1.14 ^b	1.29
4	0.52	0.66	0.74	1.16	1.29	1.34

^a Cell is calibrated against Fc/Fc^+ (0.47 V). ^b Peaks are unresolved.

Since exploratory experiments showed that the presence of a trace of a Brønsted acid has a very pronounced effect on the ESR spectra of the oxidized oligomers, the influence of acid on the redox properties was investigated. The addition of small portions of trifluoroacetic acid (TFA) to the electrolyte solution has a distinct effect on the voltammograms of the *N*-phenyl oligo(aniline)s **1**, **3**, and **4**. The first set of oxidation waves shifts 0.4 - 0.5 V to higher potential, whereas the reduction waves remain at the same position (Figure 6.3). Remarkably, this effect occurs much more rapidly in case of the star-shaped hexa(amine) **4**. With only 0.1% (v/v) of TFA the oxidation waves of **4** start shifting, whereas ten times more acid is needed to cause the same effect for compounds **1** and **3**.

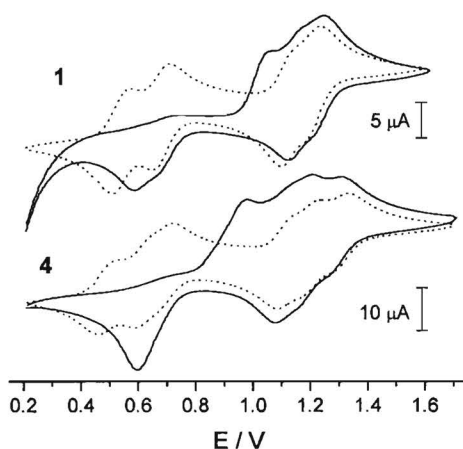


Figure 6.3. Effect of TFA on the cyclic voltammogram of oligo(*N*-phenylaniline)s recorded at RT in $\text{CH}_2\text{Cl}_2/\text{TBAH}$ (0.1 M), scan rate 100 mV/s. (top): Tetra(amine) **1** without TFA (.....) and with 4% (v/v) TFA (—). (bottom): Branched hexa(amine) **4** without TFA (.....) and with 4% (v/v) TFA (—). Potential vs SCE, calibrated against Fc/Fc^+ (0.45 V).

The increase of the first oxidation potentials in the presence of TFA can be rationalized by protonation of the *p*-phenylenediamine units at one of the nitrogen atoms. Since protonated amines carry a positive charge, withdrawal of an electron will be more difficult. Acid has no effect on the position of the second set of oxidation waves in the investigated acidity range, suggesting that deprotonation occurs as soon as a protonated *p*-phenylenediamine unit is oxidized. The fact that the reduction waves are not influenced by the acid is in full agreement with this explanation. Remarkably, the threshold for the acid-induced shift of the first oxidation waves is much lower for compound **4** than for the linear compounds **1** and **3**. Furthermore, on TPBD, lacking a 1,3-benzenediamine unit, addition of acid has no effect at all.²⁰ These differences are tentatively ascribed to a stabilization of the protonated 1,3-benzenediamine and 1,3,5-benzenetriamine rings via tautomeric intermediates (Figure 6.4).

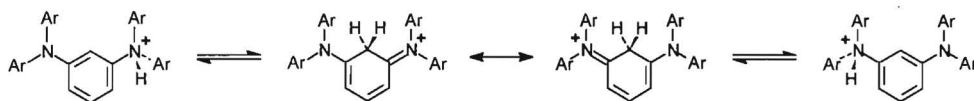


Figure 6.4. Stabilization of protonated 1,3-benzenediamines via tautomerization.

6.4 UV/visible/nearIR Measurements.

Quantitative conversion of the amines to the different oxidation states has been achieved by chemical oxidation with either thianthrenium perchlorate ($\text{Thi}^+\text{ClO}_4^-$)²¹ or phenyliodine(III) bis(trifluoroacetate) (PIFA)²² in dichloromethane or acetonitrile. The reaction was monitored by UV/visible/nearIR spectroscopy (Table 6.2).

The absorption spectrum of neutral **1** in dichloromethane shows a maximum at 3.93 eV and does not differ much from the absorption spectrum of TPBD. Apparently, the addition of a second *p*-phenylenediamine unit at the *meta* position of one of the outer phenyl rings does not influence the effective conjugation length significantly. Upon stepwise addition of small portions of $\text{Thi}^+\text{ClO}_4^-$, the absorption of neutral amine decreases, and new bands appear at 1.44 and 3.02 eV, with an isosbestic point at 3.42 eV (Figure 6.5). The new absorption bands have a close resemblance to the bands of singly oxidized TPBD. When 1 equiv of oxidant is added, the band at 3.93 eV has decreased to half the original intensity. Based on the difference between the oxidation potentials for the removal of the first and the second electron, one can expect that no significant disproportionation will occur, and most molecules will be singly oxidized to the mono(cation radical) $1^{+\bullet}$. Apparently, the optical spectrum of $1^{+\bullet}$ can be described with a superposition of the absorption bands of neutral and

singly oxidized *p*-phenylenediamine units. After addition of 2 equiv, the absorption at 3.93 eV has disappeared completely and the bands at 1.44 and 3.02 eV have reached maximum intensity. This demonstrates that in the di(cation radical) $\mathbf{1}^{2\cdot 2+}$ one electron is removed from each *p*-phenylenediamine unit. Further oxidation leads to a constant decrease in the bands at 1.44 eV and 3.04 eV, which are replaced by a new band at 2.09 eV. During this process isosbestic points are observed at 1.86, 2.80, and 3.81 eV. The absorption at 2.09 eV is similar to the absorption band of doubly oxidized TPBD, indicating that a second electron is removed from each *p*-phenylenediamine unit. When finally an excess of a reducing agent, like hydrazine monohydrate, is added to the fully oxidized aniline oligomer, the initial spectrum of $\mathbf{1}$ is recovered, demonstrating the reversibility of the oxidation process.

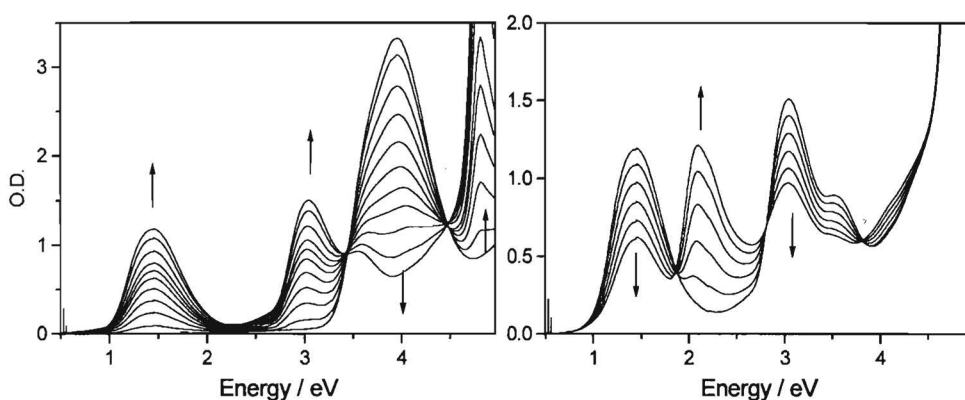


Figure 6.5. UV/visible/nearIR spectra of the stepwise oxidation of $\mathbf{1}$ with $\text{Th}^+\text{ClO}_4^-$ in CH_2Cl_2 at 295 K. (left): Oxidation of neutral $\mathbf{1}$ to the intermediate oxidation state $\mathbf{1}^{2\cdot 2+}$. (right): Further oxidation to $\mathbf{1}^{3+ \cdot 23}$. The band at 4.80 eV is caused by neutral thianthrene.

Careful analysis of the near-infrared region of the spectrum of $\mathbf{1}^{+\cdot}$ reveals a very weak band around 0.9 eV, which reaches a maximum after addition of 1 equiv of oxidizing agent (Figure 6.6). Because this band is not only very weak, but also very broad and partially overlapped by the much stronger band at 1.44 eV, the energy of the absorption maximum cannot be determined accurately. The broad band has the characteristics of an intervalence transition. Because $\mathbf{1}^{+\cdot}$ is a mixed-valence compound, intramolecular electron transfer can occur, giving rise to an intervalence band.²⁴⁻²⁶ For this band, the evolution of the optical density as a function of the average number of removed electrons is expected to increase linearly, until one electron is removed. At that stage $\mathbf{1}^{+\cdot}$ has reached the maximal concentration, and upon further oxidation to $\mathbf{1}^{2\cdot 2+}$ the intensity of the intervalence band will decrease again. The observed behavior of the absorption at 0.9 eV is in excellent agreement with this prediction (Figure 6.6). An intervalence band of $\mathbf{1}^{3+ \cdot 23}$, which is a mixed-valence

compound as well, is not observed in the region between 0.4 eV and the onset of the low-energy cation band. This may be due to a low intensity, or the absorption may be obscured by another band.

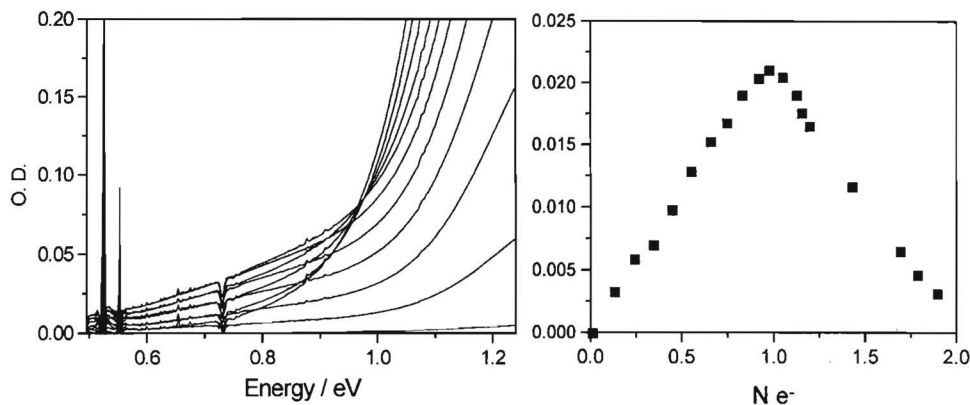


Figure 6.6. (left): Enlarged nearIR region of the electronic spectra during the stepwise oxidation from **1** to **1²⁺²⁺**. (right): Evolution of the intensity of the intervalence band of **1⁺** as a function of the average number of electrons removed.

Comparable optical spectra are recorded for the stepwise oxidation of the linear and star-shaped hexamers **3** and **4** (Table 6.2). The evolution of the intervalence bands for these compounds, however, is somewhat different. For the oxidation of **3** to **3³⁺³⁺**, the intensity of the intervalence bands goes through a maximum, whereas further oxidation again leads to an increasing signal. Unlike in the case **1³⁺**, an intervalence band for **3²⁺⁴⁺** and **3⁵⁺** is observed. The expected final decrease of this intervalence band intensity is not observed, because the oxidation strength of thianthrenium perchlorate is not sufficient to reach the **3⁶⁺** state. Remarkably, the intensity of the intervalence band related to **4⁺** and **4²⁺²⁺** already decreases well before an average of one electron per molecule has been removed. This indicates that for this oligomer a disproportionation equilibrium may exist, which favors tri(cation radical) **4³⁺³⁺** over the mono and di(cation radical). For higher oxidation states **3²⁺⁴⁺** and **3⁵⁺** a more distinct intervalence band is obtained.

When PIFA is used as oxidizing agent in dichloromethane/trifluoroacetic acid (9:1 v/v) solution the reaction does not progress beyond the intermediate oxidation state, which is characterized by the bands at 1.4 and 3.0 eV, even when an excess of PIFA is added. So, this method is very convenient to obtain the intermediate oxidation states **1²⁺²⁺**, **3³⁺³⁺**, and **4³⁺³⁺**.

Table 6.2. Spectral Data for the Oligo(amine)s and Corresponding Cation Radicals in CH_2Cl_2

Neutral compound		Intermediate oxidation state		Fully oxidized state	
eV (nm)		eV (nm)		eV (nm)	
TPBD	3.97 (312)	TPBD ²⁺	1.44 (861); 3.05 (407)	TPBD ²⁺	2.09 (593)
1	3.93 (316)	1²⁺²⁺	1.44 (861); 3.02 (411)	1⁴⁺	2.10 (590)
3	4.01 (309)	3³⁺³⁺	1.44 (861); 3.07 (404)	3⁶⁺	2.11 (588)
4	(3.93 (316))	4³⁺³⁺	1.34 (925); 2.97 (418)	4⁶⁺	2.08 (596)

6.5 Electrospray Mass Spectrometry

Electrospray mass spectrometry (ES-MS) is a very gentle technique, which allows pre-existing ions in solution to be transferred to the gas phase with minimal fragmentation. It has been widely used in the study of large biomolecules, such as proteins, which are converted to poly-cationic species by addition of dilute acid to the solution. Because doped aniline oligomers are charged species, no additional ionization technique is needed to obtain an ES-MS of these oligo(cation radical)s. Using a syringe pump, solutions of doped oligo anilines in dichloromethane were directly injected into the spectrometer.

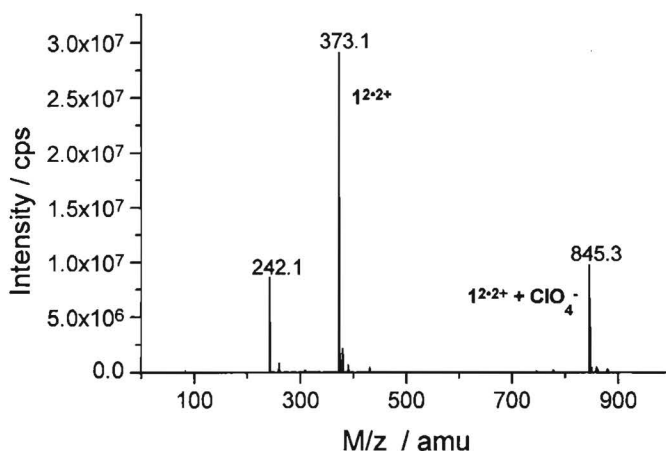


Figure 6.7. ES-MS of di(cation radical) 1^{2+2+} in CH_2Cl_2 . The peak at 242 amu results from a tetrabutylammonium cation contamination.²⁷

During the stepwise oxidation of compound **1** with $\text{Thi}^+\text{ClO}_4^-$, a series of ES-MS spectra is recorded. Even when no oxidant is added, significant signals are obtained that can be attributed to mono(cation radical) ($m/z = 746.3$), di(cation radical) ($m/z = 373.1$), and an adduct of a perchlorate anion to the di(cation radical) ($m/z = 845.3$). This is an indication that some oxidation occurs during the measurement. Upon addition of $\text{Thi}^+\text{ClO}_4^-$, the signal of mono(cation radical) decreases in favor of the signals of the doubly charged compound (Figure 6.7). There is, however, no quantitative correlation between the degree of oxidation and the ratio of the observed signals. Similar effects have also been encountered with ES-MS measurements on thiophene oligomers. Oxidation states with more than two charges are not observed, even if the average oxidation state –as inferred from UV/visible/nearIR measurements– is well beyond the doubly charged state. For oligomers **3** and **4**, no ES-MS measurements, other than the determination of the M^+ -peaks, have been carried out so far.

6.6 ESR Spectroscopy

When < 1 equiv of $\text{Thi}^+\text{ClO}_4^-$ is added to a solution of **1** in dichloromethane, the ESR spectrum at room temperature reveals nine poorly resolved lines which arise from hyperfine interaction ($A_{\text{iso}}(\text{N}) = 8$ MHz) with all four nitrogen nuclei in the molecule (Figure 6.8). This suggests a fast intramolecular electron-transfer between the neutral and singly oxidized *p*-phenylenediamine moieties of I^{++} , which is in agreement with UV/vis/nearIR measurements on the same species. The electron-transfer can be suppressed by lowering the temperature as demonstrated by the anisotropic spectrum recorded in frozen solution. This spectrum results from interaction with only two ^{14}N nuclei and can be simulated with $A_{\parallel}(\text{N}) = 37$ and $A_{\perp}(\text{N}) = 5$ MHz. Addition of acid also results in the localization of the unpaired electron in one of the *p*-phenylenediamine moieties, as evidenced by the five-line ESR spectrum with $A_{\text{iso}}(\text{N}) = 16$ MHz recorded in the presence of TFA at room temperature (Figure 6.8). This effect can be explained by protonation of the unoxidized half of the molecule, making this unit a weaker electron donor. By heating the acidified sample, the nine-line pattern reappears. Apparently, the charge transfer is a thermally activated process.

When 2 equiv of oxidant are added to **1**, the lines in the room temperature spectrum broaden significantly, leaving one featureless transition. This broadening is ascribed to the presence of triplet-state diradicals, causing line broadening via efficient spin-spin relaxation.

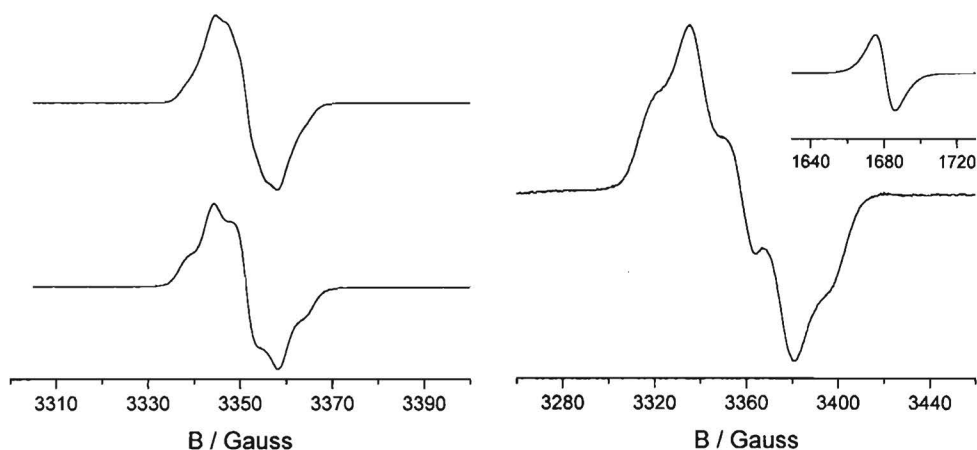


Figure 6.8. ESR spectra. (top, left): Cation radical I^{2+} in CH_2Cl_2 , recorded at RT. (bottom, left): Cation radical I^{2+} in $\text{CH}_2\text{Cl}_2/\text{TFA}$ (99:1 v/v), recorded at RT. (right): Di(cation radical) I^{2+2+} in $\text{CH}_2\text{Cl}_2/\text{TFA}$ (99:1 v/v), recorded at 110 K. The central line in the $\Delta M_s = \pm 1$ spectrum is due to some doublet impurity. Inset shows half-field signal recorded at 4 K.

The anisotropic spectrum of **1** oxidized with 2 equiv of $\text{Thi}^+\text{ClO}_4^-$, recorded in dichloromethane containing some TFA at 110 K, reveals the characteristic zero-field splitting associated with a high-spin state and a $\Delta M_s = \pm 2$ transition at half field. These ESR signals are attributed to the di(cation radical) 1^{2+2+} in a triplet state. The zero-field parameters ($D = 110$ MHz; $E \approx 0$ MHz) have been determined by simulation of the $\Delta M_s = \pm 1$ transitions of the ESR spectrum. Assuming a point-dipole approximation for the zero-field splitting, $D = 110$ MHz corresponds to an average distance between the unpaired electrons of 8.7 Å. This is consistent with a separation of 9.8 Å between the centers of the *p*-phenylenediamine moieties, as estimated from standard bond lengths, assuming a stretched planar geometry. In dichloromethane without TFA, the anisotropic spectrum reveals just one strong line at $g = 2$ and no transition at half field. In other solvents like chloroform, acetonitrile, and THF no additional acid is needed to bring about the zero-field splitting and half-field signal. Therefore, the unusual behavior in pure dichloromethane cannot simply be attributed to the absence of acidic protons and it is tentatively ascribed to conformational effects that may occur in a dichloromethane matrix.

The ESR spectrum of 3^{2+} is obtained after oxidation of **3** with < 1 equiv of oxidant. The room temperature spectrum reveals a 1:2:3:2:1 five-line pattern ($A_{\text{iso}}(\text{N}) = 16$ MHz), irrespective of the presence of acid. This pattern results from interaction with only two nitrogen atoms (Figure 6.9). Due to the inequivalence of the three *p*-phenylenediamine units, the singly oxidized hexa(amine) 3^{2+} does not display intramolecular electron transfer, as

observed for 1^{++} . When more oxidant is added, the spectrum changes gradually into a nine-line pattern ($A_{\text{iso}}(\text{N}) = 8 \text{ MHz}$), which is reached just before 2 equiv are added (Figure 8). This pattern is caused by a diradical with a strong exchange interaction ($|J| \gg |A(\text{N})|$), but weak dipolar spin-spin interaction between the unpaired electrons. Electrochemical studies indicated that in the di(cation radical) 3^{2+2+} the charges –and therefore also the unpaired electrons– are localized within the two outer *p*-phenylenediamine units as a result of electrostatic repulsion. The long distance will reduce the dipolar spin-spin interaction. Generally, when the exchange interaction is large as compared to the hyperfine coupling ($|J| \gg |A(\text{N})|$), the ESR spectrum of the diradical exhibits a hyperfine pattern corresponding to twice the number of nuclei, with a coupling constant $A(\text{N})/2$.^{28,29} The experimental nine-line spectrum with $A_{\text{iso}}(\text{N}) = 8 \text{ MHz}$ is in agreement with this description.

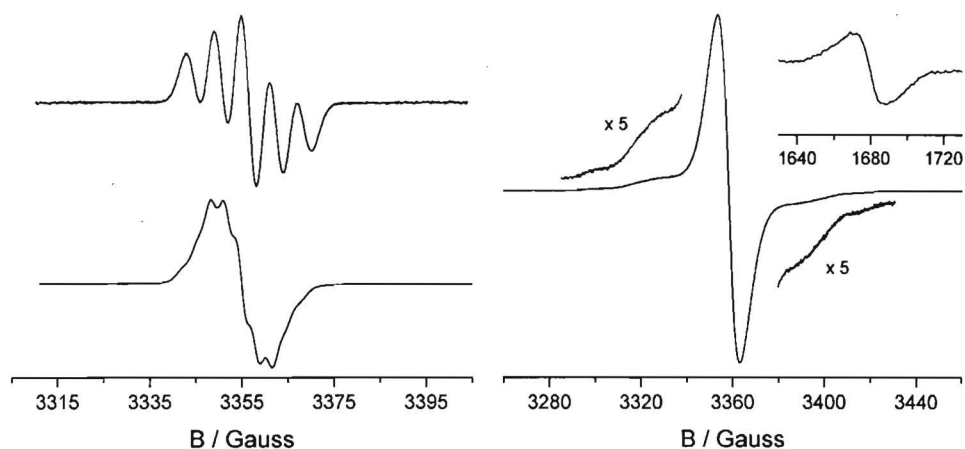


Figure 6.9. ESR spectra. (top, left): Cation radical 3^{++} in CH_2Cl_2 , recorded RT. (bottom, left): Di(cation radical) 3^{2+2+} in CH_2Cl_2 , recorded at RT. (right): Tri(cation radical) 3^{3+3+} in $\text{CH}_2\text{Cl}_2/\text{TFA}$ (99:1 v/v), recorded at 110 K. Inset shows half-field signal recorded at 4 K.

Oxidation beyond the dicationic state causes broadening of the room temperature spectrum due to the presence of a high-spin species. In frozen solution, the anisotropic spectrum of the tri(cation radical) 3^{3+3+} is dominated by a strong transition at $g = 2$ (Figure 6.9). Alongside of this line, broad shoulders are observed that are attributed to the tri(cation radical) 3^{3+3+} in a quartet state, and can be simulated using $D = 77 \text{ MHz}$ and $E \approx 0 \text{ MHz}$ as zero-field parameters. According to the simulation, the quartet spectrum does not completely account for the intense central transition. The $\Delta M_s = \pm 2$ transition of 3^{3+3+} is significantly broader than the half-field signal of the triplet state 1^{2+2+} . This is consistent with the expected zero-field splitting on the half-field signal of a quartet state.³⁰⁻³² The actual

D -splitting on the $\Delta M_s = \pm 2$ transition, however, is obscured by the broad lines that result from hyperfine interaction with the nitrogen nuclei. A $\Delta M_s = \pm 3$ transition could not be detected, not even at 4 K. This can be rationalized by the theoretical ratio of the $|\Delta M_s| = 1, 2,$ and 3 transitions which is $1 : (D/B_0)^2 : (D/B_0)^4$.³²⁻³⁵ Due to the relatively small D value, the $\Delta M_s = \pm 3$ transition signal is extremely weak and not detected.

In a dipolar approximation, the magnitude of D is proportional to d^{-3} , where d is the average distance between the unpaired electrons. In case of a triradical, the experimental D will be the average of the interactions between each pair of electrons. Assuming the distance between the unpaired electrons in adjacent units of 3^{3+} to be similar to the distance in 1^{2+2+} , it is possible to make an estimate for $D(3^{3+3+}) \approx [2 D(1^{2+2+}) + D(1^{2+2+}) / 8] / 3 \approx 78$ MHz, which is in excellent agreement with the experimental value of 77 MHz.

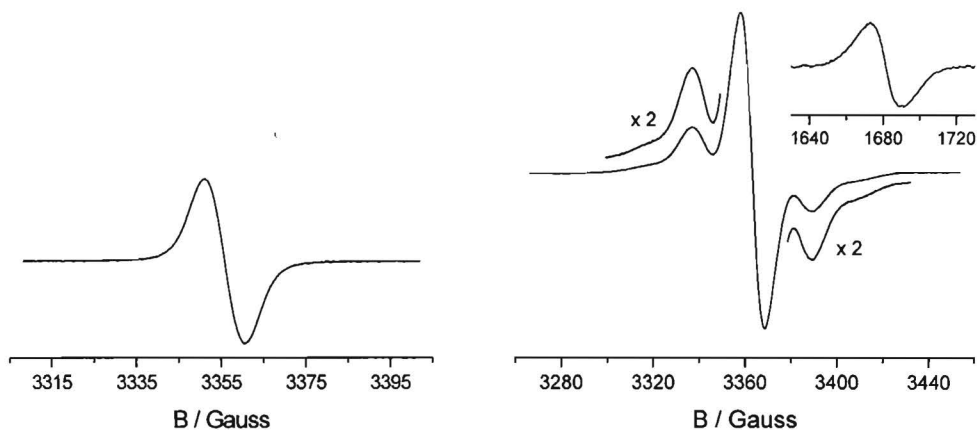


Figure 6.10. ESR spectra. (left): Branched oligomer **4**, oxidized to a minimal extent in CH_2Cl_2 , recorded at RT. (right): Tri(cation radical) 4^{3+3+} in $\text{CH}_2\text{Cl}_2/\text{TFA}$ (99:1 v/v), recorded at 4 K. Inset shows half-field signal recorded at 4 K.

In contrast with oligomers **1** and **3**, oxidation of **4** immediately leads to one broad ESR transition at room temperature, even when much less than 1 equiv of oxidant is used (Figure 6.10). This behavior does not change when TFA is added. Apparently, high-spin species are generated at a very low oxidation level. This is confirmed by the spectra recorded at low temperature. After addition of only 1 equiv of oxidant the spectrum reveals the five-line pattern of a quartet state, which, apart from an increasing intensity, does not change upon addition of more oxidant up to 3 equiv (Figure 6.10). In the $g = 4$ region a very broad $\Delta M_s = \pm 2$ transition is detected, but again no signals could be observed in the $\Delta M_s = \pm 3$ region. These signals are attributed to the tri(cation radical) 4^{3+3+} in a quartet state. The observation of the quartet tri(cation radical) at low doping level can be explained by a disproportionation

equilibrium that favors the tri(cation radical) over the mono(cation radical).^{36,37} The early decrease of the intensity of the intervalence band in the optical spectra recorded during the stepwise oxidation of **4** is in agreement with this explanation. Spectral simulation of the $\Delta M_s = \pm 1$ part of the ESR spectrum provides an estimate of the zero-field splitting parameters $D = 68$ MHz and $E \approx 0$, suggesting an average distance of 10.5 Å between the unpaired electrons. The increased average distance for **4**^{3•3+} as compared to **1**^{2•2+} and **3**^{3•3+} can be explained by the increased electrostatic repulsion resulting from the star-shaped topology of **4**^{3•3+}.

6.7 Determination of Ground States

6.7.1 Variable Temperature ESR Spectroscopy

Variable temperature ESR experiments were carried out between 4 and 100 K, in order to determine the ground states of the observed high-spin molecules. In this temperature range, the signal intensity of both the $\Delta M_s = \pm 1$ and $\Delta M_s = \pm 2$ transitions of **1**^{2•2+} follows Curie's law ($I = C/T$), indicating that no population or depopulation of the triplet state occurs in this temperature region (Figure 6.11). This means that the energy gap from the triplet to the singlet state is either much larger or much smaller than the thermal energy in this temperature range (4-100 K: $\Delta E_{ST} < 8$ cal/mole or $\Delta E_{ST} > 200$ cal/mole).³⁸⁻⁴⁰ In either case, the high-spin state corresponds to a low-energy state.

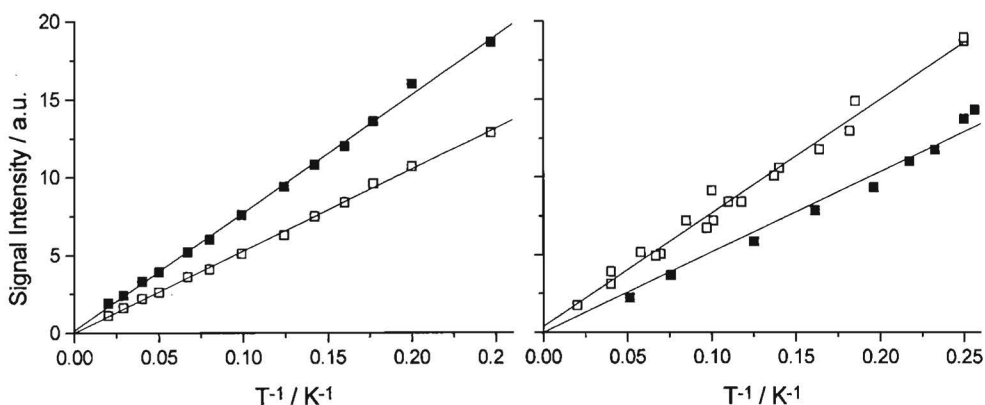


Figure 6.11. Temperature dependence of the ESR signal intensity. (left): $\Delta M_s = \pm 1$ (\square) and $\Delta M_s = \pm 2$ signal (\blacksquare) of di(cation radical) **1a**^{2•2+}. (right): $\Delta M_s = \pm 1$ signal (\square) of tri(cation radical) **4**^{3•3+} and $\Delta M_s = \pm 2$ signal (\blacksquare) of tri(cation radical) **3**^{3•3+}. Solid lines are least-square fits to Curie's law.

For tri(cation radical) 3^{3+} , only the $\Delta M_s = \pm 2$ transition was monitored as a function of the temperature, because the central peak in the $\Delta M_s = \pm 1$ spectrum interferes too much with the quartet signal in this region. For tri(cation radical) 4^{3+} , on the other hand only the $\Delta M_s = \pm 1$ transitions were monitored, because the half-field signal was too weak to be measured accurately at temperatures above 10 K. Both quartet signals exhibit Curie behavior, consistent with a high-spin ground state.

6.7.2 Magnetization Studies

In addition to ESR measurements, preliminary magnetization studies were carried out to gain insight into the ground state of the di(cation radical) 1^{2+} . Because this method is less sensitive than ESR, more concentrated samples ($[1^{2+}] \approx 1$ mM) had to be prepared. A small excess of $\text{Thi}^+\text{ClO}_4^-$ was used in combination with TFA to generate the intermediate oxidation state.

ESR measurements on these samples revealed a relatively large doublet contamination, which according to UV/visible/nearIR spectroscopy was not due to mono- or tri(cation radical). Furthermore, the intensity of the doublet peak was higher when the sample was cooled down slowly. Because of its sensitivity towards cooling rate and concentration, this doublet peak is attributed to molecular aggregates in which part of the spins are canceled out, due to intermolecular antiferromagnetic interactions. This association behavior was suppressed by the addition of a large excess of camphorsulfonic acid in combination with fast cooling. Exchange of the trifluoroacetate anion for the much bulkier camphorsulfonate counter ion results in samples with significantly less doublet impurity.

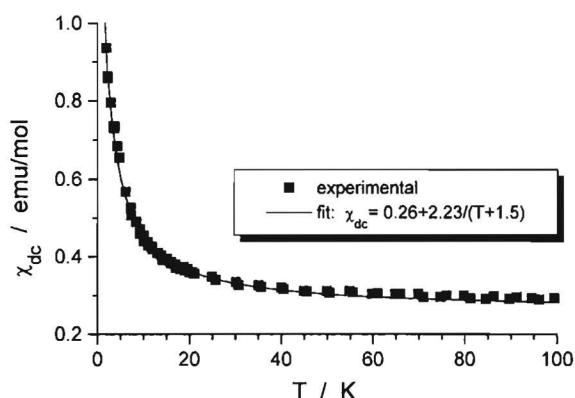


Figure 6.11. Susceptibility of 1^{2+} vs temperature, measured at 0.1 Tesla. Solid line is least-square fit to Curie-Weiss law, corrected for the diamagnetic contribution.

Magnetic susceptibility measurements between 2 and 100 K at 0.1 Tesla were carried out in a SQUID magnetometer.⁴¹ The experimental susceptibility data were fitted to the Curie-Weiss law with an additional diamagnetic contribution. From the fit a Weiss constant $\theta = -1.5$ K is obtained, indicating weak antiferromagnetic intermolecular interactions (Figure 6.11). This temperature dependence is in agreement with the variable temperature ESR experiments.

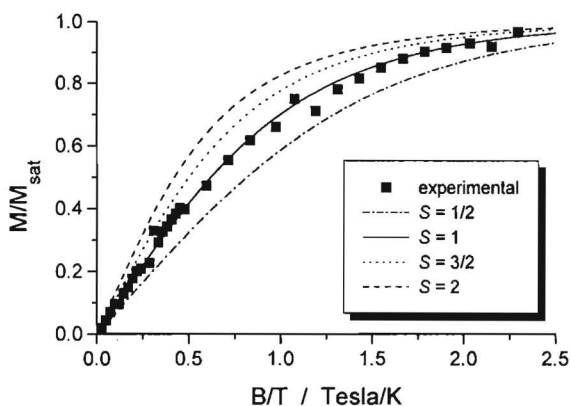


Figure 6.12. Normalized magnetization of I^{2+2+} vs the ratio of magnetic field and temperature, measured at 2.1 K. Lines represent Brillouin functions for different spin states.

The magnetization measurements were carried out at 2.1 K, varying the magnetic field between 0 and 5 Tesla. The plot of the normalized magnetization (M/M_{sat}) vs the ratio of magnetic field and temperature (H/T) is consistent with a Brillouin function of a spin state of $S = 1$ (Figure 6.12). Because the exact spin content of the sample was unknown, no decisive answer can be given whether the triplet is the ground state, or degenerate with a singlet state. Therefore, additional quantitative measurements on I^{2+2+} are required. Measurements on tri(cation radical)s 3^{3+3+} and 4^{3+3+} have not performed so far.

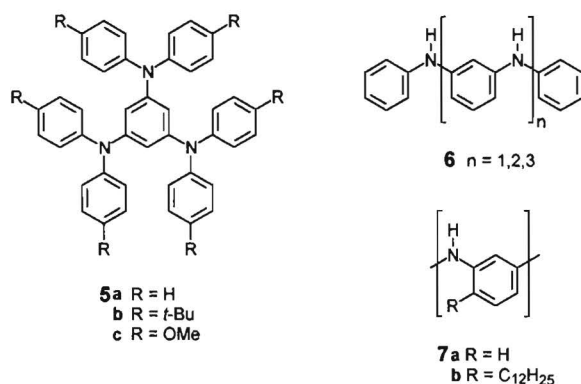
6.8 Discussion

One of the major challenges in the field of organic ferromagnets is the design and preparation of open-shell units that combine stability with the possibility to be incorporated in a chain or network proving the ferromagnetic interaction between the unpaired electrons. In this chapter it has been demonstrated that it is possible to apply the concepts used in the area of (semi)conducting polymers to prepare high-spin molecules with intramolecular ferromagnetic coupling. Taking advantage of the open-shell character of the charge carriers in

conducting polyaniline, ferromagnetic spin alignment has been achieved in a series of oligomers, by simply changing the interconnection of the aniline units from an all-*para* to an alternating *meta* and *para* topology.

The precursor oligo(*m-p*-aniline)s are accessible via a series of copper-catalyzed Ullmann-type reactions. At room temperature, these compounds can be oxidized to the corresponding high-spin oligo(cation radical)s. The ferromagnetic spin-spin interaction between two adjacent singly oxidized *p*-phenylenediamine units is a consequence of the topology of the connecting *meta* phenylene rings. Delocalization of the unpaired electron within each *p*-phenylenediamine unit provides the desired chemical stability. Reversible oxidation has been achieved electrochemically or chemically, using $\text{Thi}^+\text{ClO}_4^-$ or PIFA in combination with TFA.

Comparison with previously reported oligo(cation radical)s of aryl amines shows that the stability of the doped *m-p*-aniline oligomers is unprecedented. Papers concerning 1,3,5-tris(diarylamino)-benzene derivative **5a**, initially claimed a stable quartet tri(cation radical) after oxidation.¹² Recent studies, however, demonstrate that the observed species is a doublet radical cation of a benzidine-like structure, resulting from oxidative coupling at the *para* position of one of the outer phenyl rings.^{13,14} Introduction of substituents at these positions as in compounds **5b** and **5c** affords more stable cation radicals, especially if an electron-releasing methoxy group is used. Quartet state tri(cation radical) **5c**^{3•3+} has actually been prepared, but its stability is still very limited; this species can only be kept at -80 °C for a few minutes.¹⁴ Facile intramolecular coupling at the *ortho* positions, leading to carbazole-like products, is thought to be responsible for the observed instability of these cation radicals.^{15,16,42} The same reaction probably accounts for the instability of cation radicals of *meta* aniline oligomers⁴³ and the extremely low spin concentration (< 1 spin per 60 aniline units) observed for doped poly-*m*-anilines.^{44,45}



ESR spectroscopy has provided insight into the spin distribution and the nature of the intramolecular spin-spin interaction of the various redox states of the oligo(*m-p*-aniline)s.

High-spin states have been observed for all aniline oligomers in the intermediate oxidation state, despite the extended delocalization within the *p*-phenylenediamine units. Due to this delocalization, the zero-field splitting parameter D is small compared to high-spin molecules with more localized unpaired electrons like carbenes and triarylmethyl radicals.^{46,48} However, no direct relation exists between the zero-field splitting and the exchange energy ($|2J|$), which determines the actual energy difference between the high-spin and low-spin states. Variable temperature ESR measurements on all high-spin *m-p*-aniline oligomers presented in this study, reveal Curie behavior between 4 K and 100 K, consistent with a high-spin ground state. The strength of the spin alignment probably results from the fact that most of the spin density is found at the two nitrogen atoms of each *p*-phenylenediamine unit, one of which is directly coupled with the *m*-phenylene linking moiety. Clearly, the *p*-phenylenediamine radical cation is a very suitable spin-carrying unit for high-spin systems, because it meets the required delicate balance between localization and delocalization of spin.

6.9 Conclusion

It has been shown that a polaronic triplet di(cation radical) 1^{2+} can be generated by oxidative doping of neutral precursors. Moreover, this triplet di(cation radical) structure can successfully be extended to higher spin multiplicities in one and two dimensions. The outstanding chemical stability of the cationic oligoradicals and their intramolecular ferromagnetic spin-spin interaction, demonstrate the feasibility of the concept of alternating *meta* and *para* oligo(aniline)s as building blocks for future polaronic ferromagnetic polymers.

6.10 Experimental Section

6.10.1 General Methods

For general procedures and equipment see Chapter 3. The electrochemical setup that has been used for cyclic voltammetry measurements has been described in Chapter 5, the electrospray mass spectrometer in Chapter 6. The UV/visible/nearIR spectra were recorded on a Perkin Elmer Lambda 900 spectrophotometer with a sealed 10 mm cuvette.

6.10.2 Synthesis

The syntheses of 4-iodo-*N,N*-diphenylaniline,¹⁹ and *N,N',N''*-triphenyl-1,3,5-benzene-triamine,⁴⁹ have been carried out according to literature procedures.

***N,N'*-Bis[4-(diphenylamino)phenyl]-*N,N'*-diphenyl-1,3-benzenediamine 1.**

n-Butyllithium (1.0 mL 1.6M in hexane, 1.6 mmol) was added slowly to a solution of *N,N'*-diphenyl-1,3-benzenediamine (0.18 g, 0.70 mmol) in diphenyl ether (15 mL) at room temperature. After stirring for 15 min 4-iodo-*N,N'*-diphenylaniline (0.52 g, 1.40 mmol) and copper(I) iodide (13 mg, 0.07 mmol) were added and the mixture was heated to 200 °C for 48 h. After cooling, ethyl acetate (50 mL) was added and the reaction mixture was filtered over hyflo. The filtrate was washed with a saturated aqueous solution of ammonium chloride and dried over magnesium sulfate. Evaporation of the solvent, flash column chromatography of the residue (SiO₂, hexane/CHCl₃ 3:1 - 2:1) and recrystallization from benzene afforded pure **1** (0.32 g, 61%) as white crystals: mp 216-218 °C; ¹H NMR (CDCl₃) δ 6.68 (2H, dd, *J* = 8.0 Hz and 2.0 Hz, H_{A-4}), 6.86 (1H, t, *J* = 2.0 Hz, H_{A-2}), 6.94-7.01 (14H, m, H_{B-4}, H_{C-2}, H_{C-3}, H_{D-4}), 7.06-7.12 (13H, m, H_{A-5}, H_{B-2}, H_{D-2}), 7.19 (12H, m, H_{B-3}, H_{D-3}); ¹³C NMR (CDCl₃): δ 117.43 (C_{A-4}), 118.57 (C_{A-2}), 122.40 (C_{B-4}, C_{D-4}), 123.69 (C_{B-2}), 123.77 (C_{D-2}), 125.33 (C_{C-3}), 125.56 (C_{C-2}), 129.08 (C_{B-3}), 129.17 (C_{D-3}), 129.65 (C_{A-5}), 142.58 (C_{C-1}), 142.96 (C_{C-4}), 147.57 (C_{B-1}), 147.87 (C_{D-1}), 148.60 (C_{A-1}). Anal Calcd for C₅₄H₄₂N₄: C, 86.83; H, 5.67; N, 7.50. Found: C, 86.76; H, 5.78; N, 7.66. ES-MS *m/z* (M⁺) calcd 746.3, obsd 746.3.

***N*-[4-(Diphenylamino)phenyl]-*N,N'*-diphenyl-1,3-benzenediamine 2.** In a procedure similar to the synthesis of **1**, *N,N'*-diphenyl-1,3-benzenediamine (0.78 g, 3.0 mmol) was reacted with *n*-BuLi, 4-iodo-*N,N'*-diphenylaniline (1.11 g, 3 mmol) and copper(I) iodide (0.04 g, 0.2 mmol). Flash column chromatography (SiO₂, hexane/CHCl₃ 3:1 - 2:1) afforded **1** (0.29 g, 13%) and **2** (0.65 g, 43%) as a grey solid: mp 178 °C; ¹H NMR (CDCl₃) δ 5.6 (1H, b s, NH), 6.63 (1H, m, H_{A-6}), 6.66 (1H, m, H_{A-4}), 6.77 (1H, t, *J* = 2.1 Hz, H_{A-2}), 6.89 (1H, tt, *J* = 7.3 Hz and 1.1 Hz, H_{B-4}), 6.9-7.0 (9H, m, H_{B-2}, H_{C-2}, H_{C-3}, H_{B-4}, H_{D-4}), 7.05-7.15 (7H, m, H_{A-5}, H_{B-2}, H_{D-2}), 7.15-7.25 (8H, m, H_{B-3}, H_{D-3}, H_{B-3}); ¹³C NMR (CDCl₃) δ 111.58 (C_{A-4}), 112.67 (C_{A-2}), 116.00 (C_{A-6}), 117.61 (C_{B-2}), 120.82 (C_{B-4}), 122.36 (C_{D-4}), 122.52 (C_{B-4}), 123.69 (C_{D-2}), 124.03 (C_{B-2}), 125.42 (C_{C-3}), 125.63 (C_{C-2}), 129.15 (C_{B-3}, C_{D-3}), 129.22 (C_{B-3}), 129.84 (C_{A-5}), 142.73, 142.82, 142.89, 143.78 (C_{A-3}, C_{B-1}, C_{C-1}, C_{C-4}), 147.66 (C_{B-1}), 147.82 (C_{D-1}), 148.96 (C_{A-1}).

***N,N'*-Bis{3-[*N*-(4-diphenylamino)phenyl-*N*-phenyl]aminophenyl}-*N,N'*-diphenyl-1,4-benzenediamine 3.** To a solution of **2** (0.46 g, 1.1 mmol) in diphenyl ether (10 mL), sodium hydride (0.05 g, 2 mmol), 1,4-diiodobenzene (0.17 g, 0.5 mmol), and copper(I) iodide (20 mg, 0.1 mmol) were added and the mixture was heated to 200 °C for 48 h. After cooling, ethyl acetate (50 mL) was added and the reaction mixture was filtered over hyflo. The filtrate was washed with a saturated aqueous solution of ammonium chloride and dried over magnesium sulfate. Evaporation of the solvent and flash column chromatography (SiO₂,

hexane/CHCl₃ 3:1 - 2:1) afforded **3** (0.28g, 51 %) as a light grey solid: mp 234 °C; ¹H NMR (CDCl₃) δ 6.61 (2H, dd, *J* = 8.0 Hz and 2.1 Hz, H_{C-6}), 6.65 (2H, dd, *J* = 8.0 Hz and 2.1 Hz, H_{C-4}), 6.85 (2H, t, *J* = 2.1 Hz, H_{C-2}), 6.9-7.0 (20H, m, H_A, H_{B-4}, H_{D-4}, H_{E-2}, H_{E-3}, H_{F-4}), 7.05-7.08 (18H, m, H_{B-2}, H_{C-5}, H_{D-2}, H_{F-2}), 7.15-7.25 (16H, m, H_{B-3}, H_{D-3}, H_{F-3}); ¹³C NMR (CDCl₃) δ 117.41 (C_{C-4}, C_{C-6}), 118.53 (C_{C-2}), 122.36, 122.37 (C_{B-4}, C_{D-4}), 122.39 (C_{F-4}), 123.65, 123.68 (C_{B-2}, C_{D-2}), 123.76 (C_{F-2}), 125.32 (C_{E-3}), 125.51, 125.54 (C_{A-2}, C_{E-2}), 129.07 (C_{B-3}, C_{D-3}), 129.14 (C_{F-3}), 129.67 (C_{C-5}), 142.57, 142.62 (C_{A-1}, C_{E-1}), 142.91 (C_{E-4}) 147.52, 147.54 (C_{B-1}, C_{D-1}), 147.85 (C_{F-1}), 148.54, 148.57 (C_{C-1}, C_{C-3}). ES-MS *m/z* (M⁺) calcd for C₇₈H₆₀N₆ 1080.5, obsd 1080.5.

***N,N',N''*-Tris[4-(diphenylamino)phenyl]-*N,N',N''*-triphenyl-1,3,5-benzenetriamine**

4. To a solution of *N,N',N''*-triphenyl-1,3,5-benzenetriamine (0.74 g, 2.0 mmol) in diphenyl ether (25 mL) sodium hydride (0.25 g, 10 mmol), 4-iodo-*N,N*-diphenylaniline (2.71 g, 7.3 mmol) and copper(I) iodide (0.12 g, 0.6 mmol) were added and the mixture was heated to 200 °C for 48 h. After cooling, ethyl acetate (50 mL) was added and the reaction mixture was filtered over hyflo. The filtrate was washed with a saturated aqueous solution of ammonium chloride and dried over magnesium sulfate. Evaporation of the solvent and flash column chromatography of the residue (SiO₂, hexane/CHCl₃ 3:1 - 2:1) afforded pure **4** (0.80 g, 37%): mp 239 °C; ¹H NMR (330K, CDCl₃): δ 6.36 (3H, b s, H_A), 6.8-6.94 (21H, m, H_{B-4}, H_{C-2}, H_{C-3}, H_{D-4}), 6.95-7.05 (18H, m, H_{B-2}, H_{D-2}), 7.13 (6H, t, *J* = 7.5 Hz, H_{B-3}), 7.17 (12H, t, *J* = 7.5 Hz, H_{D-3}); ¹³C NMR (330K, CDCl₃): δ 112.79 (C_{A-2}), 122.48 (C_{B-4}), 122.51 (C_{D-4}), 123.85 (C_{B-2}), 123.93 (C_{D-2}), 125.34 (C_{C-3}), 125.69 (C_{C-2}), 129.00 (C_{B-3}), 129.19 (C_{D-3}), 142.64 (C_{C-1}), 143.24 (C_{C-4}), 147.56 (C_{B-1}), 148.09 (C_{D-1}), 149.28 (C_{A-1}). ES-MS *m/z* (M⁺) calcd for C₇₈H₆₀N₆ 1080.5, obsd 1080.5.

6.11 References

- 1 Fukutome, H.; Takahashi, I.; Ozaki, M. *Chem. Phys. Lett.* **1987**, *133*, 34.
- 2 Kaisaki, D. A.; Chang, W.; Dougherty, D. A. *J. Am. Chem. Soc.* **1991**, *113*, 2764.
- 3 Tanaka, K.; Ago, H.; Yamabe, T. *Synth. Met.* **1995**, *72*, 225.
- 4 Torrence, J. B.; Oostra, S.; Nazzari, A. *Synth. Met.* **1987**, *19*, 709.
- 5 Murray, M. M.; Kaszynski, P.; Kaisaki, D. A.; Chang, W.; Dougherty, D. A. *J. Am. Chem. Soc.* **1994**, *116*, 8152.
- 6 Bushby, R. J.; Ng, K. M. *Chem. Commun.* **1996**, 659.
- 7 Patil, A. O.; Heeger, A. J.; Wudl, F. *Chem. Rev.* **1988**, *88*, 183.
- 8 Brédas, J. L.; Street, G. B. *Acc. Chem. Res.* **1985**, *18*, 309.
- 9 Hill, M. G.; Mann, K. R.; Miller, L. L.; Penneau, J.-P. *J. Am. Chem. Soc.* **1992**, *114*, 2728.

- 10 Wudl, F.; Angus, R. O.; Lu, F. L.; Allemand, P. M.; Vachon, D. J.; Nowak, M.; Liu, Z. X.; Heeger, A. J. *J. Am. Chem. Soc.* **1987**, *109*, 3677.
- 11 Stafström, S.; Brédas, J. L.; Epstein, A. J.; Woo, H. S.; Tanner, D. B.; Huang, W. S.; MacDiarmid, A. G. *Phys. Rev. Lett.* **1987**, *59*, 1464.
- 12 Yoshizawa, K.; Tanaka, K.; Yamabe, T.; Yamauchi, J. *J. Chem. Phys.* **1992**, *96*, 5516.
- 13 Yoshizawa, K.; Hatanak, M.; Ago, H.; Tanaka, K.; Yamabe, T. *Bull. Chem. Soc. Jpn.* **1996**, *69*, 1417.
- 14 Stickley, K. R.; Blackstock, S. C. *J. Am. Chem. Soc.* **1994**, *116*, 11576.
- 15 Stickley, K. R.; Blackstock, S. C. *Tetrahedron Lett.* **1995**, *36*, 1585.
- 16 Sasaki, S.; Iyoda, M. *Chem. Lett.* **1995**, 1011.
- 17 Nakamura, Y.; Iwamura, H. *Bull. Chem. Soc. Jpn.* **1993**, *66*, 3724.
- 18 Okada, K.; Imakura, T.; Oda, M.; Murai, H.; Baumgarten, M. *J. Am. Chem. Soc.* **1996**, *118*, 3047.
- 19 Strohriegl, P.; Jesberger, G.; Heinze, J.; Moll, T. *Makromol. Chem.* **1992**, *193*, 909. The reported values have been scaled by +0.12 V to correct for the difference in E^0 of the Fc/Fc⁺ couple, due to different experimental conditions.
- 20 Durand, G.; Morin, G.; Trémillon, B. *Nouv. J. Chem.* **1979**, *7*, 463.
- 21 Murata, Y.; Shine, H. J. *J. Org. Chem.* **1969**, *34*, 3368.
- 22 Ebersson, L.; Hartshorn, M. P.; Persson, O. *Acta Chem. Scand.* **1995**, *49*, 640.
- 23 This notation is preferred over 1^{3+} because two electrons in one *p*-phenylenediamine unit are expected to be in a closed-shell configuration.
- 24 Sedó, J.; Ruiz, D.; Vidal-Gancedo, J.; Rovira, C.; Bonvoisin, J.; Launay, J. -P.; Veciana, J. *Adv. Mater.* **1996**, *8*, 748.
- 25 Bonvoisin, J.; Launay, J. -P.; Van der Auweraer, M.; De Schryver, F. C. *J. Phys. Chem.* **1994**, *98*, 5052.
- 26 Ribou, A. -C.; Launay, J. -P.; Takahashi, K.; Nihira, T.; Tarutani, S.; Spangler, C. W. *Inorg. Chem.* **1994**, *33*, 1325.
- 27 ES-MS turned out to be very sensitive for the detection of the tetrabutylammonium cations of TBAH, which is present as a contamination in the glovebox, in which the samples were prepared.
- 28 Luckhurst, G. R. *Mol. Phys.* **1966**, *10*, 543.
- 29 Luckhurst, G. R. In *Spin Labeling Theory and Applications*; Berliner, L. J., Ed.; Academic Press: New York, 1976, p133.
- 30 Rajca, A.; Rajca, S.; Desai, S. R. *J. Am. Chem. Soc.* **1995**, *117*, 806.
- 31 Rajca, A.; Utamapanya, S. *J. Am. Chem. Soc.* **1993**, *115*, 2396.
- 32 Brickmann, J.; Kothe, G. *J. Chem. Phys.* **1973**, *59*, 2807.
- 33 Weissman, S. I.; Kothe, G. *J. Am. Chem. Soc.* **1975**, *97*, 2537.
- 34 Novak, C.; Kothe, G.; Zimmermann, H. *Ber. Bunsen-Ges. Phys. Chem.* **1974**, *78*, 265.
- 35 Müller, U.; Baumgarten, M. *J. Am. Chem. Soc.* **1995**, *117*, 5840.
- 36 Wolf, M. O.; Fox, H. H.; Fox, M. A. *J. Org. Chem.* **1996**, *61*, 287.
- 37 Grzeszczuk, M.; Smith, D. E. *J. Electroanal. Chem.* **1984**, *162*, 189.
- 38 Iwamura, H.; Koga, N. *Acc. Chem. Res.* **1993**, *26*, 346.
- 39 Kanno, F.; Inoue, K.; Koga, N.; Iwamura, H. *J. Phys. Chem.* **1993**, *97*, 13267.
- 40 Ling, C.; Lahti, P. M. *J. Am. Chem. Soc.* **1994**, *116*, 8784.

- 41 Magnetization measurements were performed by J. Sinzig, Kamerlingh Onnes Laboratory, Leiden University, The Netherlands.
- 42 Fox, M. A.; Dulay, M. T.; Krosley, K. *J. Am. Chem. Soc.* **1994**, *116*, 10992.
- 43 Ito, A.; Saito, T.; Tanaka, K.; Yamabe, T. *Tetrahedron Lett.* **1995**, *36*, 8890.
- 44 Yoshisawa, K.; Tanaka, K.; Yamabe, T.; Yamauchi, J. *J. Chem. Phys.* **1992**, *96*, 5516.
- 45 Ito, A.; Ota, K.-I.; Tanaka, K.; Yamabe, T.; Yoshizawa, K. *Macromolecules* **1995**, *28*, 5618.
- 46 Wasserman, E.; Murray, R. W.; Yager, W. A.; Trozzolo, A. M.; Smolinsky, G. *J. Am. Chem. Soc.* **1967**, *89*, 5076.
- 47 Itoh, K. *Chem. Phys. Lett.* **1967**, *1*, 235.
- 48 Luckhurst, G. R.; Pedulli, G. F.; Tiecco, M. *J. Chem. Soc. (B)* **1971**, 329.
- 49 Buu-Hoï, Ng. Ph. *J. Chem. Soc.* **1952**, 4346.

Chapter 7

Stable High-Spin Cation Radicals of *m-p*-Aniline Oligomers by “Acid Doping”

Abstract

The formation of stable cation radicals of aniline oligomers ($3^{2\cdot 2+}$ and $5^{3\cdot 3+}$) via a proton-triggered redox reaction between a fully oxidized oligo(amine) and corresponding fully reduced oligo(imine) is described. In this reaction the amine is oxidized, while the protonated imine is reduced, both yielding the same oligo(cation radical). The cation radicals are characterized with UV/Visible/NIR and ESR spectroscopy ($3^{2\cdot 2+}$: $D = 118$ MHz; $E \approx 0$ MHz; $5^{3\cdot 3+}$: $D = 73$ MHz; $E \approx 0$ MHz). Variable temperature ESR measurements are consistent with high-spin ground states. The high stability under ambient conditions demonstrates that alternating meta and para aniline oligomers are interesting building blocks for future polaronic ferromagnets.

7.1 Introduction

In the previous chapter it was shown that poly(*m-p*-aniline) is a very promising candidate for a polaronic ferromagnet in which dopable segments are interlinked by ferromagnetic coupling units. Oxidation of oligomers to an intermediate oxidation state in which one electron per two aniline units is removed, affords stable high-spin oligo(cation radical)s, because the alternating sequence of *meta* and *para* connected anilines in the repeat unit, combines chemical stability from the *p*-phenylenediamine units with ferromagnetic interaction via a *m*-phenylene ring.¹

In contrast to the doping of other π -conjugated polymers, the preparation of conducting polyaniline from the emeraldine base involves a completely different type of process. This “acid doping” process is a proton-triggered internal redox reaction.²⁻⁴ The

emeraldine base consists of an alternating sequence of fully oxidized *p*-benzoquinonediimine and fully reduced *p*-phenylenediamine units, which are linked via *p*-phenylene rings. Protonation of the emeraldine base at the imine nitrogen atoms induces an internal redox reaction, in which one electron is transferred from each *p*-phenylenediamine to a *p*-benzoquinonediiminium unit. In the resulting conducting emeraldine salt, all aniline units have the same intermediate oxidation state and all nitrogen atoms are equivalent (Figure 7.1). This internal redox reaction exactly produces one unpaired electron per two aniline units.

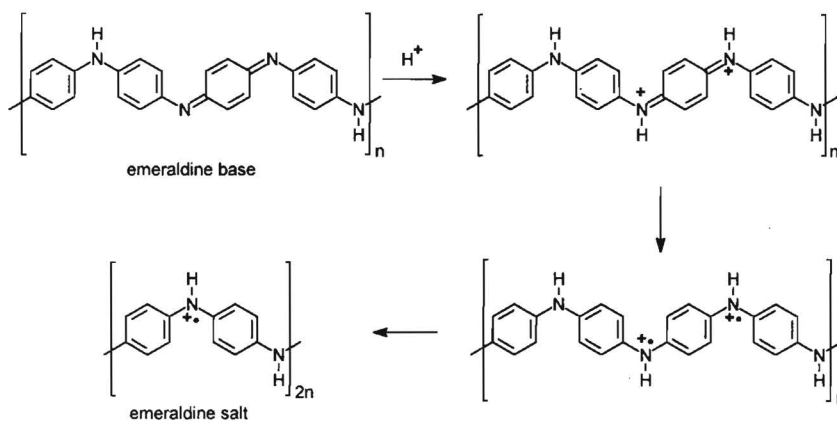


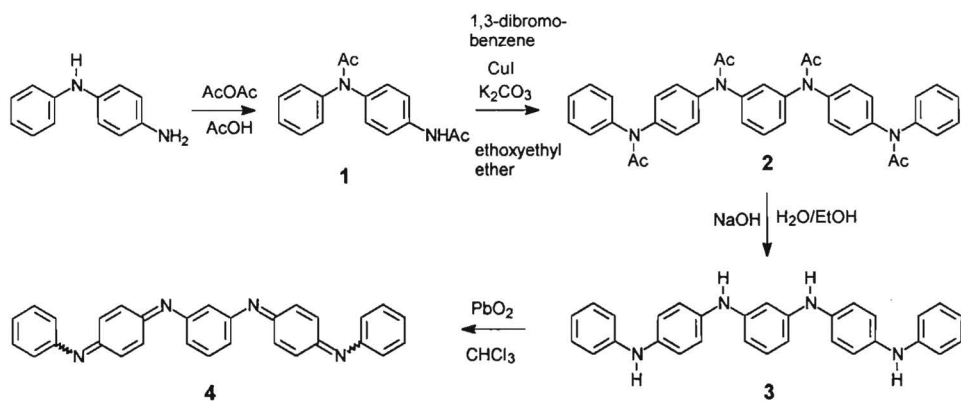
Figure 7.1. Mechanism of the “acid doping” process of the emeraldine base of polyaniline to the conducting emeraldine salt.

In principle, the same proton-induced spin unpairing can also be used to generate high-spin polyaniline. To test this proposition, high-spin aniline oligomers have been prepared via a similar “acid doping” process. For this purpose, oligo(aniline)s in a fully reduced form (3, 5) and fully oxidized form (4, 6) have been synthesized. A 1:1 mixture of a fully reduced oligomer and corresponding fully oxidized oligomer, has the required overall oxidation state and by simply adding a drop of acid a redox reaction is initiated that produces the oligomer in the intermediate oxidation state as the single product.

7.2 Synthesis

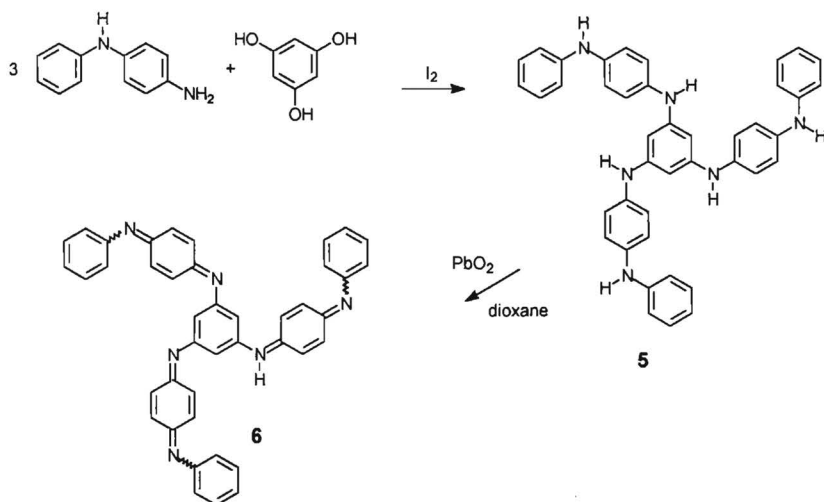
Tetra(amine) **3** was synthesized starting from *N*-phenyl-1,4-benzenediamine (Scheme 7.1). Diacetylation with acetic anhydride in acetic acid gave compound **1**, and subsequent coupling with 1,3-dibromobenzene, using potassium carbonate and copper(I) iodide as a catalyst, afforded tetra(amide) **6**. Finally, hydrolysis with sodium hydroxide in water/ethanol

led to compound **2** (Scheme 7.1). Oxidation of **3** with lead(IV) oxide in chloroform gave tetra(imine) **4** as a mixture of three *cis-trans* isomers. These isomers could not be separated because isomerization takes place during column chromatography.



Scheme 7.1. Synthesis of linear oligomers **3** and **4**.

Hexa(amine) **5** was prepared by an iodine-catalyzed condensation reaction between phloroglucinol and *N*-phenyl-1,4-benzenediamine (Scheme 7.2). Oxidation to the hexa(imine) **6** with lead(IV) oxide was carried out in dioxane.



Scheme 7.2. Synthesis of branched oligomers **5** and **6**.

7.3 Cyclic Voltammetry

Cyclic voltammetry of compounds **3** and **5** was carried out in acetonitrile with 0.1 M TBAH, in the presence of 0.01 M perchloric acid, because it is well-known that the removal of two electrons from a *p*-phenylenediamine unit with secondary amines leads to deprotonation and irreversible oxidation processes.^{5,6} In the presence of acid, deprotonation is suppressed and the voltammogram of tetra(amine) **3** reveals two broad reversible oxidations (Figure 7.2). The peak-to-peak separations of 95 mV and 81 mV are significantly larger than 59 mV. From the rather large peak-to-peak separation between the oxidation waves observed for compound **3** and comparison with the values reported for *N,N'*-diphenyl-1,4-benzenediamine (DPBD), we conclude that these waves each represent a two-electron process. Apparently, both *p*-phenylenediamine moieties are oxidized simultaneously under these conditions.

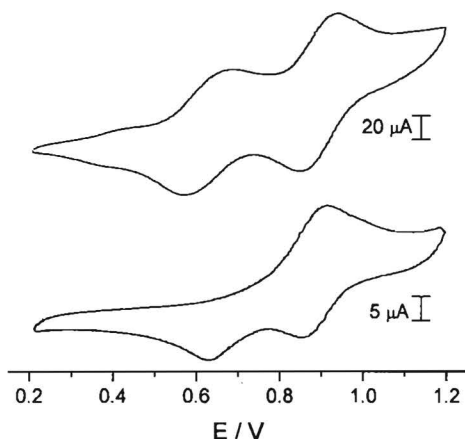


Figure 7.2. Cyclic voltammogram of aniline oligomers recorded at RT in CH_2Cl_2 /TBAH (0.1 M) / HClO_4 (0.01 M), scan rate 100 mV/s. (top): Tetra(amine) **3**. (bottom): Hexa(amine) **5**. Potential vs SCE calibrated against Fc/Fc^+ (0.43 V).

Hexa(amine) **5** was measured at lower concentration because otherwise the voltammogram only reveals very broad uninformative oxidation/reduction waves. At lower concentration, only one oxidation wave is observed at a potential, which is comparable to the second oxidation wave of **3** (Figure 7.2). During the reversing scan, two waves are detected, but their currents are smaller than the current of the oxidation wave. Identical behavior is observed for successive scans. Because the oxidation wave is twice as large as either one of the reduction waves, we assume that the first wave, which is associated with the simultaneous oxidation of all three *p*-phenylenediamine units, is overlapping the second wave. A similar shift of the first set of oxidation potentials has been observed for *N*-phenyl substituted oligo(aniline)s (see paragraph 6.3) and is ascribed to protonation.

7.4 UV/visible/nearIR Spectroscopy

Quantitative conversion of the amines to the different oxidation states has been achieved by chemical oxidation with either thianthrenium perchlorate ($\text{Thi}^+\text{ClO}_4^-$)⁷ or phenyliodine(III) bis(trifluoroacetate) (PIFA)⁸ in dichloromethane or acetonitrile with 10% (v/v) of TFA added to the solution to stabilize the generated cation radicals. The reaction was monitored by UV/visible/nearIR spectroscopy (Table 7.1).

The optical spectrum of **3** recorded in dichloromethane exhibits only one band at 4.05 eV, very similar to the spectrum of DPDB (4.08 eV). In dichloromethane/TFA, the spectrum of **3** displays two absorption bands at 3.31 eV and 4.27 eV, whereas in acidic media the spectrum of DPDB changes only with respect to the position of the single absorption band, which is shifted to higher energy (4.31 eV). The fact that **3** is more sensitive towards acids is comparable to the behavior of different *N*-phenyl aniline oligomers with respect to acid (see 6.3). The shift of the absorption to higher energy is ascribed to protonation, leading to quaternization of the amines, shortening the effective conjugation length. The absorption around 3.31 eV in the spectrum of **3** is tentatively attributed to an intramolecular electron-transfer. This explanation is in agreement with the absence of such a band in the corresponding spectrum of DPDB. Acidification of hexa(amine) **5** in dichloromethane affords two absorption bands at 3.00 and 3.92 eV, respectively.

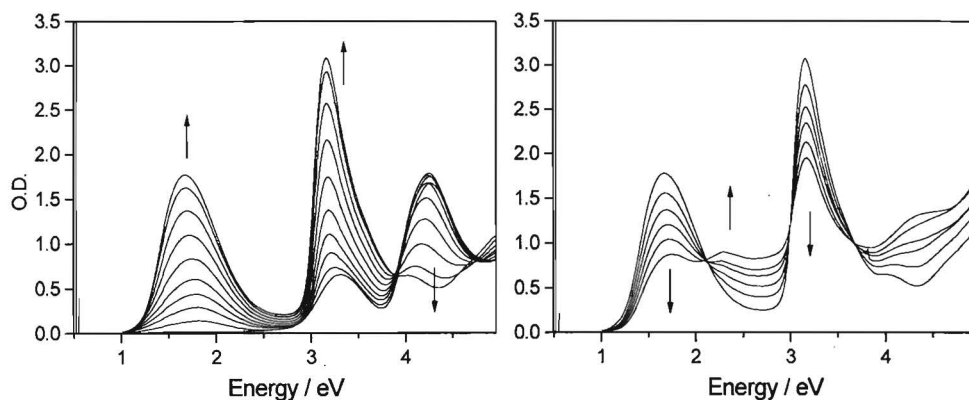


Figure 7.3. UV/visible/nearIR spectra of the stepwise oxidation of **3** with PIFA in $\text{CH}_2\text{Cl}_2/\text{TFA}$ (9:1 v/v) at 295 K. (left): Oxidation of neutral **3** to the intermediate oxidation state 3^{2+2+} . (right): Further oxidation to 3^{3+9} .

Oxidation of **3** in dichloromethane/TFA with PIFA results in cation bands at 1.67 and 3.17 eV, and an isosbestic point at 3.90 eV (Figure 7.3). For **5**, similar cation bands are found at 1.67 and 3.13 eV. The maximum absorbance corresponds to the intermediate oxidation

states 3^{2+2+} and 5^{3+3+} , and is reached after addition of 2 and 3 equiv of oxidant for **3** and **5**, respectively. Eventually, when more equivalents are added, the cation bands decrease and a new band at 2.31 eV (**3**) or 2.33 eV (**5**) emerges which is attributed to doubly oxidized *p*-phenylenediamine units. The oxidation potential of PIFA is not high enough to achieve complete conversion to the fully oxidized states 3^{4+} and 5^{6+} .⁹ During the oxidation processes, no absorption bands can be detected at low energy, which can be attributed to intervalence transitions.

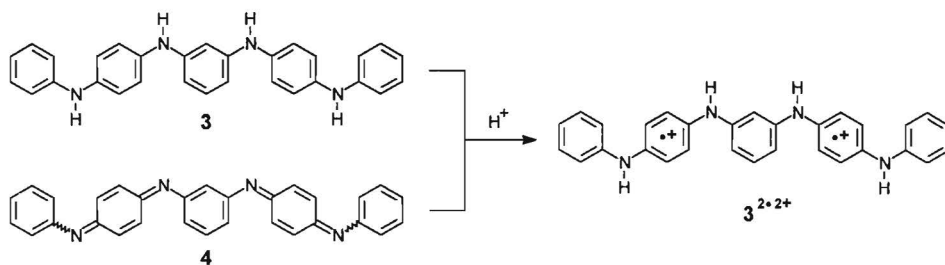
Table 7.1. Spectral Data for the Oligo(amine)s, Oligo(imine)s, and Cation Radicals

	Neutral compound		Intermediate oxidation state		Fully oxidized state	
	eV (nm)		eV (nm)		eV (nm)	
DPBD	4.08 (304) ^a		DPBD ^{•+}	1.78 (697); 3.25 (381)	DPBD ²⁺	2.30 (539)
	4.31 (288) ^b			–		–
3	4.05 (306) ^a			–		–
	3.31 (374); 4.27 (290) ^b		3^{2+2+}	1.67 (743); 3.17 (391)	3^{4+c}	2.31 (537)
5	4.01 (309) ^a			–		–
	3.00 (413); 3.92 (316) ^b		5^{3+3+}	1.67 (743); 3.13 (396)	5^{6+c}	2.33 (533)
4	2.74 (452); 4.05 (306) ^a			–		–
6	2.72 (456); 4.01 (309) ^a			–		–

^a In dichloromethane. ^b In dichloromethane/TFA 9:1 v/v. ^c Complete conversion is not achieved.

7.5 “Acid Doping”

In addition to chemical oxidation, the intermediate oxidation states of the secondary oligo(amine)s, 3^{2+2+} and 5^{3+3+} , can conveniently be obtained via an “acid doping” process. When equimolar amounts of oligo(amine) (**3**, **5**) and corresponding oligo(imine) (**4**, **6**) are dissolved in acetonitrile, no reaction occurs, as indicated by the UV/visible/nearIR spectrum, which is a superposition of the absorptions of amine and imine. Upon addition of 1% (v/v) of TFA, the spectrum changes completely. The initial bands disappear and two new peaks emerge, identical to the absorptions of the intermediate oxidation state, 3^{2+2+} and 5^{3+3+} , obtained in the oxidative doping experiment. The mechanism is a proton-triggered redox reaction between the amine and corresponding imine (Scheme 7.3), similar to the acid doping process used for the preparation of conducting polyaniline from the emeraldine base.



Scheme 7.3. "Acid doping" of a 1:1 mixture of oligo(amine) **3** and oligo(imine) **4** to the di(cation radical) 3^{2+2+} .

In this process the amine is oxidized to the intermediate oxidation state by the protonated imine, while at the same time the protonated imine is reduced to exactly the same species. The spectra of the neutral oligo(amine)s can be retrieved when an excess of hydrazine monohydrate is added to the sample. Because the overall process then is reduction of the oligo(imine), a double intensity of the oligo(amine) absorption is found.

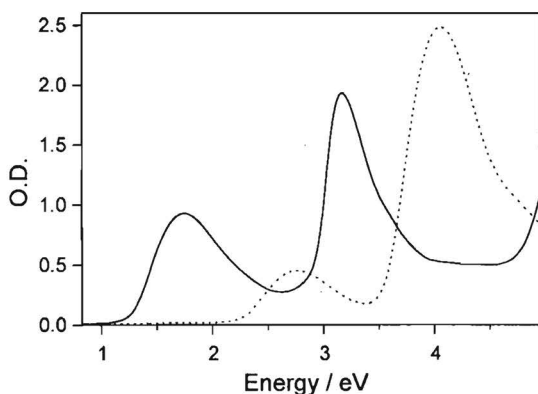


Figure 7.4. UV/visible/nearIR spectra of a 1:1 mixture of **3** and **4** in acetonitrile (.....) and after the addition of 1% (v/v) of TFA (—).

7.6 ESR Spectroscopy

The ESR spectrum of 3^{3+} is obtained after doping of **3** with < 1 equiv of PIFA in the presence of TFA, and exhibits a well-resolved complex pattern, dominated by hyperfine interaction with two ^{14}N nuclei and two amine protons (Figure 7.5). The isotropic couplings of

$A_{\text{iso}}(\text{N}) = 15$ and $A_{\text{iso}}(\text{H}) = 18$ MHz are in good agreement with values reported for the cation radical of DPBD.⁵ Interaction with only two nitrogen nuclei demonstrates that the unpaired electron is localized within half of the molecule, and that no fast charge transfer occurs on the ESR timescale.

The di(cation radical) 3^{2+2+} is most conveniently prepared from the 1:1 mixture of **3** and **4**, by the “acid doping” process. The triplet ESR spectrum recorded at 110 K reveals zero-field splitting ($D = 118$ MHz; $E \approx 0$ MHz) and a $\Delta M_s = \pm 2$ transition at half-field (Figure 7.5). Assuming a point-dipole approximation for the zero-field splitting, $D = 118$ MHz corresponds to an average distance between the unpaired electrons of 8.7 Å. This is consistent with the separation of 9.8 Å between the centers of the two *p*-phenylenediamine units, as estimated from standard bond lengths, assuming a stretched planar geometry.

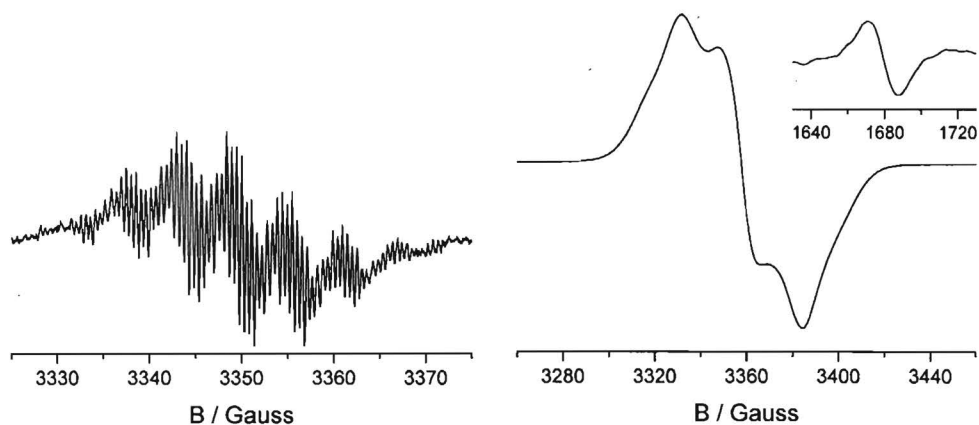


Figure 7.5. ESR spectra. (left): Cation radical $3^{+\bullet}$ in $\text{CH}_2\text{Cl}_2/\text{TFA}$ (9:1 v/v) recorded at RT. (right): Di(cation radical) 3^{2+2+} in $\text{CH}_2\text{Cl}_2/\text{TFA}$ (9:1 v/v) recorded at 110 K. The central line in the $\Delta M_s = \pm 1$ spectrum is due to some doublet impurity. Inset shows half-field signal recorded at 4 K.

For compound **5** a similar but less well-resolved room-temperature ESR spectrum is recorded for a partially oxidized sample. If > 1 equiv of oxidant is used, the anisotropic spectrum clearly displays zero-field splitting, and gradually changes from a combination of doublet and triplet to a combination of triplet and quartet signals. Eventually, after the addition of 3 equiv, a five-line spectrum is obtained ($D = 73$ MHz; $E \approx 0$ MHz), as well as a broad $\Delta M_s = \pm 2$ transition at half-field (Figure 7.6).

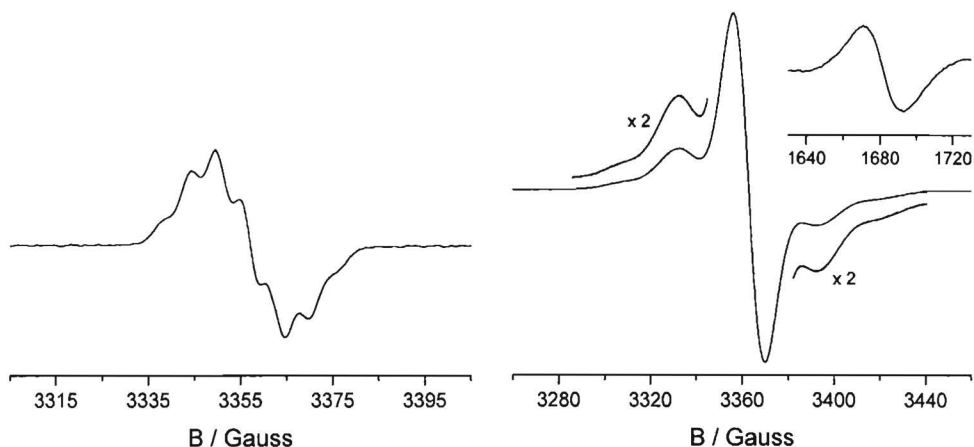


Figure 7.6. ESR spectra. (left): Cation radical 5^{2+} in $\text{CH}_2\text{Cl}_2/\text{TFA}$ recorded at RT. (right): Tri(cation radical) $5^{3\cdot 3+}$ in $\text{CH}_2\text{Cl}_2/\text{TFA}$ (99:1 v/v) recorded at 110 K. Inset shows half-field signal recorded at 4 K.

These signals are attributed to $5^{3\cdot 3+}$ in a quartet state. The $\Delta M_s = \pm 2$ transition of $5^{3\cdot 3+}$ is significantly broader than the half-field signal of the triplet state $3^{2\cdot 2+}$ due to zero-field splitting on the half-field signal of a quartet state. The actual D -splitting on the $\Delta M_s = \pm 2$ transition, however, is obscured by the broad lines that result from hyperfine interaction. A $\Delta M_s = \pm 3$ transition could not be detected, not even at 4 K. This can be rationalized by the theoretical ratio of the $|\Delta M_s| = 1, 2,$ and 3 transitions which is $1 : (D/B_0)^2 : (D/B_0)^4$.¹⁰⁻¹³ Due to the relatively small D value, the $\Delta M_s = \pm 3$ transition signal is extremely weak and therefore not detected.

The zero-field parameters suggest an average distance of 10.2 Å between the unpaired electrons, consistent with an estimate of 9.8 Å for a planar structure. The increased average distance for $5^{3\cdot 3+}$ as compared to $3^{2\cdot 2+}$ has also been observed for the *N*-phenyl substituted derivatives, and can be explained by the increased electrostatic repulsion resulting from the star-shaped topology of $5^{3\cdot 3+}$.

The "acid doping" of a 1:1 mixture of **5** and **6** also affords the quartet tri(cation radical) $5^{3\cdot 3+}$ displaying identical ESR spectra.

7.7 Determination of Ground States

To assess the ground states of $3^{2\cdot 2+}$ and $5^{3\cdot 3+}$, Curie studies were performed between 4 and 100 K. The observed Curie behavior of both the $\Delta M_s = \pm 1$ and $\Delta M_s = \pm 2$ transitions of tetra(amine) in the intermediate oxidation state $3^{2\cdot 2+}$, is consistent with a high-spin ground state, but the possibility of a ground-state degeneracy can not be excluded.¹⁴⁻¹⁶

The $\Delta M_S = \pm 2$ transition of tri(cation radical) $5^{3\cdot 3+}$ was too weak to be monitored accurately at temperatures above 10 K. Therefore, only the temperature dependence of the $\Delta M_S = \pm 1$ transition is presented. This thermal behavior also follows Curie's law, which is in good agreement with a high-spin quartet ground state. By quantitative magnetization measurements one can discriminate between a high-spin ground state and the possibility of a ground-state degeneracy. Therefore, these experiments eventually will have to be carried out, in order to obtain a decisive answer concerning the ground state of the high-spin aniline oligomers.

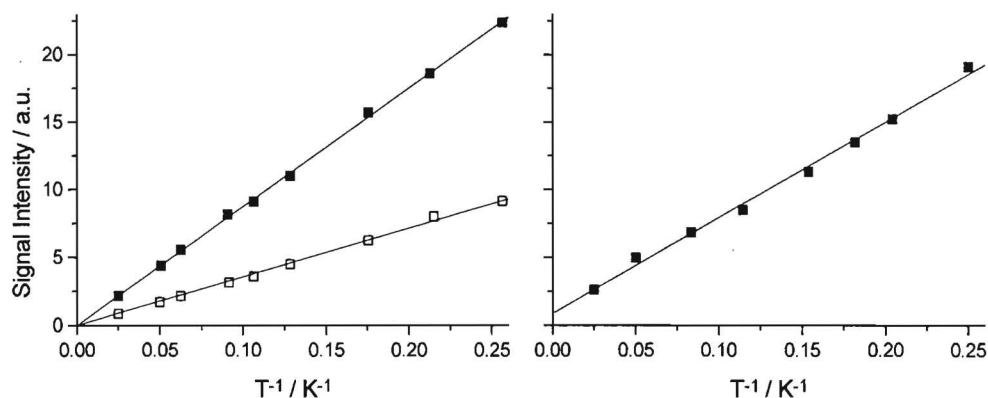


Figure 7.7. Temperature dependence of the ESR signal intensity. (left): $\Delta M_S = \pm 1$ (■) and $\Delta M_S = \pm 2$ signal (□) of di(cation radical) $3a^{2\cdot 2+}$ (right): $\Delta M_S = \pm 1$ transition of tri(cation radical) $5^{3\cdot 3+}$. Solid lines are least-square fits to Curie's law.

7.8 Conclusion

It is demonstrated that in addition to redox doping, acid doping can be used as a very convenient method to generate polaronic high-spin molecules. The remarkable chemical stability of the oligo(cation radicals), $3^{2\cdot 2+}$ and $5^{3\cdot 3+}$ confirms the feasibility of alternating *meta* and *para* oligo(aniline)s as building blocks for future polaronic ferromagnetic polymers.

7.9 Experimental Section

7.9.1 General Methods

For general procedures and equipment see Chapter 3. The electrochemical setup that has been used for cyclic voltammetry measurements and the electrospray mass spectrometer

have been described in Chapter 5 and 6, respectively. The UV/visible/nearIR spectra were recorded on a Perkin Elmer Lambda 900 spectrophotometer with a sealed 10 mm cuvette.

7.9.2 Synthesis

***N*-Phenyl-*N,N'*-1,4-phenylenebis(acetamide) 1.** Acetic anhydride (3.8 mL, 40 mmol) was added slowly to *N*-phenyl-1,4-benzenediamine (3.68 g, 20 mmol) in acetic acid (20 mL). After the addition was complete, the reaction mixture was heated to 70 °C for 2 h. The acetic acid was removed by distillation under reduced pressure. Column chromatography of the residue (SiO₂, EtOAc) and subsequent recrystallization from hexane/EtOAc (1:1) provided **1** (3.83 g, 87 %) as a white crystalline solid: mp 137 °C; ¹H NMR (330 K, CDCl₃) δ 2.09 (3H, s, CH₃), 2.16 (3H, s, CH₃), 7.18 (2H, d, *J* = 8.7 Hz, H_{A-2}), 7.20-7.25 (3H, m, H_{B-4}, H_{B-2}), 7.30 (1H, bs, N-H), 7.33 (2H, dd, *J* = 8.4 Hz and 6.9 Hz, H_{B-3}), 7.43 (2H, bd, *J* = 8.7 Hz, H_{A-3}); ¹³C NMR (330K, CDCl₃): δ 23.45 (CH₃), 23.86 (CH₃), 120.80 (C_{A-3}), 126.87 (C_{B-4}), 127.23, 127.60 (C_{A-2}, C_{B-2}), 129.19 (C_{B-3}), 137.41 (C_{A-4}), 138.61 (C_{A-1}), 143.15 (C_{B-1}), 168.73, 170.53 (CO). Anal. Calcd for C₁₆H₁₆N₂O₂: C, 71.62; H, 6.01; N, 10.44. Found: C, 72.14; H, 5.94; N, 10.54.

***N,N'*-Bis[4-(*N*-phenyl)acetylaminophenyl]-1,3-phenylenebis(acetamide) 2.** A mixture of diamide **1** (2.69 g, 10 mmol), 1,3-dibromobenzene (1.18 g, 10 mmol), K₂CO₃ (1.38 g, 10 mmol), and CuI (0.05 g, 0.25 mmol) in ethoxyethyl ether (25 mL) was heated under reflux for 24 h. The hot reaction mixture was filtered over Hyflo and the residue was thoroughly extracted with EtOAc. The combined organic fractions were concentrated by vacuum distillation, and the crude product was purified by column chromatography (SiO₂, CHCl₃/MeOH 9:1) and additional recrystallization from hexane/EtOAc, providing **2** (3.11 g, 51 %) as a white solid: mp 160-165 °C; ¹⁸ ¹H NMR (330 K, CDCl₃): δ 1.98 (6H, s, CH₃), 1.99 (6H, s, CH₃), 7.06 (2H, d, *J* = 8.1 Hz, H_{A-4}), 7.16 (4H, d, *J* = 8.8 Hz, H_{C-2}), 7.2-7.3 (12H, m, H_{A-2}, H_{A-5}, H_{B-2}, H_{B-3}, H_{C-4}), 7.35 (4H, t, *J* = 7.7 Hz, H_{C-3}); ¹³C NMR (330 K, CDCl₃): δ 23.74 (CH₃), 125.46 (C_{A-4}), 126.65 (C_{A-2}), 127.44, 127.54, 127.87, 128.06 (C_{B-2}, C_{B-3}, C_{C-2}, C_{C-4}), 129.61 (C_{C-3}), 129.91 (C_{A-5}), 140.72, 141.86 (C_{B-1}, C_{B-4}), 143.13 (C_{C-1}), 143.83 (C_{A-1}), 170.01, 170.10 (CO). Anal. Calcd for C₃₀H₂₆N₄: C, 74.74; H, 5.61; N, 9.17. Found: C, 74.30; H, 4.89; N, 9.39.

***N,N'*-Bis[4-(phenylamino)phenyl]-1,3-benzenediamine 3.** A solution of tetra(amide) **2** (1.22 g, 2 mmol) and sodium hydroxide (1.0 g, 40 mmol) in EtOH/H₂O (1:1, 40 mL) was heated under reflux for 48 h. During the reaction the initially homogeneous solution underwent a liquid/liquid phase separation and eventually precipitation occurred. After cooling, the precipitate was filtered off, washed with water, and dried under reduced pressure. Recrystallization from benzene gave pure **3** (0.73 g, 83 %) as a white crystalline solid: mp 211 °C (dec); ¹H NMR (CDCl₃): δ 5.52 (2H, b s, NH), 5.56 (2H, b s, NH), 6.48 (2H, dd, *J* = 8.0 and 2.2 Hz, H_A-4), 6.59 (1H, t, *J* = 2.2 Hz, H_A-2), 6.86 (2H, tt, *J* = 7.3 and 1.1 Hz, H_C-4), 6.97 (4H, m, H_C-2), 7.05 (8H, s, H_B-2, H_B-3), 7.09 (1H, t, *J* = 8.0 Hz, H_A-5), 7.23 (4H, m, H_C-3); ¹³C NMR (CDCl₃) δ 103.75 (C_A-2), 108.29 (C_A-4), 116.45 (C_C-2), 120.15 (C_C-4), 120.79, 121.33 (C_B-2, C_B-3), 129.34 (C_C-3), 130.19 (C_A-5), 136.92, 137.25 (C_B-1, C_B-4), 144.26 (C_C-1), 145.58 (C_A-1); ES-MS *m/z* (*M*⁺) calcd 442.2, obsd 442.4. Anal. Calcd for C₃₀H₂₆N₄: C, 81.42; H, 5.92; N, 12.66. Found: C, 81.54; H, 5.85; N, 12.71.

***N,N'*-Bis-[4-(phenylimino)-cyclohexa-2,5-dienylidene]-1,3-benzenediamine (EE + EZ + ZZ) 4.** To tetra(amine) **3** (110 mg, 0.025 mmol) in chloroform (5 mL) was added PbO₂ (0.6 g, 2.5 mmol). The mixture was stirred at room temperature for 15 min. The dark red solution was filtered over silica, and the solvent was removed from the filtrate by evaporation. The product (98 mg, 90 %) was isolated as a mixture of three cis-trans isomers (**4a-c**). These isomers could not be separated by column chromatography due to fast isomerization: ¹H NMR (CDCl₃) δ 6.37, 6.41, 6.46 ((0.2+0.5+0.3) H, 3 t, *J* = 1.9 Hz, H_A-2a-c), 6.67 (0.4H, dd, *J* = 8.0 and 1.9 Hz, H_A-4a), 6.69, 6.70 (1H, 2 d, *J* = 8.0 Hz, H_A-4b, H_A-6b), 6.72 (0.6H, dd, *J* = 8.0 and 1.9 Hz, H_A-4c), 6.75 - 7.15 (12H, m, H_B-2, H_B-3, H_C-3), 7.20 (2H, m, H_C-4), 7.31 - 7.43 (9H, m, H_A-5, H_C-2); ¹³C NMR (CDCl₃) δ 112.22 (C_A-2), 117.09, 117.16, 117.19, 117.22 (C_A-4, C_A-6), 120.49, 120.57 (C_C-2), 124.45, 124.49, 124.72, 125.07, 125.11, 125.40 (*syn*-(C_B-2, C_B-3, C_B-5, C_B-6)), 125.20, 125.23 (C_C-4), 128.91, 128.95 (C_C-3), 129.53, 129.58, 129.64 (C_A-5), 136.26, 136.30, 136.77, 137.44, 137.48, 137.98 (*anti*-(C_B-2, C_B-3, C_B-5, C_B-6)), 149.92, 149.94 (C_C-1), 150.74, 150.77, 150.82 (C_A-1, C_A-3), 158.20, 158.22, 158.28, 158.31 (C_B-1), 158.67, 158.74 (C_B-4); ES-MS *m/z* (*M* + H⁺) calcd 439.2, obsd 439.4.

***N,N',N''*-Tris[4-(phenylamino)phenyl]-1,3,5-benzenetriamine 5.** A mixture of phloroglucinol (0.25 g, 2 mmol), *N*-phenyl-1,4-benzenediamine (1.47 g, 8 mmol) and iodine (0.03 g, 0.12 mmol) was stirred at 180 °C for 6 h. The water formed during the reaction was removed from the mixture by careful evacuation of the reaction vessel. After cooling the solid residue was suspended in MeOH/CHCl₃, using an ultrasonic bath. The grey solid was filtered off and washed thoroughly with CHCl₃ and recrystallized from acetonitrile to give pure **5** (0.98 g, 78 %) as a white crystalline solid: mp 210 °C; ¹H NMR (acetone-d₆) δ 6.27 (3H, s, H_A), 6.74 (3H, tt, *J* = 7.3 Hz and 1.1 Hz, H_{C-4}), 6.99 (6H, dd, *J* = 7.5 Hz and 1.2 Hz, H_{C-2}), 6.99 (3H, s, N-H), 7.08 (6H, d, *J* = 9.0 Hz, H_{B-2}), 7.10 (3H, s, N-H), 7.12 (6H, d, *J* = 9.0 Hz, H_{B-3}), 7.16 (6H, dd, 7.5 Hz and 7.3 Hz, H_{C-3}); ¹³C NMR (acetone-d₆) δ 96.3 (C_{A-2}), 116.3 (C_{C-2}), 119.6 (C_{C-4}), 121.2, 121.3 (C_{B-2}, C_{B-3}), 130.0 (C_{C-3}), 137.5, 138.7 (C_{B-1}, C_{B-4}), 144.3 (C_{C-1}), 147.6 (C_{A-1}); ES-MS *m/z* (M⁺) calcd 624.3, obsd 624.5.

***N,N',N''*-Tris-[4-(phenylimino)-cyclohexa-2,5-dienylidene]-1,3,5-benzenediamine (EEE + EEZ + EZZ + ZZZ) 6.** To hexa(amine) **5** (110 mg, 0.025 mmol) in dioxane (5mL) was added PbO₂ (0.6 g, 2.5 mmol). The mixture was stirred at room temperature for 30 min. The dark red solution was filtered over silica and the solvent was removed by evaporation. The product (98 mg, 90 %) was isolated as a mixture of four cis-trans isomers (**6a-d**). These isomers could not be separated by column chromatography due to fast isomerization: ¹H NMR (CDCl₃) δ 6.17, 6.20, 6.24, 6.27 ((0.12+0.34+0.39+0.15) 3H, 4 s, H_{A-2a-d}), 6.75-7.10 (18H, m, H_{B-2}, H_{B-3}, H_{B-5}, H_{B-6}, H_{C-2}), 7.17 (3H, m, H_{C-4}), 7.33-7.41 (6H, m, H_{C-3}); ¹³C NMR (CDCl₃) δ 108.72, 108.80 (C_{A-2}, C_{A-4}, C_{A-6}), 120.49, 120.56 (C_{C-2}), 124.34, 124.39, 124.44, 124.88, 124.98, 124.01, 125.05, 125.59 (*syn*(C_{B-2}, C_{B-3}, C_{B-5}, C_{B-6})), 125.27, 125.32 (C_{C-4}), 128.92, 128.94 (C_{C-3}), 136.05, 136.07, 136.11, 137.00, 137.21, 137.24, 137.28, 138.24 (*anti*(C_{B-2}, C_{B-3}, C_{B-5}, C_{B-6})), 149.86 (C_{C-1}), 151.38, 151.41, 151.45, 151.46, 151.51 (C_{A-1}, C_{A-3}, C_{A-5}), 158.06, 158.08, 158.11, 158.14, 158.16, 158.19 (C_{B-1}), 158.92, 158.97(C_{B-4}); ES-MS *m/z* (M + H⁺) calcd 619.3, obsd 619.3.

7.10 References

- 1 Wienk, M. M.; Janssen, R. A. J. *Chem. Commun.* **1996**, 267.
- 2 Huang, W. -S.; Humphrey, B. D.; MacDiarmid, A. G. *J. Chem. Soc., Faraday Trans.* **1986**, 82, 2385.
- 3 Wudl, F.; Angus, R. O.; Lu, F. L.; Allemand, P. M.; Vachon, D. J.; Nowak, M.; Liu, Z. X.; Heeger, A. J. *J. Am. Chem. Soc.* **1987**, 109, 3677.
- 4 MacDiarmid, A. G.; Epstein, A. J. *Faraday Discuss. Chem. Soc.* **1989**, 88, 317.
- 5 Wolf, J. F.; Forbes, C. E.; Gould, S.; Shacklette, L. W. *J. Electrochem. Soc.* **1989**, 136, 2887.
- 6 Moll, T.; Heinze, J. *Synth. Met.* **1993**, 55-57, 1521.
- 7 Murata, Y.; Shine, H. J. *J. Org. Chem.* **1969**, 34, 3368.
- 8 Ebersson, L.; Hartshorn, M. P.; Persson, O. *Acta Chem. Scand.* **1995**, 49, 640.
- 9 This notation is preferred, because two electrons in one *p*-phenylenediamine unit are expected to be in a closed-shell configuration.
- 10 Weissman, S. I.; Kothe, G. *J. Am. Chem. Soc.* **1975**, 97, 2538.
- 11 Weissman, S. I. *J. Am. Chem. Soc.* **1975**, 97, 2537.
- 12 Novak, C.; Kothe, G.; Zimmermann, H. *Ber. Bunsen-Ges. Phys. Chem.* **1974**, 78, 265.
- 13 Müller, U.; Baumgarten, M. *J. Am. Chem. Soc.* **1995**, 117, 5840.
- 14 Iwamura, H.; Koga, N. *Acc. Chem. Res.* **1993**, 26, 346.
- 15 Kanno, F.; Inoue, K.; Koga, N.; Iwamura, H. *J. Phys. Chem.* **1993**, 97, 13267.
- 16 Ling, C.; Lahti, P. M.; *J. Am. Chem. Soc.* **1994**, 116, 8784.
- 17 The appearance of the ¹H NMR spectrum is very sensitive towards temperature and concentration.
- 18 Between 160 and 165 °C a liquid crystalline phase is observed by polarization microscopy.

Epilogue

In this thesis, various phosphorus and nitrogen-centered radicals have been evaluated as spin-carrying unit in high-spin molecules. These studies reveal that it is indeed possible to construct such high-spin molecules, but it became clear that (in)stability of the spin-carrying unit is a very important issue. Phosphoryl and phosphinyl radicals can both be employed, but due to the difficult generation and chemical instability, these phosphorus-centered radicals afford no distinct advantages over other organic radicals, commonly used for high-spin systems. Cation radicals of methylene phosphoranes can not only be generated more efficiently, but these open-shell moieties are significantly more stable as well. Finally, cation radicals of *m-p*-aniline oligomers are shown to be remarkably stable, and this is not at the expense of the spin coupling, because for all oligomers, high-spin states are obtained. It is concluded that the singly oxidized *p*-phenylenediamine unit is a very suitable spin-carrying unit for the construction of high-spin systems, because it meets a very delicate balance between localization and delocalization of spin.

So, where to go from here? Will it be possible to make organic ferromagnetic materials, simply by making polymers instead of oligomers? One should realize that, in order to obtain bulk magnetic properties, spin coupling over a long distance in at least two, but preferably three dimensions is required. Therefore, extension of aniline oligomers to larger spin multiplicities is merely the next step.

One problem that still needs to be solved, is the interruption of the spin coupling, that may occur due to structural defects or an improperly tuned oxidation state. Possibly, this problem can be solved by making networks, in which several spin-coupling pathways are possible,¹ or by the development of architectures in which the spin-carrying unit is no longer in the backbone of the polymer, but is present as a side group on a conjugated backbone.²

Ultimately, if sufficiently high spin multiplicities can not be achieved via extension of the intramolecular spin coupling, intermolecular interactions between high-spin molecules have to be addressed as well. Recent studies have shown that it is indeed possible to gain control over the intermolecular spin coupling, by manipulation of the supramolecular arrangement.³

1 Rajca, A. *Chem. Rev.* **1994**, *94*, 871.

2 Nishide, H.; Kaneko, T.; Toriu, S.; Kuzumaki, Y.; Tsuchida, E. *Bull. Chem. Soc. Jpn.* **1996**, *69*, 499.

3 Cerujeda, J.; Mas, M.; Molins, E.; Lanfranc de Panthou, F.; Laugier, J.; Park, J. G.; Paulsen, C.; Rey, P.; Povira, C.; Veciana, J. *J. Chem. Soc., Chem. Commun.* **1995**, 709.

Summary

In this thesis, the design, synthesis, and characterization of various novel high-spin molecules is described. High-spin molecules consist of organic radicals, which function as spin-carrying moieties, that are covalently linked via ferromagnetic coupling units, in such a way that the electron spins are aligned in a parallel fashion. The research described in this thesis focuses on the evaluation of various phosphorus and nitrogen-centered radicals as spin-carrying unit, in combination with a well-established ferromagnetic coupling unit, *m*-phenylene.

A short introduction into high-spin molecules is given in Chapter 1. Furthermore, the aims of research are formulated and a short description is given of the subjects treated in the following chapters. An elaborate survey of the field of high-spin molecules is presented in Chapter 2. The mechanisms governing spin-spin interactions within, as well as between organic molecules are discussed and several examples of high-spin molecules, classified by the nature of their spin-carrying units, are evaluated. Furthermore, the techniques, commonly used to study such molecules are shortly addressed.

Chapters 3 and 4 deal with phosphinyl and phosphoryl diradicals. Both species are prepared in a toluene matrix at cryogenic temperatures, via a photoinduced dissociative electron capture reaction from the corresponding bis(phosphonous chloride) and bis(phosphinic chloride), respectively. As a result of the *m*-phenylene coupling unit between the radical centers, parallel alignment of the electron spins is achieved, giving rise to a triplet state for both diradicals. Variable temperature ESR measurements reveal Curie behavior between 4 and 100 K, which is consistent with a low-energy triplet state, that is either the ground state or part of a (near) degeneracy with a low-spin singlet state. These diradicals are the first examples of high-spin molecules, in which heavy-atom radicals are ferromagnetically coupled. Apparently, the reduced spin-coupling, which is anticipated for second-row atom based radicals, does not rule out ferromagnetic interactions, not even for phosphoryl radicals in which the pyramidal geometry and spin delocalization are expected to decrease spin coupling even further. Attempts to employ acylphosphine oxides as more efficient precursors for phosphoryl radicals were not successful.

Di and tri(cation radical)s of methylene phosphoranes are the subject of Chapter 5. The preparation of these organic radicals by chemical oxidation of the neutral precursor molecules is much more efficient than the in situ photochemical method, used for the generation of phosphinyl and phosphoryl radicals. Moreover, these oligo(cation radical)s are stable in cold solution, which is also a marked improvement. ESR measurements on these species in frozen solution reveal high-spin triplet and quartet states for the di and tri(cation radical),

respectively. Temperature dependent studies reveal Curie behavior for all high-spin states, consistent with a high-spin ground state, though strictly, (near) degeneracy with a low-spin state can not be excluded. Sterically crowded bis and tris(phosphines) have also been synthesized as precursors for oligo(cation radical)s, but no stable open-shell species are obtained upon oxidation of the molecules.

In Chapter 6, poly(*m-p*-aniline) is introduced as a potential polaronic ferromagnetic polymer. In a polaronic ferromagnetic material, unpaired electrons are introduced by redox doping of π -conjugated segments, comparable to the well-established doping of conducting polymers. Spin alignment is achieved by linkage of these segments via ferromagnetic coupling units. Linear and branched *N*-phenylaniline oligomers, characterized by an alternating sequence of *meta* and *para*-connected aniline units, have been prepared as model compounds. Oxidation of these oligomers to an intermediate oxidation state –in which one electron is removed per two aniline units– affords cation radicals, which are stable at ambient temperature, as inferred from electrochemical measurements and UV/visible/nearIR studies. ESR studies in frozen solution reveal high-spin triplet and quartet states for di and tri(cation radical)s, respectively. Whereas the *para* connectivity provides effective delocalization of the unpaired electron, thus stabilizing the radicals, the *meta* connectivity affords the desired parallel spin alignment. The temperature dependence of the ESR signals, attributed to the high-spin states is in accordance with Curie's law between 4 and 100 K, from which can be concluded that the low energy high-spin states are the ground state or (near) degenerate with a low-spin state. This is confirmed by magnetization studies, performed on one of the compounds.

Similarly, cation radicals of unsubstituted *m-p*-aniline oligomers, which are the subject of Chapter 7, also combine ferromagnetic spin alignment with a remarkable stability. Moreover, in addition to oxidative doping, the intermediate oxidation state, which is needed for high-spin behavior, can very conveniently be reached via an "acid doping" process. A redox reaction between equimolar amounts of the fully reduced oligo(amine) and the corresponding fully oxidized oligo(imine) is triggered by the addition of a small amount of a Brønsted acid. In this process, the amines are oxidized to the desired intermediate oxidation state by the protonated imines, while at the same time, the protonated imines are reduced to exactly the same species. Variable temperature ESR measurements are consistent with high-spin ground states.

Finally, in the epilogue, the results are placed in a larger context and some of the prospects are briefly discussed.

Samenvatting

Dit proefschrift beschrijft het ontwerp, de synthese en de karakterisering van een aantal nieuwe high-spin moleculen. Deze moleculen zijn opgebouwd uit organische radicalen die fungeren als spincentra, die met elkaar verbonden zijn door een ferromagnetische koppelings-eenheid, waardoor de elektronspins gelijk gericht worden. Het in dit proefschrift beschreven onderzoek, richt zich met name op de evaluatie van verschillende fosfor- en stikstof-gecentreerde radicalen als spincentrum, in combinatie met een veelgebruikte ferromagnetische koppelingseenheid, *m*-fenyleen.

In Hoofdstuk 1 wordt een korte inleiding over high-spin moleculen gegeven. Bovendien worden de onderzoeksdoelen geformuleerd en wordt er een korte beschrijving gegeven van de onderwerpen van de volgende hoofdstukken. Hoofdstuk 2 is een overzicht over high-spin moleculen; de mechanismen die de spinkoppeling bepalen –zowel binnen een organisch molecuul alsmede tussen verschillende moleculen– worden behandeld, en verscheidene high-spin moleculen, ingedeeld naar spincentra worden besproken. Verder worden de technieken die het meest gebruikt worden om dergelijke moleculen te analyseren kort op een rij gezet.

Hoofdstuk 3 en 4 gaan achtereenvolgens over fosfynyl- en fosforyldiradicalen. Beiden worden bij lage temperatuur in een toluëenmatrix gegenereerd, via een fotogeïnduceerde dissociatieve electron-capture reactie. De *m*-fenyleen koppelingseenheid tussen de spincentra heeft een parallelle oriëntatie van de elektronspins tot gevolg, wat resulteert in een triplet-toestand voor beide diradicalen. Variabele-temperatuur ESR metingen geven Curie gedrag te zien. Dat is in overeenstemming met een triplet-grondtoestand, of met een triplet die (vrijwel) gedegenereerd is met een low-spin singulet-toestand. Deze diradicalen zijn de eerste voorbeelden van high-spin moleculen, waarin radicalen gecentreerd op een tweede-rij atoom ferromagnetisch zijn gekoppeld. De zwakkere spinkoppeling, verwacht voor een radicaal van een tweede-rij atoom, sluit ferromagnetische koppeling blijkbaar niet uit, zelfs niet in het geval van fosforyldiradicalen, waarvoor –vanwege de pyramidale geometrie en delocalisatie van spin– de spinkoppeling naar verwachting nog zwakker zal zijn. Pogingen om acylfosfine oxides te gebruiken als efficiëntere precursors voor fosforylradicalen zijn niet succesvol gebleken.

Di- en triradicaalkationen van methyleenfosforanen worden besproken in Hoofdstuk 5. Het maken van deze organische radicalen door middel van chemische oxidatie is veel efficiënter dan de in situ fotochemische reacties, die gebruikt werden voor het maken van de fosfynyl- en fosforylradicalen. Bovendien zijn deze radicaalkationen stabiel in oplossing bij lagere temperatuur, wat ook een duidelijke verbetering is. ESR metingen, uitgevoerd aan bevroren oplossingen, wijzen op een triplet-toestand voor het diradicaalkation en een

kwartet-toestand voor het triradicaalkation. Temperatuurafhankelijke ESR metingen aan deze high-spin toestanden zijn in overeenstemming met de wet van Curie, en een high-spin grondtoestand, al kan formeel de mogelijkheid niet worden uitgesloten dat high- en low-spin toestanden gedegeneerd zijn. Verder zijn ook bis- en trisfosfines gesynthetiseerd als precursors voor oligoradicaalkationen, maar oxidatie van deze verbindingen levert geen stabiele radicalen op.

In Hoofdstuk 6 wordt poly(*m-p*-aniline) als potentieel polaronisch polymeer geïntroduceerd. In een polaronische ferromagneet worden ongepaarde elektronen verkregen door het oxidatief of reductief dopen van π -geconjugeerde segmenten, vergelijkbaar met het dopen van geleidende polymeren. Parallele spins kunnen bereikt worden door het koppelen van deze gedoopte segmenten via ferromagnetische koppelingseenheden. Zowel lineaire als vertakte *N*-phenylaniline-oligomeren, gekenmerkt door een alternerende volgorde van *meta* en *para* gekoppelde aniline-eenheden, zijn gesynthetiseerd als modelverbindingen. Oxidatie tot een intermediaire oxidatietoestand –waarin één elektron is verwijderd per twee aniline-eenheden– geeft radicaalkationen die stabiel zijn bij kamertemperatuur, zoals blijkt uit elektrochemische en UV/visible/nearIR metingen. ESR metingen aan bevroren oplossingen wijzen op een triplet-toestand voor het diradicaalkation en op een kwartet-toestand voor de triradicaalkationen. Het *para* koppelingspatroon maakt delocalisatie van het ongepaarde elektron mogelijk, waardoor de radicaalkation gestabiliseerd worden; het *meta* koppelingspatroon zorgt voor de gewenste parallelle spins. De temperatuurafhankelijkheid van de ESR signalen van de high-spin toestanden is in overeenstemming met de wet van Curie, waaruit geconcludeerd kan worden, dat het grondtoestanden betreft, wellicht gedegeneerd met een low-spin toestand. Dit wordt bevestigd door magnetisatiemetingen aan een van de verbindingen.

Ook radicaalkationen van ongesubstitueerde *m-p*-aniline-oligomeren (Hoofdstuk 7) combineren ferromagnetische spinkoppeling met een buitengewone stabiliteit. Daarnaast kan de intermediaire oxidatietoestand, die vereist is voor ferromagnetische eigenschappen, door middel van “zure doping” verkregen worden. Een redoxreactie tussen equimolaire hoeveelheden van een volledig gereduceerd oligoamine en een volledig geoxideerd oligoimine wordt in gang gezet door het toevoegen van een kleine hoeveelheid van een Brønsted zuur. Tijdens deze reactie wordt het oligo(amine) geoxideerd tot de gewenste intermediaire oxidatietoestand, door het geprotoneerde oligo(imine), wat op zijn beurt gereduceerd wordt tot precies het zelfde deeltje. Variabele-temperatuur ESR metingen aan deze structuren zijn in overeenstemming met high-spin grondtoestanden.

Tot slot, in de epiloog worden de resultaten in een grotere context bekeken en de toekomstperspectieven worden kort besproken.

Curriculum Vitae

Martijn Wienk kwam op 30 april 1965 in Oldenzaal ter wereld. Na het behalen van zijn VWO diploma aan het Carmellyceum in 1983 begon hij met de studie Chemische Technologie aan de toenmalige Technische Hogeschool Twente. In 1988 studeerde hij af op onderzoek aan polymeer-gebonden crown ethers in vloeistofmembranen. Het onderzoek was uitgevoerd binnen de vakgroep Organische Chemie, onder leiding van prof. dr. E. J. R. Sudhölter en prof. dr. ir. D. N. Reinhoudt. Na vervangende dienst binnen dezelfde groep en een reis naar Azië, begon hij in 1992 aan een 2-jarige onderzoekers opleiding aan de Technische Universiteit Eindhoven. Dit onderzoek betrof high-spin moleculen op basis van fosforyl radicalen en werd begeleid door dr. ir. R. A. J. Janssen en prof. dr. E. W. Meijer. Na afronding van deze studie in 1994, vervolgde hij het onderzoek als AIO-4 en de resultaten staan beschreven in dit proefschrift.

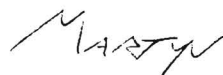
Dankwoord

Promoveren is een hele bevalling, maar gelukkig sta je er als promovendus nooit helemaal alleen voor. Ik wil graag van de gelegenheid gebruik maken om een aantal mensen te bedanken. Allereerst mijn copromotor, René Janssen; ik had me geen betere begeleider kunnen wensen. De bevrogen, ongecompliceerde wijze waarop hij met wetenschap in de weer is, bleek erg aanstekelijk, en het was dan ook een genoegen om met hem samen te werken. Van mensen met wie je het altijd eens bent valt niet veel te leren. Misschien wel juist daarom heb ik van mijn promotor Bert Meijer in de afgelopen vijf jaar veel opgestoken, al lukt het me nog niet altijd om het ook in de praktijk te brengen.

Verder heb ik altijd dankbaar gebruik gemaakt van Jef Vekemans' kennis en ervaring op het gebied van synthese en zijn bereidheid om steeds weer twee minuutjes voor me uit te trekken. Om dezelfde reden heb ik de aanwezigheid en inzet van Johan Janssen en Steven van Es weten te waarderen. Edsko Havinga, wil ik bedanken voor het kritisch volgen van mijn onderzoek, en Joost van Dongen voor ES-MS metingen en al het andere werk dat hij voor de vakgroep verricht. Ik denk dat sommige mensen –zeer ten onrechte– zijn bijdrage aan deze vakgroep onderschatten.

De rest van de vakgroep dank ik voor een plezierige werkomgeving, waarin ik mij altijd thuis heb gevoeld. Een aantal mensen wil ik met name noemen: Bas de Waal en Jos Versleijen, voor het synthetische werk dat zij mij uit handen genomen hebben. Zo ook Paul van Mil, Doina Despotovici en Ronald Mikkenie. Jammer dat het onderzoek toendertijd niet overdreven vruchtbaar was; met wat meer positieve resultaten was het werk ongetwijfeld leuker geweest. Marwijn Christiaans, Koen Pieterse en Michiel Bouman voor de regelmatig vereiste bemiddeling tussen mij en de zegening die een p.c. heet te zijn. Hans Damen voor de onderkoelde wijze waarop hij het magazijn runt en Henk Eding, omdat hij door zijn voortdurende aanmoedigingen om op te ruimen, almaar weer te kennen heeft gegeven dat hij het vertrouwen in mij nog steeds niet heeft verloren. Van buiten de vakgroep wil ik Arie Schouten (kristalstructuren), Ed Reijerse (ESR-simulaties), Joachim Sinzig (magnetisatie metingen) en Uwe Seegelbacher (electrochemie/ESR) hartelijk bedanken voor hun bijdrage.

Tot slot, alle mensen die inhoud gegeven hebben aan mijn leven buiten de universiteit. Het thuisfront in de persoon van Annemieke, Gerard, Henk, Joep, Lily, Stijn, Teo en Ted, de waterpolo mannen van Njord, mijn ouders (waar zou ik zijn zonder hen), en natuurlijk Marga. Hoe waardevol vrijheid is, blijkt uit alles wat je ervoor terugkrijgt als je het inruilt.



Stellingen

behorende bij het proefschrift

"High-Spin Molecules of Phosphorus and Nitrogen-Centered Radicals"

van

Martijn M. Wienk

1. Door de spinconcentratie in polyradicalen op te geven in spins per gram, kan ten onrechte het idee gewekt worden dat er sprake zou kunnen zijn van intramoleculaire spin-koppeling in materialen met hooguit één spin per vijftig monomere eenheden.
Yoshizawa, K.; Tanaka, K.; Yamabe, T.; Yamauchi, J. *J. Chem. Phys.* **1992**, *96*, 5516.
2. Irreversibele oxidatie kan nooit een stabiel radicaalkation als primair product opleveren.
Yoshizawa, K.; Chano, A.; Ito, K.; Tanaka, K.; Yamabe, T.; Fujita, H.; Yamauchi, J.; Shiro, M. *J. Am. Chem. Soc.* **1992**, *114*, 5994.
3. Het gebruik van de term "self assembly", daar waar uiteenlopende fenomenen als kristallisatie, fasenscheiding en adsorptie bedoeld worden, is een verwerpelijk modeverschijnsel.
Chen, T. -A.; Wu, X.; Rieke, R. D. *J. Am. Chem. Soc.* **1995**, *117*, 233.
Yang, Y.; Heeger, A. J. *Nature*, **1994**, *372*, 344.
Bain, C. D.; Whitesides, G. M. *Angew. Chem., Adv. Mater.* **1989**, *101*, 522.
4. Een functioneel molecuule resulteert niet automatisch in een functioneel materiaal.

5. Kleurenplaatjes in wetenschappelijke tijdschriften vallen niet alleen op door de kleur, maar ook doordat tijdschriftenbundels op die pagina's makkelijker openvallen.
J. Am. Chem. Soc. 1990 - heden
6. Landen die economische vluchtelingen weigeren, zouden ook belastingvluchtelingen moeten weren.
7. Het is opvallend dat "misdaden tegen de mensheid" altijd alleen door de uiteindelijke verliezers van een conflict gepleegd blijken te zijn.
8. Met een groeiend aantal managers in een organisatie komen er steeds meer mensen die *menen* te weten hoe iets moet, en steeds minder mensen die *weten* hoe het moet.
10. Bij het aannemen van impopulaire wetsvoorstellen, zoals het aanleggen van de HSL door het groene hart, zijn de initiële protesten van de regeringsfracties altijd opvallend luidruchtiger dan het uiteindelijke leidzame instemmen.
11. Arrogantie en macht vertonen kip/ei karakteristieken. Het is niet duidelijk wat oorzaak is en wat gevolg.
12. Ondertiteling van buitenlandse programma's op televisie is niet alleen goed voor het leren van een vreemde taal, maar zal in toenemende mate van belang zijn voor het ontwikkelen van de leesvaardigheid.